UNSTEADY AERODYNAMIC FORCES ON PARACHUTE CANOPIES

R. J. HARWOOD

University of Leicester

Ph.D. 1988

Text cut off in original

INDEX

Index.

ABSTRACT

Unsteady Aerodynamic Forces on Parachute Canopies.

R.J. Harwood.

A research programme has been conducted, the objective of which has been the determination of unsteady force coefficients for a range of parachute canopy models. These coefficients are required for prediction of the aerodynamic stability of full scale parachutes under conditions of unsteady motion during descent.

The method of obtaining these coefficients required the collection of force and acceleration data for parachute canopy models which were tested in unsteady conditions. This was achieved by imposing oscillatory motion on individual canopies during towing tests, which were conducted under water in a ship testing tank.

Two modes of unsteady motion were imposed on a canopy under test; one in which it was oscillated along its axis, and one in which it was oscillated laterally. A mathematical model describing such modes of motion consists of a general equation for the unsteady force developed on a bluff body.

In this model the force F(t) is expressed using two components; a velocity dependent force component, and an acceleration dependent force component. Each component of the aerodynamic force contains an unknown parameter denoted by the terms 'a' and 'b' in the equation, which is shown below;

$$F(t) = a(t)\cdot v^2(t) + b(t)\cdot \dot{v}(t).$$

An identification technique is used to determine the mean values per cycle of each parameter by substitution of the data obtained from these tests as functional variables in the mathematical model. Mean values of the velocity dependent force and stability coefficients; C_T and $\partial C_N/\partial\alpha$, and the added mass coefficients k_{11} and k_{33} are then obtained from these parameters.

The results of this programme indicate a strong dependence in oscillatory motion of the mean value per cycle for the axial added mass coefficient k_{11} on the unsteady force parameter called the Keulegan-Carpenter number K_C;

$$K_C = \hat{U}\cdot T/D_o.$$

Where; $\hat{U}$ = the velocity amplitude of the oscillation, T = the period of an oscillation, and D_o = a typical canopy dimension.

The velocity dependent axial force coefficient C_T exhibits a similar, although not as substantial dependency.

Good agreement has been obtained between steady-state test results from this programme and results from other independent work. The effects of values obtained in this investigation are considered in the linearised dynamic stability model developed by Doherr and Saliaris (4), and their influence on the descent characteristics of full-scale parachutes is assesed.

Acknowledgements

The author would like to express his gratitude to the following for their help in completing this work; to Dr D.J.Cockrell for his guidance encouragement and suggestions throughout the project, to staff and collegues of the Engineering Department of the University of Leicester in particular Mr P. Barwell and Dr A.C. Baxter who sacrificed their own time in agreeing to assist with the experiments, and without whom this work would not have been made possible, to Dr R. Ziarati and his staff at Southampton Institute of Higher Education for their cooperation in conducting these tests.

The encouragement of Dr R. Bartlett and staff of the parachute section, Royal Aerospace Establishment is greatly appreciated.

Finally the author would like to thank Professor G.D.S. MacLellan for permitting the use of the staff and facilities of Leicester University Engineering Department during the course of this project.

OBJECTIVE

To determine the aerodynamic and inertial characteristics for certain specified parachute canopy shapes and types, thus extending the understanding of ways in which dynamic stability characteristics of parachute canopies depend on the variation of canopy shape.

NOMENCLATURE

NOMENCLATURE

A General expression for the area of an object.

â Acceleration number; $\hat{a} = \dot{V} \cdot l / V^2$.

a Velocity dependent force parameter of Morison's equation.

a_o, a_1; Polynomial coefficients of the stability eigenvalues λ^n.

α Angle of attack.

α_{11} Axial added mass component.

α_{33} Lateral added mass component.

α_{35} Added mass coupling term for motion either along the z-axis and about the y-axis, or along the y-axis and about the z-axis.

α_{55} Added Moment of inertia about the y-axis.

b_o, b_1, b_2; Polynomial coefficients of the stability eigenvalues λ^n.

b Acceleration dependent force parameter of Morison's equation.

c_o, c_1; Polynomial coefficients of the stability eigenvalues λ^n.

C_T Total axial force coefficient, for varying angle of attack α.

C_D Velocity dependent, axial force coefficient for which the angle of attack $\alpha = 0$.

C_D^* Velocity dependent force coefficient C_D corrected for blockage.

C_N Velocity dependent, lateral force coefficient.

C_M Inertial force coefficient.

d_o, d_1, d_2; Polynomial coefficients of the stability eigenvalues λ^n.

D_o Nominal diameter of parachute canopy.

ϕ Potential function for an ideal fluid.

$\nabla\phi$ Derived velocity for an ideal fluid flow.

F General expression for force.

F^* An expression for the mean force.

g Acceleration due to gravity, $m.s^{-2}$.

K_C Keulegan-Carpenter number $K_C = \hat{U} \cdot T/D_o$.

k_{ij} The added mass coefficient Tensor.

k_{11} Axial added mass coefficient.

k_{33} Lateral added mass coefficient.

λ General stability eigenvalue.

M Moment about y-axis.

m Mass of an object in a fluid.

m_a Added mass of an object in a fluid.

$(m + m_a)$ Virtual mass of an object in a fluid.

N_p External aerodynamic force in the lateral direction.

P_o Porosity of parachute canopy fabric; cu.ft/sq.ft/sec.

R_e Reynolds number $R_e = \rho \cdot D_o \cdot V/\mu$.

S_o Nominal surface area of a parachute canopy.

τ Polpitiye phase-lag parameter.

T Oscillational period.

T_e Kinetic energy of object and fluid.

T_p External aerodynamic force in the tangential (axial) direction.

$\hat{U}$ Velocity amplitude of oscillatory motion.

u Velocity in x direction.

$\dot{u}$ Acceleration in x direction.

v Velocity in y direction.

$\dot{v}$ Acceleration in y direction.

V_u Unsteady velocity component.

V_s Steady velocity component.

V_o Nominal volume of a parachute canopy.

υ General representative volume of an object.

w Velocity in z direction.

$\dot{w}$ Acceleration in z direction.

X Total force in x direction refered to parachute body axes.

Y Total force in y direction refered to parachute body axes.

Z Total force in z direction refered to parachute body axes.

LIST OF TABLES

LIST OF TABLES

Chapter 2.

Chapter 3.

Chapter 4.

Chapter 5.

Chapter 6.

Chapter 7.

Table Title

LIST OF FIGURES

LIST OF FIGURES

For Mum Dad and Janine

CHAPTER 1

1. INTRODUCTION

Preface.

The motion of parachutes in unsteady flow poses an interesting and relevant problem to fluid dynamicists. Both canopy deployment and oscillatory motion during fully deployed descent pose unsteady flow problems, though the former is not considered in the present context.

Although a parachute generally descends with an effectively steady downward velocity, it oscillates in pitch and varies its line of motion, so altering its angle of attack. This alteration of the shape presented to the relative airflow affects the aerodynamic forces which the parachute experiences. Since the main purpose of a parachute canopy is to provide drag for its payload any alteration to this drag will affect its descent rate. Variations to the lateral aerodynamic force component similarly affect the stability characteristics of the canopy.

Dimensional analysis techniques readily demonstrate that the aerodynamic forces experienced by a parachute depend on the shape which it presents to the flow, the nature of the motion e.g. linear or rotational, experienced by the parachute relative to the fluid, effects such as vortex shedding which cause the system to develop a memory to the flow history, the magnitude of the instantaneous velocities and accelerations applied to the parachute and both the Reynolds number and the Mach number of the flow.

Instantaneous aerodynamic forces are therefore related to the instantaneous velocity and the instantaneous acceleration in a highly complex manner.

It is convenient to model these forces as if they consisted of two main components, one of which is velocity-dependent, and the other which is acceleration dependent, and to disregard the complex flow history effects. These velocities and accelerations could be either linear or rotational or they could be both of these. When modelling a force in such a way, the problem arises of determining the dimensionless coefficients associated with the acceleration and the velocity. Since flow history effects are being disregarded it is of importance to study the consistency of these coefficients in different types of flow, such as in both steady and unsteady flows, and of scaling experimentally acquired results from models to prototype parachute canopies.

1.1. Acceleration Dependent Force & The Concept Of Added - Mass.

The forces experienced by a body in steady motion, when moving through a fluid, are aerodynamic e.g. drag and lift force components and also body forces, for example the gravitational force. Unsteady motion invokes an extra mechanism for the aerodynamic forces, in the form of inertial forces.

When an object moves through a fluid, the fluid gains kinetic energy due to the motion of the object. Its effect is to translate and rotate the surrounding fluid, some of which will be entrained into the object's wake. Since localised masses of fluid are set into motion an object passing through a fluid has an associated "added mass", which is representitive of this fluid's motion. This can be illustrated by the following demonstration for the one-dimensional motion of an object within an ideal fluid.

Let 'F' be the total force applied to an object along its line of motion. If the object moves with velocity 'U', then the rate at which work is done is;

$$F \cdot U = dT_e/dt$$

Where; T_e = Kinetic energy of the object & fluid, such that;

$$T_e = 1/2 \cdot (M + M_a) \cdot U^2 .$$

M = Mass of object.

M_a = A localized mass of fluid.

$1/2 \cdot M_a \cdot U^2$ = The kinetic energy imparted by the object to the fluid.

The term M_a is referred to as the added mass. Thus, the sum; $(M + M_a)$, is generally referred to as the virtual mass of the object.

Since the added mass of an ideal fluid can be shown to be invarient with time, differentiating kinetic energy with respect to time gives;

$$dT_e/dt = (M + M_a) \cdot U \cdot dU/dt$$

$$\rightarrow \quad F \cdot U = (M + M_a) \cdot U \cdot dU/dt$$

$$\rightarrow \quad F = (M + M_a) \cdot dU/dt \qquad [1.2].$$

Although this is a statement of Newton's second law, it is derived by assuming the work done on the fluid is wholly converted to kinetic energy and no heat is dissipated into the surroundings. This is not true for real fluids, for unlike ideal fluids kinetic energy is dissipated as internal energy of the real fluid during motion.

The added mass associated with an object is loosely considered to be that part of the fluid in the locality of the object that is set into motion by the object's movement. In an infinite fluid, fluid particles in the vicinity of the object will acquire the local velocity of the object. But

fluid particles further away will not be influenced to the same extent and those particles at an infinite distance experience no change in their velocity due to the object's motion. Thus the motion of the object will produce a distribution of velocities in the surrounding fluid field. Instead of accounting for the individual effects of all elemental masses both far and near, the exchange of momentum between object and fluid is collectively described by what is called the "added mass". The added mass is then assigned a velocity which is equal to that of the object.

One consequence of the effect of added mass is apparent from equation 1.2;

$$F = (M + M_a)\cdot dU/dt.$$

If as in the case of a large aircraft in air, 'M' is very much greater than M_a, that is, the aircraft's mass is very much greater than the mass of fluid which the aircraft sets into motion, then predominantly;

$$F \simeq M\cdot dU/dt.$$

But when as in the case of a balloon, the density of the immersed body is approximately that of the surrounding fluid, the added mass plays a larger role in determining the motion of the object. Typical examples of objects subject to this phenomenon include; oilrigs and submarines at sea, together with balloons, airships and parachutes in both air and water.

Generally M_a is written as;

$$M_a = \rho \cdot k \cdot \upsilon \qquad [1.3].$$

Where; ρ = density of fluid in which the body is immersed, υ = a representative volume of the immersed object, and k = an added mass coefficient. For a parachute the representative volume V_o is considered to be that of a hemispherical shell the diameter of which equals the canopy nominal diameter. Thus for a parachute canopy;

$$\upsilon = V_o = \pi D_o^3/12$$

where D_o is the diameter of the canopy when laid on a flat surface. This is generally known as the nominal diameter, and V_o is generally known as the nominal volume.

1.2. Acceleration Dependent Forces In Potential Flow.

In the potential flow of ideal fluids the absence of viscosity enables them to be described by potential functions ϕ in which the fluid velocity at a point is given by the potential gradient $\nabla\phi$. The concept of added mass illustrates that an accelerating immersed object is subjected to an inertial effect associated with the rate of change of momentum of the fluid as well as that which is dependent on the object's mass.

1.3. Acceleration Dependent Forces In Real Fluids.

In real fluids, the property of viscosity leads to complications in modelling the flow. Viscosity gives rise to shear stresses within the fluid. In regions of high shear stresses, such as arise in the boundary layer surrounding an object in the flow, vorticity is generated and flow separation can occur. Since the nature of the fluid flow around an immersed object differs according to whether the fluid is real or ideal, the added mass in a real fluid will be different from the value predicted by a potential flow model. In addition, when the motion of the object is unsteady then in a real flow vorticity will be shed. Thus both the fluid viscosity and the unsteadiness of the motion will cause inertial coefficients to differ from their potential flow values. Since they cannot be determined analytically in a real fluid, for in the presence of vorticity no potential function can exist in unsteady viscous flow, experimental work must be performed in order to determine the velocity dependent coefficients and the added mass components of aerodynamic forces.

1.4. Experimental Results For Unsteady Flow Around Bluff Bodies.

Over the last sixty years, the results obtained in unsteady flows can be divided into those derived analytically and those obtained empirically. Experimentally-determined

added mass coefficients tend to differ from those derived analytically. These differences arise from the difficulties in modelling analytically the states of flow in real fluids. Since much of the experimental work has been performed over a period of time, with little appreciation of the parameters on which the required added mass coefficients may depend, its present day value is very variable.

CHAPTER 2

2. SURVEY OF LITERATURE FOR BLUFF BODIES IN UNSTEADY MOTION

Introduction.

About one hundred and fifty years ago Bessel (34), performed experiments oscillating spherical pendula in both air and water, and in order to obtain realistic results, found it necessary to consider the mass of the sphere to be apparently higher than its measured value. Bessel represented this increase in inertia by a mass equal to k times the mass of the fluid displaced by the sphere. Bessel's k values for air and water were 0.6 and 0.5 respectively.

A mathematical study of this phenomenon was undertaken by Poisson, who disregarded the viscosity of the fluids and thus considered unsteady motion through ideal fluids. He obtained k = 0.5 for a sphere.

In this way both initial theoretical and experimental studies of added masses commenced in the nineteenth century.

2.1. The Concept of Added Mass.

Milne-Thomson (6), discussed the concept of added mass using a potential flow model and showed how it arises in an ideal fluid. The argument which he presented is summarised in Section 1.1. However, this argument may be developed further to prove the presence of added mass components in each of the three dimensions, and the presence of added moments of inertia associated with rotational motion, additionally there exist other components of added mass in the form of couples between the different degrees of freedom. The mathematical

model of added mass uses a description in the form of a second order tensor associated with each added mass component in each degree of freedom. Full derivations can be found in Lamb (30) and Milne-Thomson (6).

The concept of added mass thus has a firm place in the study of ideal fluid flow. The work of Milne-Thomson in theoretical modelling of fluid flow invoked experimental studies in order to detect similar inertial effects in real fluids. Amoung others Yee Tak Yu (20), outlined an experimental method for the determination of added moments of inertia. He used a torsional pendulum, to which discs and cylinders could be attached when it was immersed in a fluid and rotated. His method was used for the determination of added moments of inertia. These were directly related to the parameters of period and amplitude which are not difficult to measure.

Sir Charles Darwin (22), studied the trajectories of fluid particles. The motion of a body through a fluid induces a "drift", in the fluid, that is, the action of a body moving through a fluid causes an amount of fluid to be displaced. Thus, after the body has passed a particular point, the fluid in the locality of that point will have shifted to a new position, further along the path of the body's motion. Darwin concluded that in an ideal fluid the volume of the fluid caused to drift in this way is equal to the volume of the added mass. This shows the close resemblance between an idealized hydrodynamic fluid as described by Milne-Thomson,

and a real fluid the behaviour of which was studied by Yee Tak Yu, and others.

The work of these and other authors, written much more recently than that of Bessel and Poisson, established inertial effects in real fluids which correspond to equivalent added masses of fluid, as predicted by potential flow. They provided strong evidence, both theoretical and empirical, in support of the concept of an added mass of fluid associated with the motion of an object through the said fluid.

Table 2.1.1. Empirical Added Mass Coefficients (41).

SHAPE	INVESTIGATOR	k_{11} (Axial)	Reynolds number	NATURE OF EXPERIMENT
Sphere	Bessel -1826	Air 0.9	-	Oscillating Pendulum
		Water 0.6	-	
	Lunnon -1928	Air & Water 0.5 - 2	10^4 -10^5	Unidirectional
	McEwan -1911	Water 0.5	-	Torsional Pendulum
	Relf & Jones - 1918	Water 0.8	-	Torsional Pendulum
	Cook - 1920	Water 0.5	10^5	Free Fall
	Frazer & Simmons 1919	Water 1 - 2	10^4	Unidirectional
Flat Plate	Gracey -1947	Air 0.94 - 0.96	-	Oscillating Pendulum
Disc	Yee Tak Yu 1942	Various Fluids 0.81		Torsional Pendulum
	Ibrahim 1965	Water 0.8	10^3	

From this table it can be seen that experimental work on added mass magnitude has been conducted by different workers over a time span of more than a century. These experiments have taken place at many research institutions and establishments, and have employed various experimental methods. When viewed as a whole these investigations indicate a lack of consistent results, as can be seen by the wide ranging values of k_{11} obtained for a sphere.

Table 2.1.2. Analytical Values of Added Mass Coefficients.

SHAPE	k_{11}	k_{22}	k_{33}	k_{44}	k_{55}	k_{66}
2-D Circ Cylinder	Varies with Length	1.0	1.0	0	-	-
Circular Disc	0	0.64	0.64	0	0.39	0.39
Elliptic Cylinder a/b	Varies					
0.25	with	4.00	0.25	1.65	-	-
0.50		2.00	0.50	0.45	-	-
2.00		0.50	2.00	0.45	-	-
4.00	Length	0.25	4.00	1.65	-	-
Sphere	0.50	0.50	0	0	0	0
Elliptic Axisym--metric Bodies a/b						
2.00	0.21	0.70	0.70	0	0.24	0.24
4.00	0.08	0.86	0.86	0	0.61	0.61
8.00	0.03	0.94	0.94	0	0.84	0.84

k_{44} = Added moment of inertia about X, associated with a coupling moment in the Y-Z plane, for which a≠b.

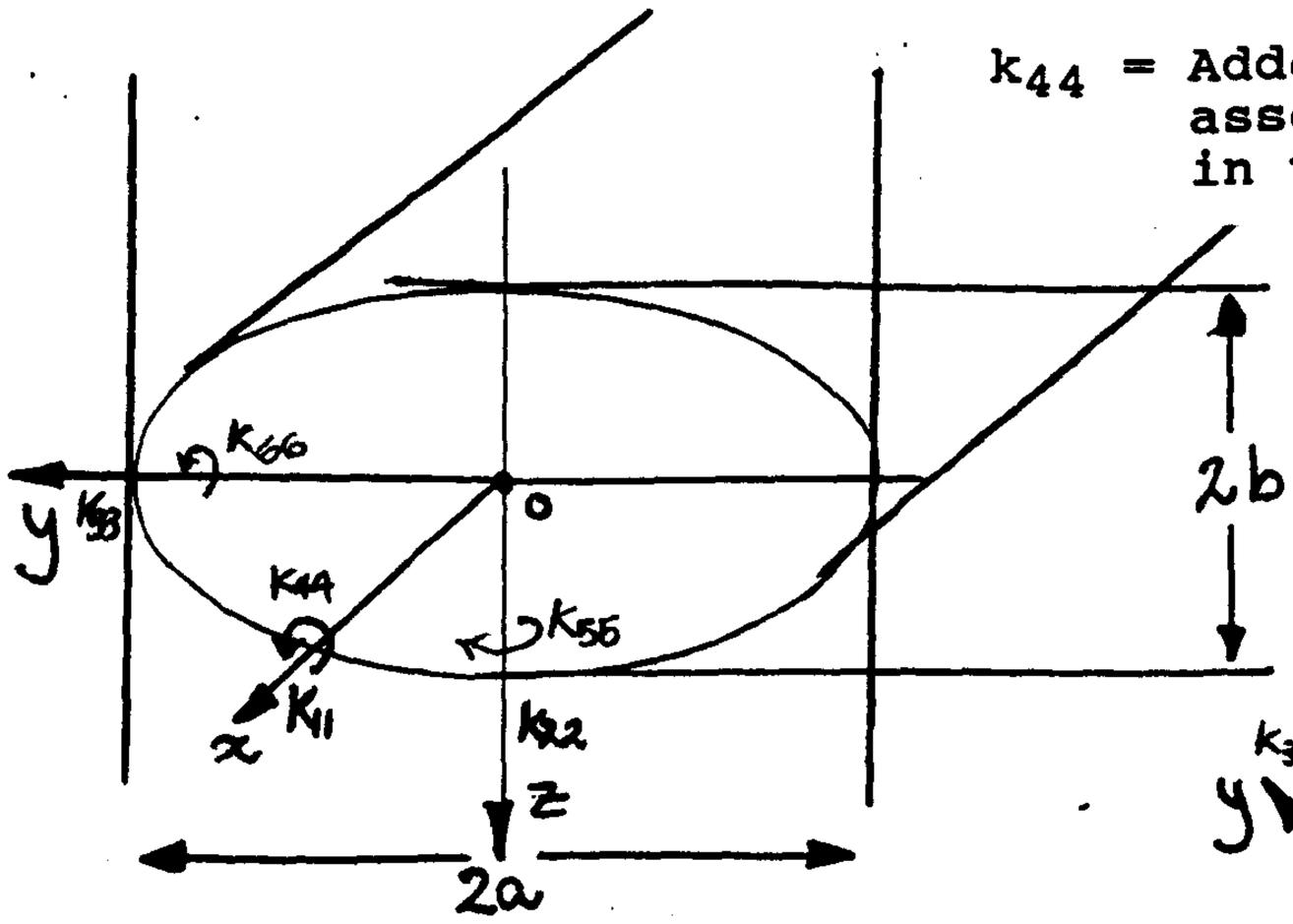

Fig I.

k_{55} =

Added moment of inertia about Z in the X-Y plane.

k_{66} =

Added moment of inertia about Y in the X-Z plane

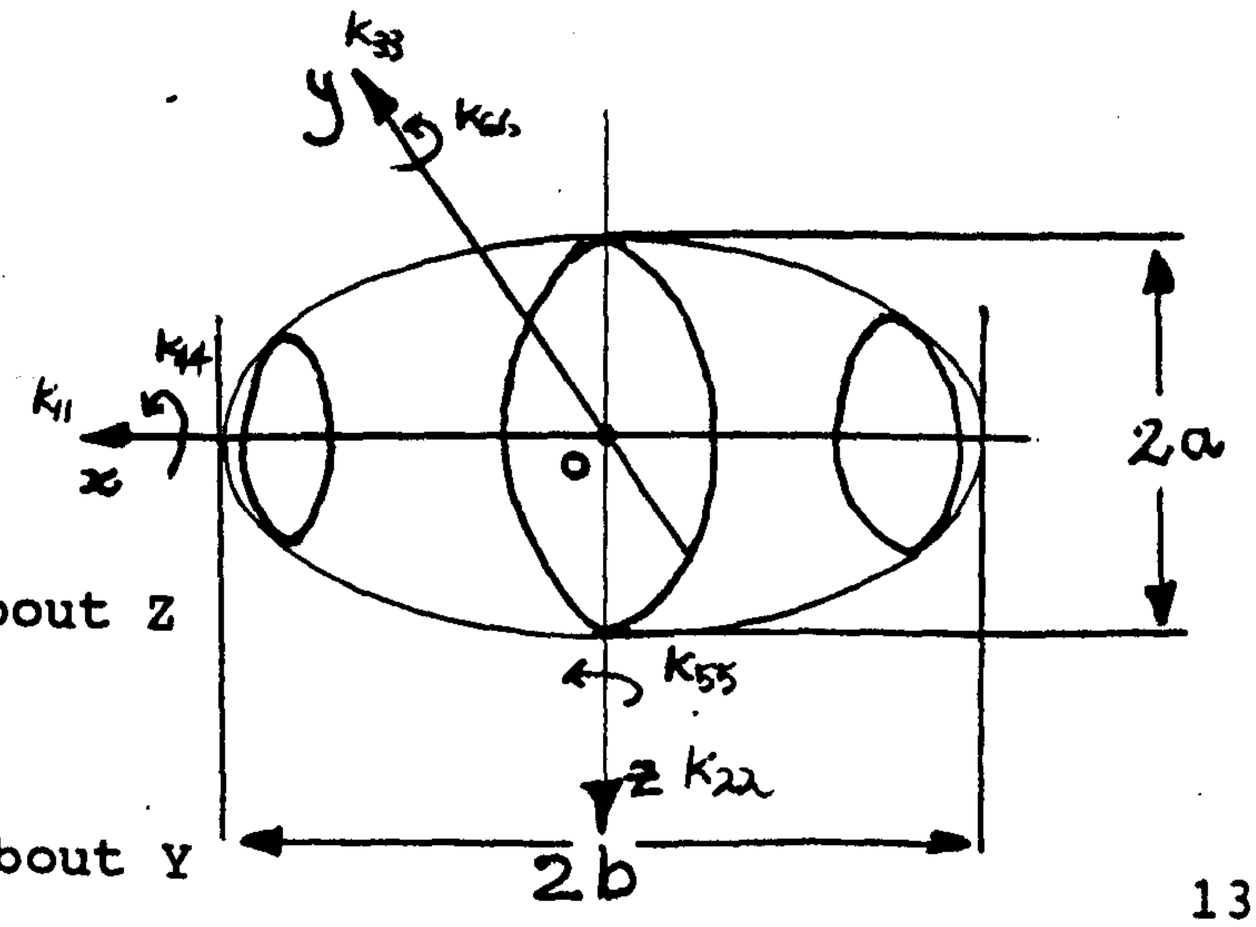

Fig. II.

2.2. Parachute Motion.

In 1944 Henn (14), published a significant work that set out the equations of motion of descending parachutes comprising canopies which were rigidly connected to their payloads. From the solutions of these equations it is possible to determine the oscillatory motion and thus the stability of the descending parachute. Henn's equations of motion indicated the influence of the added inertial effects on the motion of a descending parachute:

$$X = (m + A)\cdot\dot{u} - (m + B)\cdot v\cdot r + B\cdot s\cdot r^2 \qquad [2.1].$$

$$Y = (m + B)\cdot\dot{v} + (m + A)\cdot u\cdot r - B\cdot s\cdot\dot{r} \qquad [2.2].$$

$$N = (R + B\cdot s^2)\cdot\dot{r} - B\cdot s\cdot\dot{v} - A\cdot s\cdot u\cdot r \qquad [2.3].$$

Fig 2.1 overleaf illustrates the application of these equations to a parachute system, where: X and Y are external force components, which arise from gravitational and aerodynamic effects and are countered by the terms on the right hand side of the equations; N is the external moment in the X-Y plane; u, v, and w are translational velocity components; r is the rotational velocity component; M is the load mass; A, B, and R are added mass components in the X and Y directions and about the Z-axis respectively; s is the distance between the centre of gravity and the origin O of the coordinate system.

Fig 2.1. Henn's Coordinate System.

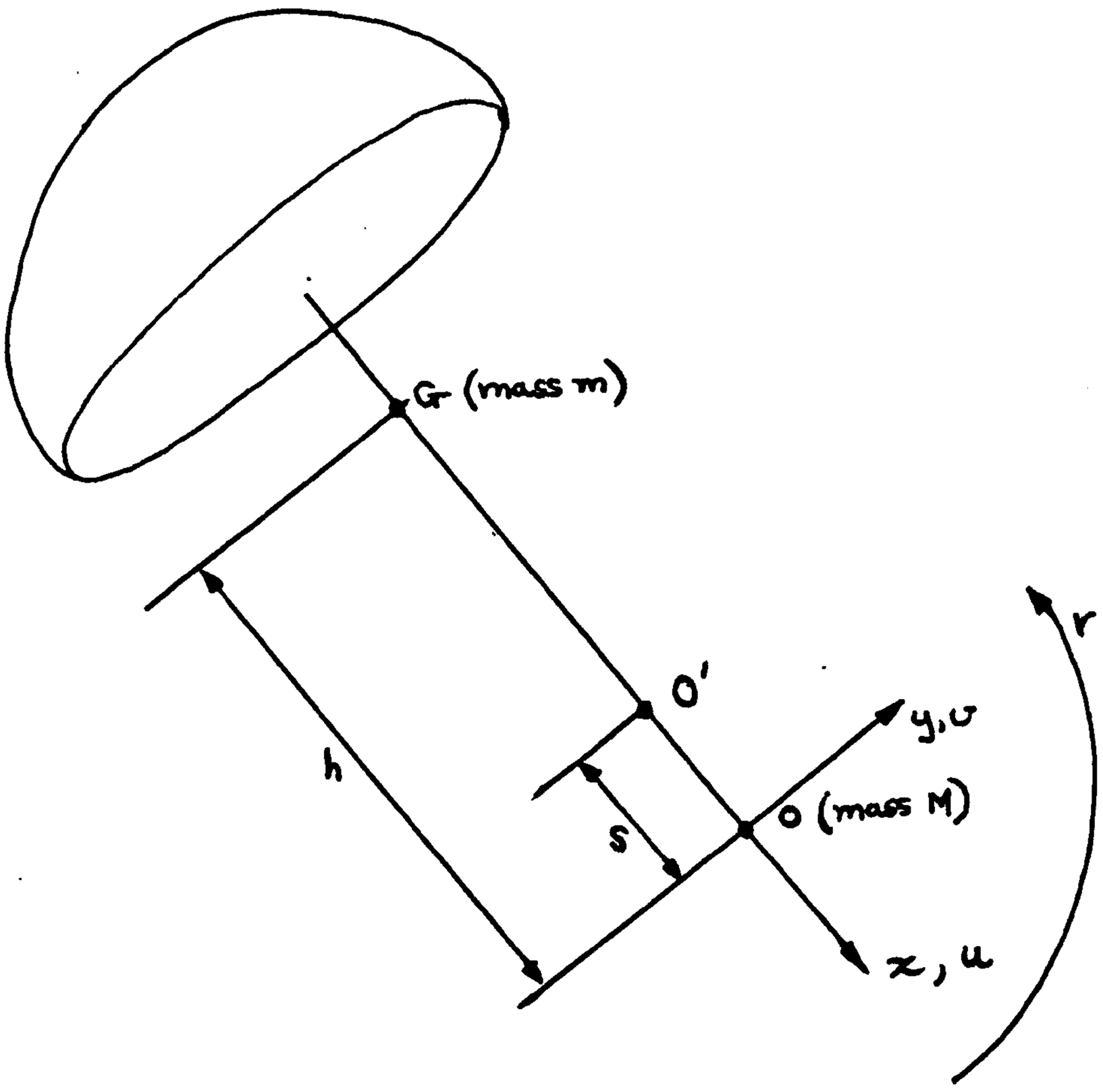

Any inertial effect for bodies immersed in fluids has to include an added mass component. Although this inertial effect may not be significant for heavier than air aircraft, a body such as a parachute is likely to have its motion influenced by the presence of an added mass of fluid because of the similarity in densities between the parachute and the air which it diplaces, as demonstrated in Chapter 1 by equations [1.2] and [1.3]. Thus, for any relationship which describes the dynamics of parachute motion, the added mass components should be included.

The equations of motion remained in the form in which they were developed by Henn until Lester (1), made a reassesment, with the object of clarifying the assumptions used in their derivation and exposing deficiencies in Henn's treatment. Referring to Lamb (30), Lester derived some new equations but made no comparisons between his mathematical model and experiment.

Lester's Equations:

$$X = (m + A)\cdot\dot{u} - (m + B)\cdot v\cdot r - (F - B\cdot s)\cdot r^2 \qquad [2.4].$$

$$Y = (m + B)\cdot\dot{v} + (m + A)\cdot u\cdot r + (F - B\cdot s)\cdot\dot{r} \qquad [2.5].$$

$$N = (R + B\cdot s^2 - 2F\cdot s)\cdot\dot{r} + (F - B\cdot s)\cdot\dot{v} - (A - B)\cdot u\cdot v + \ldots$$

$$\ldots + (F - B\cdot s)\cdot u\cdot r \qquad [2.6].$$

Where the nomenclature is the same as for Henn's equations [2.1] to [2.3]. The term F is an additional added mass term which appears in Lester's version of these equations of motion. It arises from the difference in position of the

coordinate system origin which occurs between these two systems.

These equations were developed using ideal fluid theory. Uncertainties at the time concerning the relation between added mass concepts in a real and an ideal fluid suggested that any correlation between theory and experiment might be slight. The differences that can arise in the values of added mass coefficients between theory and experiment are shown in Tables 2.1.1 and 2.1.2. Thus experimental work on the added mass of a parachute was recommended in order to assess the validity of the theoretical model. Lester came to two significant conclusions; that the equations of motion for parachutes as given by Henn were erroneous, and that since the theory, as he re-assesed it, was based on the behaviour of a model in an ideal fluid, the theoretical concept of added mass with regard to the motion of a body immersed in an ideal fluid did not necessarily describe the physical phenomena which occur in real fluids.

Lester's conclusions pointed towards a lack of knowledge concerning added mass coefficients for parachute canopies in both ideal and real fluids. This lack of knowledge prompted the work which was subsequently performed by Ibrahim (12).

2.3. Parachute Added Mass.

Ibrahim (12), modelled the potential flow around cup-shaped bodies and derived the added mass coefficients for a hemispherical shell immersed in an ideal fluid. Thus, Ibrahim modelled the deployed shape of a descending fully inflated parachute canopy, considering it to be described as a hemisphere. This potential flow model, demonstrating D'Alembert's paradox, produces no wake and develops no drag. It does provide values for the inertial coefficients but the added mass coefficients so derived may not be properly representative of those for a real fluid. Ibrahim's results therefore needed to be validated experimentally.

Further to the theoretical work covered in reference (12), Ibrahim (24) also undertook a limited programme of experimental work in order to verify his ideal fluid predictions. After the manner of Yee Tak Yu, rigid canopy models were attached to a torsional pendulum and made to oscillate in both air and water. Since the added moment of inertia in air is negligible compared with that in water, the measured periods of oscillation of this system were a means of determining the added moments of inertia of the canopies immersed in water.

Results were obtained for bodies of regular geometries such as spheres and cubes, which were compared with known theoretical results. The experimental added mass terms which assumed larger values, tended to diverge from the theoretical results. This is shown in the following figures;

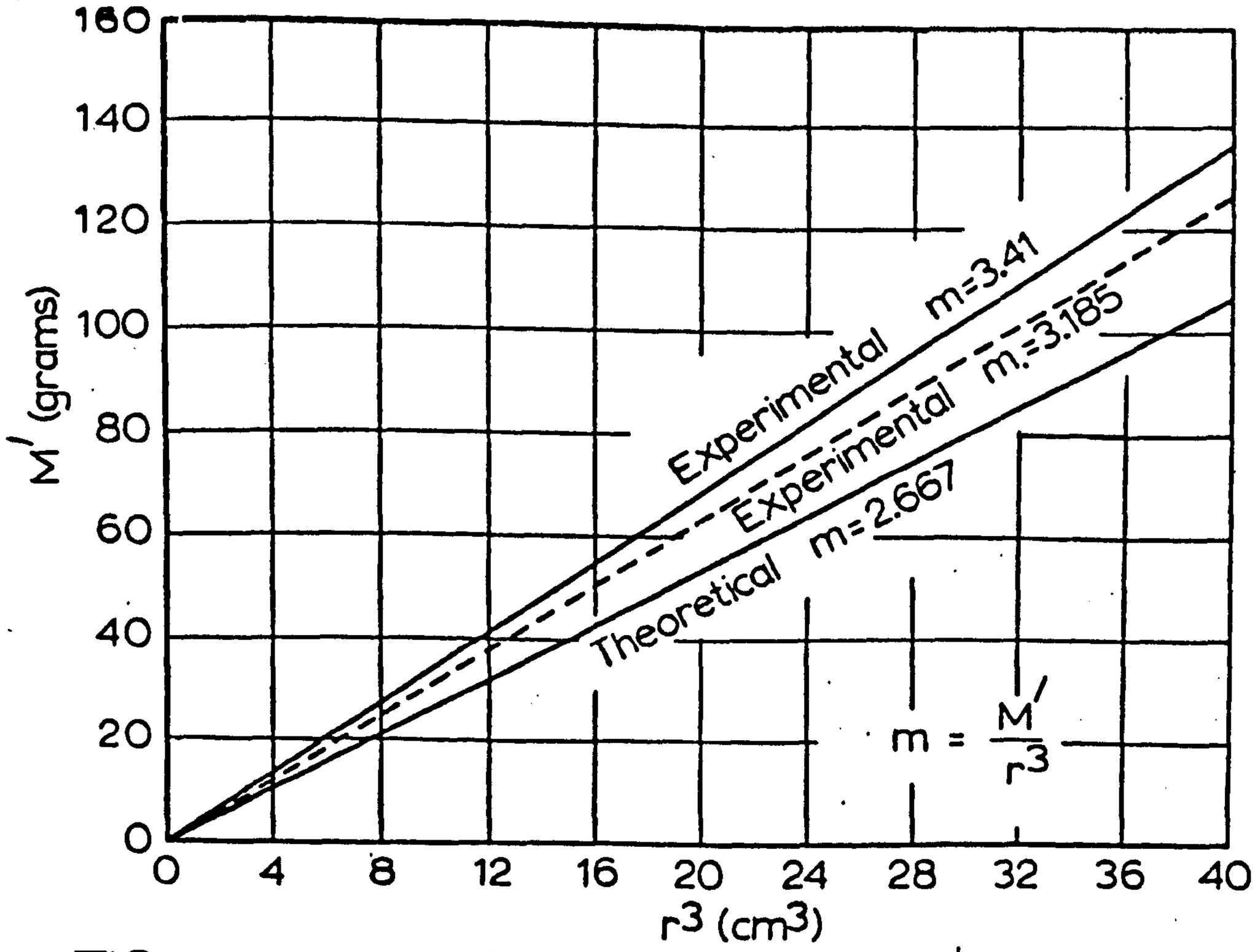

FIG 2·3·1 ADDED — MASS VERSUS RADIUS CUBED FOR CIRCULAR DISKS

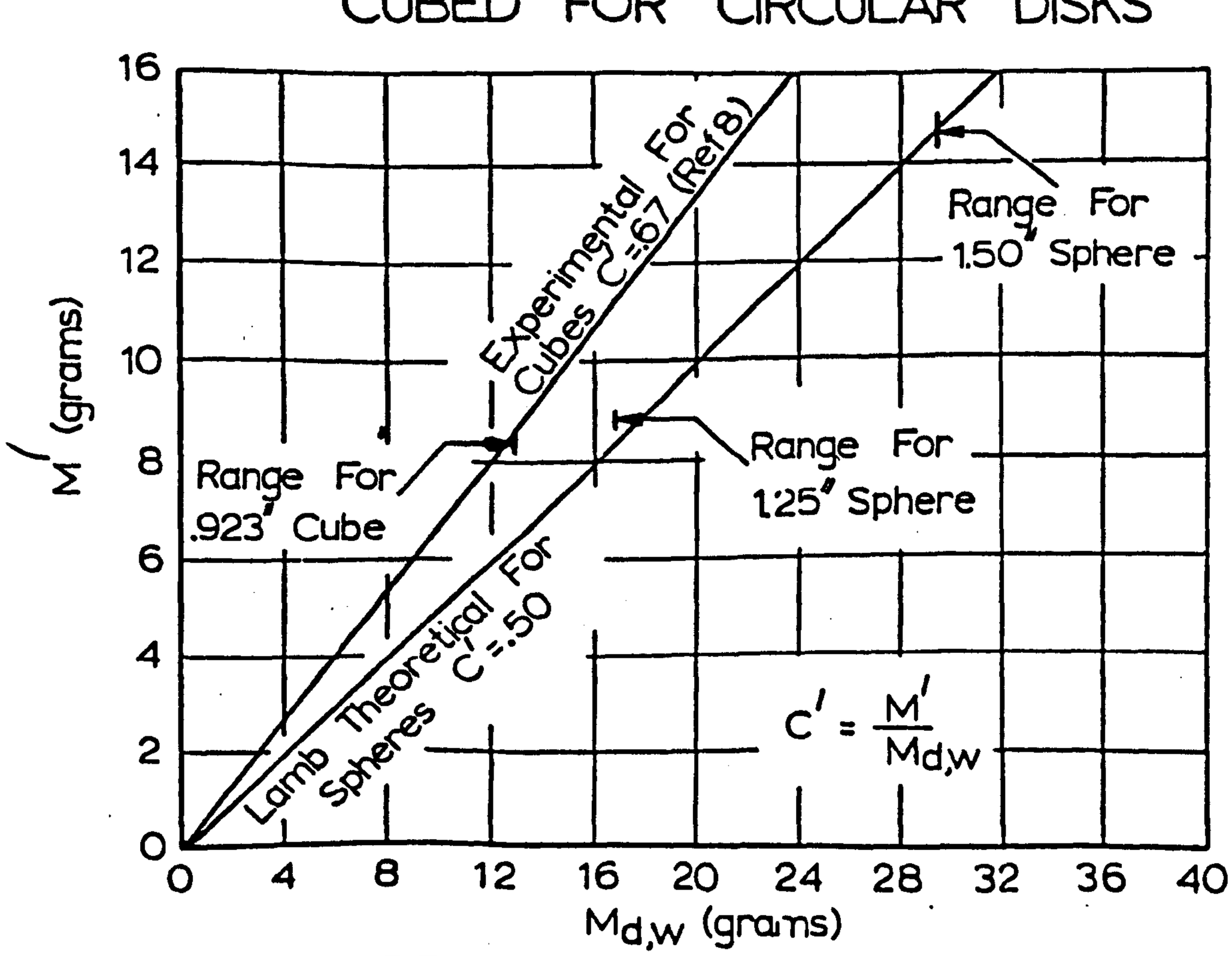

FIG 2·3·2 ADDED — MASS VERSUS DISPLACED MASS FOR SPHERES AND CUBES

Ibrahim stated that extension of the derived added moments of inertia for these rigid models to parachutes in free flight may not be possible, due the flexibility and porosity of the real parachute's cloth. It was anticipated that the added moment of inertia would be reduced with increasing fabric porosity but that flow separation would increase the added moment of inertia. Thus the significance of canopy porosity not only to the velocity-dependent aerodynamic force components but also to the added mass components, was becoming apparent.

2.4. A Mathematical Relationship For Aerodynamic Forces in Unsteady Flow.

Whilst these initial steps were being taken with the possible influence of added masses on parachute motion, in other fields of investigation work was being carried out into the nature and magnitudes of added masses in real unsteady flows. Because it models the forces acting on bluff bodies in oscillatory flow a mathematical relationship first put forward by Morison, O'Brien, Johnson, and Schaff (18), who were concerned with wave forces acting on offshore structures, is of relevance to the problem of parachute unsteady motion.

In their model the force exerted by unbroken surface waves on a pile extending upwards from the ocean floor to above the wave crest is considered to consist of two components;

(1) A drag force proportional to the square of the

velocity which may be represented in terms of a drag coefficient having substantially the same value as for steady flow.

(2) An added mass force proportional to the horizontal component of the accelerative force exerted on the mass of water displaced by the pile.

The authors concluded that the mathematical relationship, for the drag on such a bluff body in unsteady fluid flow is;

$$D = [\ (1/2)\cdot C_T\cdot \rho\cdot A\cdot V^2\ ] + [\ C_M\cdot \rho\cdot V_M\cdot dV/dt\ ] \qquad [2.7].$$

Where; D = Total Force, V = Velocity of the object relative to the flow, dV/dt = Acceleration of the object, C_T = Velocity dependent force coefficient, C_M = Inertial force coefficient, ρ = Density of fluid, A = Area of object presented to the flow, V_M = Displaced volume of fluid due to the object.

In a later paper by Morison et al (19), it was concluded that analysis of forces and piles using the relationship of equation [2.7] required the experimental determination of C_T and C_M. Unlike inviscid flow analysis, in the real flow situation the authors stated that C_M was not a constant and that C_T is not the steady-state coefficient. In this thesis the relationship set out by Morison, O'Brien, Johnson, and Schaff and expressed in equation [2.7] is referred to as Morison's equation.

Other workers have employed Morison's equation as the

basis for the determination of the velocity dependent and the inertial coefficients for a variety of bluff bodies in unsteady flow, for example; Maull and Milliner (25), studied unidirectional forces developed on a cylinder in a U-tube by oscillatory flow. Forces normal and transverse to the flow were measured as a function of time. The way in which vortices were shed from the cylinder and then formed its wake was established. Using Morison's equation they expressed for sinusoidal flow the root-mean-square value of the drag coefficient for a circular cylinder. In their experiments, conducted at Reynolds numbers of the order of the order of 4 x 10^3, the inertial force component C_M was found to be constant, taking the potential flow value of 2.0.

Although in Morison's equation the total drag force may be considered as the sum of two components; one an inertial term and one a velocity dependent term, the velocity dependent term was also found to be associated with vortex shedding from the immersed body. Since at any instant this vortex motion was found to be a function of the prior history of the flow, Morison's equation, stating aerodynamic force as a function of instantaneous velocity and instantaneous acceleration and neglecting history effects, may well be an over simplification of physical behaviour.

Sarpkaya and Isaacson (5), have described a way of modelling unsteady flow around bluff bodies such as offshore structures where the unsteadiness takes the form of wave oscillatory forces acting on such bodies in the sea. These

bodies may be the cylindrical structural members of offshore platforms such as oil rigs. The modelling process involves the determination of the average value of fluid force coefficients, using Morison's equation. The average value is taken for these coefficients because they do not have constant values but vary over the cycle. The functions of acceleration, velocity, and force are averaged over a cycle or a period, yielding averaged force coefficients.

2.5. The Keulegan-Carpenter number K_C.

An important parameter in work on oscillatory flow around bluff bodies is the Keulegan-Carpenter number K_C (32).

$$K_C = \hat{U} \cdot T/D_o$$

Where;

$\hat{U}$ = oscillatory velocity amplitude

T = oscillatory period or $2\pi/\omega$

D_o = typical system dimension.

This parameter emerged from dimensional analysis by Keulegan and Carpenter (32) as a dimensionless group on which the force acting on an object in unsteady motion would depend.

Bearman et al (31), presented measurements of the in-line and transverse loads on a small element of a vertical and horizontal cylinder in waves at Keulegan-Carpenter numbers (K_C) up to 20 and Reynolds numbers up to 5×10^5. Drag and

inertia coefficients were calculated for the vertical cylinder and Morison's equation was found to give a good fit to the measured and in-line forces.

Measurements made in random waves and in waves occuring with a constant period were found to give similar values of root-mean-square force coefficients. However, Morison's equation failed to fit the horizontal cylinder data and this was believed to be due to the presence of a strong vortex shedding component suggesting that under such conditions, constant valued velocity dependent and inertial drag coefficients might be inapplicable. The graphs shown in Fig 2.3 display the variation with Keulegan-Carpenter number of the velocity dependent and inertial coefficients which they obtained.

Although both this and Sarpkaya's investigations were concerned with the behaviour of cylinders in wave-type flow, their work deals with unsteady flow around bluff bodies and so is relavent to parachute motion. Therefore, the possible dependence of fluid dynamic forces which develop on bluff bodies on the Keulegan-Carpenter number K_C could have important consequences for the study of parachute unsteady motion.

Fig 2.3. Graphs of Keulegan-Carpenter number vs Added Mass Coefficient C_M, after Bearman et al (31).

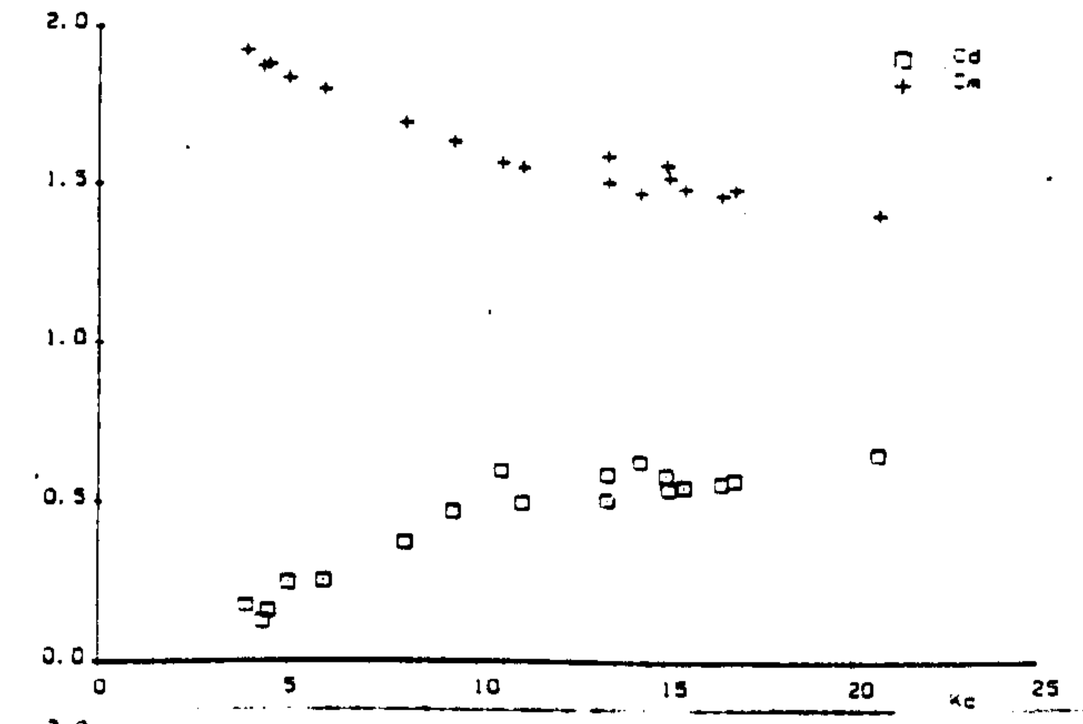

Vertical cylinder: Drag and inertia coefficients versus Keulegan Carpenter N=

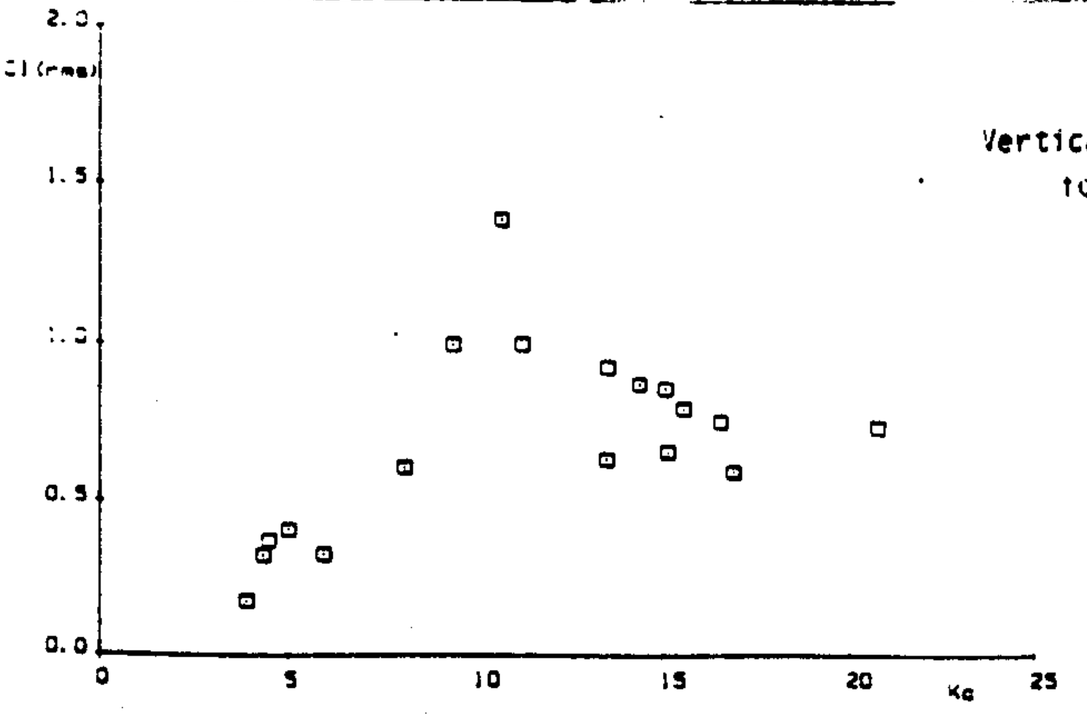

Vertical cylinder: coefficient of rms transverse force versus Keulegan Carpenter number.

2.5.1. Application to Parachute Motion.

Given a general form of Morison's equation where acceleration, velocity, and force are time dependent, and the velocity-dependent and inertial parameters may also be functions of time, then the aerodynamic force F(t) may be expressed as;

$$F(t) = a(t)\cdot v^2(t) + b(t)\cdot dV/dt.$$

Yavuz (11) used an empirical method to determine the instantaneous value of 'b' which yielded the instantaneous added mass coefficient for the parachutes being tested. This involved imposing oscillatory flow on steady motion for which it was assumed the parameter of the velocity dependent component of the total force 'a' retained its steady state value, therefore the velocity dependent force coefficient C_T would also retain its steady state value. Thus Yavuz's form of the above equation can be summarised as;

$$F(t) = a\cdot v^2(t) + b(t)\cdot dV/dt.$$

Since the equation of motion shown above can be applied to both lateral and axial oscillations knowledge of 'a' from steady-state tests yields for unsteady motion values for the steady-state components of C_T and C_N, and Yavuz's experiments thus enabled the variation with time of the added mass coefficients k_{11} and k_{33} to be determined.

In unsteady motion, the velocity dependent component of the drag may also differ from its value in steady flow and it is known that drag coefficients vary with Reynolds number which is velocity dependent. That steady state values for the velocity dependent drag coefficient are not applicable to oscillatory motion is supported by the work of Morison et al (19). In Yavuz's work all the variation in aerodynamic force in unsteady motion is assumed to be caused by modifications in the added mass and his approach may be seen as not accounting adequately for any variation in the velocity dependent force coefficients. Although it is mathematically sound there is difficulty in applying to full-scale canopies the results which he obtained because of the considerable variation with the instantaneous acceleration of these added mass coefficients .

Whilst Yavuz's advances were occuring in the empirical study of added mass coefficients, a re-appraisal of parachute motion was being made by Cockrell & Doherr (10).

2.6. A Re-Appraisal of Parachute Motion.

Cockrell and Doherr set out the problem that mathematical models of descending parachutes are subject to uncertainties in the magnitudes of the added mass and inertia coefficients. They discussed an optimizing parameter identification process which minimised the differences between the outputs from an aerodynamic force model and those from suitably devised experiments. Applying this technique to the study of

parachute descent performance formalises the processes of mathematical modelling and flight testing. In the model physical systems which are less sophisticated than the fully deployed parachute in free flight can be developed. For example, the complete analysis of a parachute's motion has to deal with translational and rotational forces, and combinations of these two. But by developing experimental methods which isolate particular forces that act on a parachute in motion, an examination of the constituent parts of the aerodynamic force can be made. However, the conclusive validation requirement of such a model is that of elaborately instrumented full scale flight tests.

This suggested some form of long term project which examined individual components of aerodynamic forces acting on a parachute model under controlled conditions. This would be followed by full-scale flight testing of a descending parachute.

Doherr and Saliaris (4), linearised the equations which Lester (1) developed, producing first-order solutions for the stability in pitch. This was done because the dynamic behaviour of full-scale parachutes is observed to be less stable than Lester's equations predicted. Two important destabilizing effects were identified, one affecting small parachute systems, the other large parachute systems.

Small parachute systems are very sensitive to stochastic aerodynamic disturbances of the airflow around the canopy. A

computer analysis of suitable static and dynamic wind tunnel tests showed that if the non-linear and the stochastic nature of aerodynamic forces were neglected, the results would be inaccurate.

On large canopies since inertia forces are volume dependent compared with velocity-dependent forces which are area dependent considerable inertia forces are developed compared to those on smaller canopies. For these larger parachutes it is essential to develop a valid mathematical model of the added mass effects, based on experiments in which the acceleration dependent aerodynamic forces are measured.

In 1984 Cockrell et al (21), discussed the significance of the added mass terms associated with parachutes in steady descent. Experiments undertaken in a ship tank were described. By the suitable choice of a coordinate system origin only two added mass coefficients were shown to be significant in Lester's equations, [2.4 - 2.6]. Using a linearised stability analysis (4) the effects caused by variation of these two coefficients were described and general conclusions drawn. These are that;

(1) k_{11} and k_{33}, the axial and lateral added mass coefficients respectively, vary with canopy shape porosity and acceleration number â. In the early stages of oscillation the acceleration number varies appreciably with time, leading to experimentally-obtained added mass coefficients which are

much larger than corresponding potential flow values.

(2) Choice of the coordinate system origin such that it is close to the canopy centre of pressure reduces the coupling added mass term 'F' in equations [2.4 - 2.6], to negligible significance, as described by Doherr and Saliaris (4).

(3) The dominant cause of varying dynamic response is the magnitude of $dC_N/d\alpha$. Only when $dC_N/d\alpha$ is small do added mass terms play a critical role in determining dynamic descent characteristics.

(4) Added mass terms do not dominate the dynamic behaviour of a descending parachute. Thus, the predictions based on the linearisation of Lester's equations are found to be valid. Therefore, a model which for small disturbances allows C_N to vary linearly the with angle of attack α, is representative of the real case.

Polpitiye (26), related the flow history of a bluff body in unsteady flow to the forces acting on the body. An empirical relationship was derived in which a time lag, τ, was introduced. Thus unlike Morison's equation, his equation of motion had three parameters which needed to be determined empirically before it could be applied;

$$F(t) = aV^2 + b \cdot dV/dt + f(t - \tau).$$

Polpitiye recommended further work to investigate the

nature of the phase lag parameter and ways in which it could possibly be applied to full scale oscillatory flow around bluff bodies.

Doherr and Saliaris (23), in a follow up to their previous work (4) concluded that added mass terms have a strong influence on the dynamic stability of parachute load systems. Appropiate experimental tests require careful mathematical modelling since added mass coefficients which are appropiate for small parachute systems appear to be less appropiate when applied to larger systems. Their work re-emphasises the need for further experimentation on parachutes with the object of finding out more about the nature of the added mass coefficients and the parameters which influence their magnitude.

Summary.

Morison's equation has been used widely in the determination of fluid dynamic force coefficients for unsteadily-moving bluff bodies. However, this model does not adequately describe bluff body motion under all conditions. It neglects flow history effects.* In addition, to determine the aerodynamic force acting on an object Morison's equation requires the determination of two parameters as in the following equation;

$$F(t) = a \cdot V^2(t) + b \cdot dV/dt(t).$$

The parameters to be determined are 'a' & 'b'. Thus there exist two unknowns for any one flow condition as described by the equation. Another relationship is necessary to derive both these parameters. One way of obtaining values of either one or other of these force parameters from acceleration, velocity, and force data is to assume that either one or the other of 'a' or 'b', is a constant. This was the approach adopted by Yavuz (11).

This is unfortunate from an engineering point of view since the parameters will need to be used both simply and effectively. For example, it may result in 'a', or 'b' being described as functions of time as Yavuz discovered with his added mass parameter. As an attempt to simplify his findings and to give Morison's equation a better theoretical basis for modelling flow, Polpitiye introduced the time lag τ but the added complexity of the expression for aerodynamic force was

*See recommendations (p.203)

not justified since values of 'a' 'b' and τ were not effectively constant over a period of oscillatory motion.

Thus it is against this background that the current investigation has been conducted. The objective is to verify Morison's equation in the case of descending parachutes and to determine the most representative values of the parameters 'a', and 'b' assuming that they remain constant over the oscillatory motion.

2.7. Research Proposals For The Current Project.

(1). To agree a range of approximately six canopy shapes whose aerodynamic and inertial characteristics will be determined in both the wind tunnel at Leicester University and the 61m long ship tank at The Southampton Institute Of Higher Education. The canopies will preferably include some whose descent characteristics are well known, together with canopies whose shapes give rise to dynamic characteristics which whilst still of interest, differ substantially from canopies previously considered.

(2). To devise and implement an experimental programme in both the wind tunnel and ship tank which will enable experimental data to be gathered both conveniently and accurately. The emphasis for this objective is on:

(a) minimisation of interference effects caused by the canopy support structure in both tunnel and tank;

(b) the effects of variation of canopy porosity;

(c) the effects of canopy forebody and determination of blockage effects of the experimental facilities due to the placement of a canopy in the flow;

(d) data processing techniques for parameter indentification to predict full scale behaviour (which as a satisfactory

mathematical model to describe unsteady bluff body motion now exists) from experimental test results;

(e) ship tank and wind tunnel flow visualisation techniques, to observe variations in both steady and unsteady flow around canopies of different shapes;

(3) interpretation of results of these experiments, updating the Leicester parachute stability prediction model, and if necessary modifying this to accomodate the results.

Footnote

In part (2), data was to be gathered both conveniently and accurately. By the term "accurately" it is implied to follow, as closely as possible, the actual motion of the parachute. The motion will therefore be that of a steady velocity onto which is superimposed oscillations, as in full scale descent. It will be useful to compare the results of such tests, i.e. drag coefficients, with the steady velocity results for the same model. It is therefore necessary for the facility to apply both oscillatory and steady state motion during tests.

The word "conveniently" implies the convenience of gathering particular added mass coefficients. Fortunately, by their nature, those added mass factors most influencing the unsteady motion are the most detectable. In this case the axial added mass coefficients k_{11} and lateral added mass coefficients k_{33} will be under investigation. It would not be convenient to try and include a facility for the

determination of a particular rotational added mass, which is presumed to have less influence on stability than say the axial or lateral added mass, since the equipment required would be more sophisticated with consequent increase in complexity and research contract cost.

CHAPTER 3

3. PARACHUTE STABILITY

Introduction

The development of ideas about added masses, and the aerodynamic drag of bodies subjected to various types of flow has been placed in both an historical and a theoretical context. The engineering application of this concept is the establishment and solution of the equations of motion for the descending parachute. An important factor governing a parachute's performance is that of stability during flight. The form which flight takes with a parachute is generally that of unsteady descent. This may be caused by gusting, the effects of canopy inflation, the position and orientation of the store or load that the parachute is carrying prior to inflation, the influence of the slipstream of the store during descent, and the possible effects of local aircraft or other bodies. To descend without undue oscillation, a parachute should exhibit good stability in pitch. Thus, pitching motion should be damped to reduce the influence of oscillatory forces on the descending parachute-store system.

This chapter aims to show the development of ideas that have concluded with the importance which added mass coefficients have to play in contemporary studies of the aerodynamic stability of parachutes. The work of Doherr & Saliaris (4), (23) is examined with an explanation of some of the concepts involved that have shaped the path of their investigation. The following analysis will demonstrate that inertia of the fluid as well as that of the body has

influence on oscillatory behaviour, therefore the importance of added mass becomes clearer. This is accomplished by linearisation of Lester's equations of motion for a parachute, and the subsequent application of Routh's criterion to determine the stability of the resulting motion as described by the result of the linearisation.

3.1. The Distinction Between Static and Dynamic Stability.

In the same sense that theories of solid body mechanics are applied to stationary rigid bodies, application of a static stability model for a parachute in pitch is an example in which the forces acting on the parachute-store system are dominated by gravity.

In static stability only the static moments acting on a parachute in steady flight when slightly disturbed from the equilibrium position are considered, based on the assumption that the linear accelerations are small, and the static forces remain in equilibrium. A parachute-store system is said to be statically stable if the static moments tend to restore the system to its equilibrium state.

Fig 3.1. States of Stability.

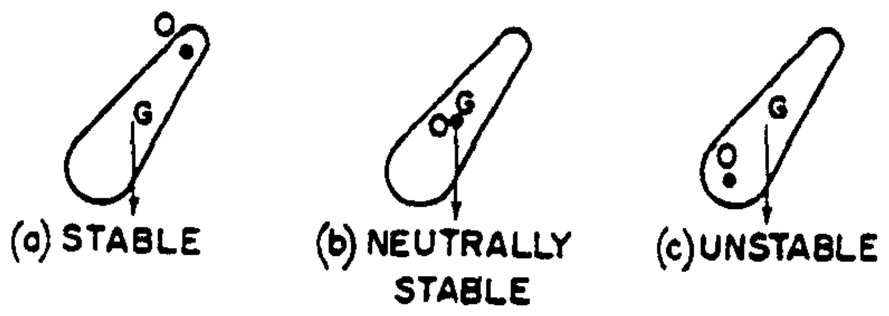

FIG. 3.1. States of stability.

Such a system is said to be stable or possess stability if, when slightly disturbed from a state of equilibrium it tends to return to and remain in that state, the disturbance only acting for a finite time. Fig 3.1 shows different states of stability which occur when the centre of gravity G is moved relative to a pivot point O.

To illustrate the concept of dynamic stability we consider the dynamic response of the system to a disturbance from the equilibrium state. The response of such a system will be encompassed by the following four categories of motion.

(i) A subsidence
(ii) Damped oscillations
(iii) A divergence
(iv) Increasing (undamped) oscillations

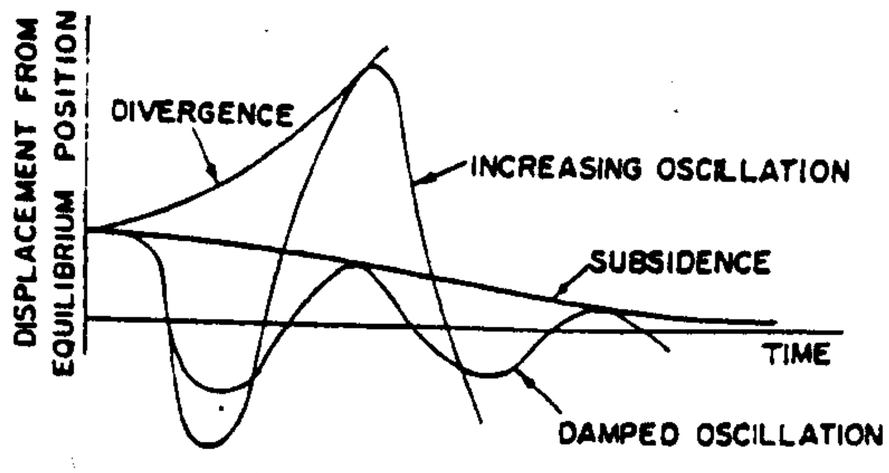

Fig 3.2. Types of Stability Response

The vertical axis in Fig 3.2 labelled "Displacement From Equilibrium Position", may refer to either a change in speed

or a change in position relative to the fixed body axes of the parachute. Thus when a parachute is subjected to, for example, a lateral gust of wind the angle of attack will be increased and the parachute-store system will start to pitch. This will result in changes in speed, accompanied by changes in the pitch angle or attitude of the parachute and store. The above graph exhibits curves representing subsidence and damped oscillatory motion. These graphs represent conditions of dynamic stability. A system is said to be dynamically unstable if it executes displacement from equilibrium represented by the curves of divergence or increasing amplitude of oscillatory motion. In divergence the parachute tends to depart continuously from its equlibrium position. Thus a divergence is a condition of both static and dynamic instability. Under conditions of subsidence, in both damped and undamped oscillations the parachute-store system tends to return to equilibrium. Hence the motions exhibit static stability. A statically unstable parachute-store system is also dynamically unstable. But it is not necessarily the case that a statically stable parachute and store is dynamically stable. The solutions to the full equations of motion are complex, but an analysis of the static stability of a parachute provides a useful first step in dealing with the problems associated with aerodynamic stability.

Since, with the exception of the Ram air (or Gliding Parachute), very little control is exerted over the motion of a parachute-store system during descent, the most desired type of parachute canopy design encompasses attributes which,

when coupled with the intended design of store to be dropped, are conducive to both dynamically and statically stable motion.

3.2. Lester's Equations.

The two-dimensional equations of motion of parachutes, comprising rigidly connected canopies and stores are described by equations which Lester (1) developed. Note the prominence of the added mass components α_{ij}. The right-handed axes O-x and O-z are fixed within the parachute and payload system, as shown in Fig 3.3.

Lester's Equations;

$$X = (m + \alpha_{11})\dot{u} + (m + \alpha_{33})qw - (mx_s - \alpha_{35})q^2 \qquad [3.1].$$

$$Z = (m + \alpha_{33})\dot{w} - (m + \alpha_{11})qu - (mx_s - \alpha_{35})\dot{q} \qquad [3.2].$$

$$M = [I_y + \alpha_{55}]\dot{q} + f(\alpha_{11} - \alpha_{33})uw - (mx_s - \alpha_{35})(\dot{w} - qu)[3.3].$$

Where; X = Total axial external force acting on the system, Z = Total lateral external force acting on the system, M = Total pitching moment about the origin O in the plane X - Z. u = system instantaneous velocity in the X direction, hence $\dot{u}$ = system instantaneous acceleration in the X direction.

Fig. 3.3. Parachute Coordinate System.

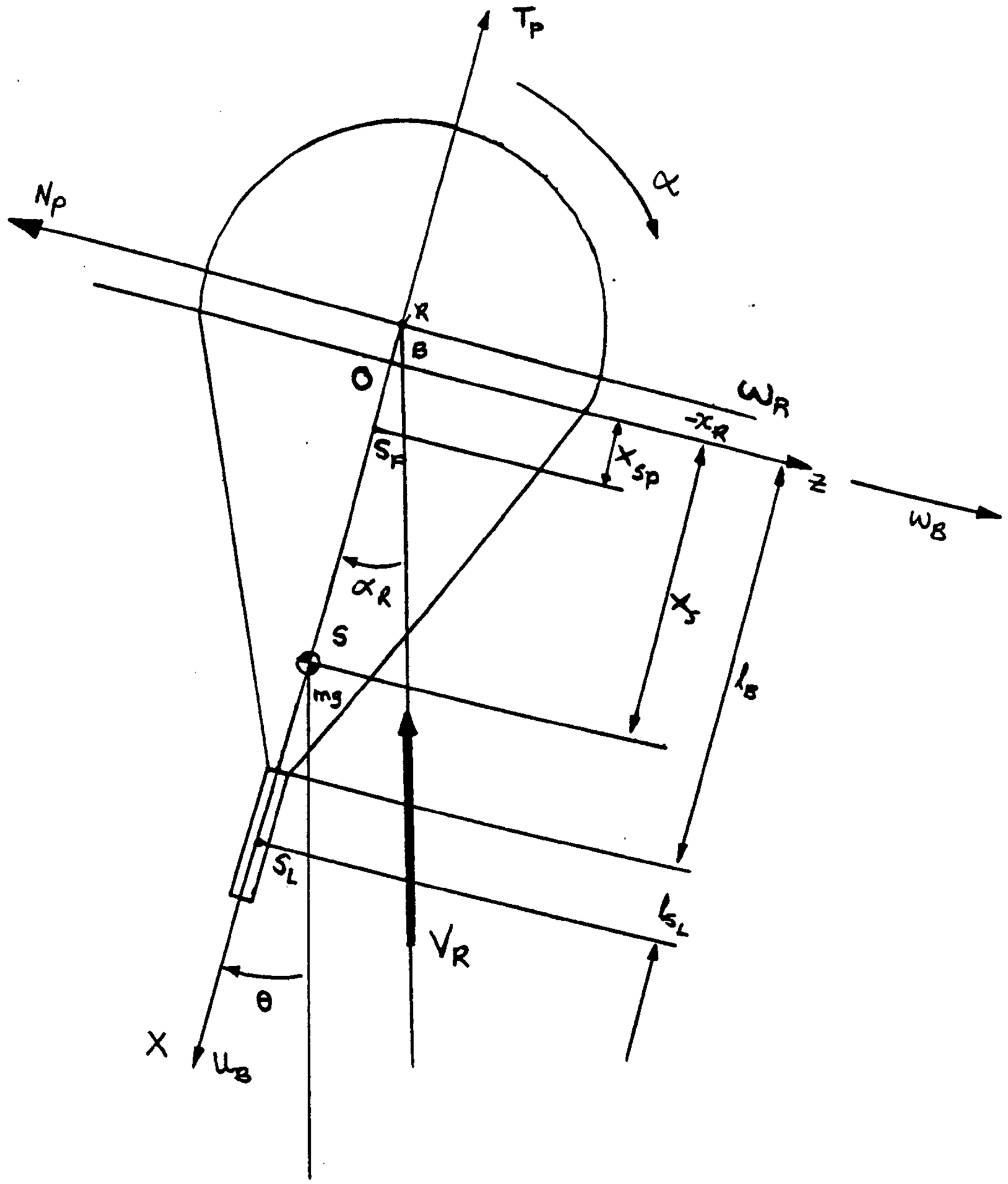

Similarly for w & q = Instantaneous velocity in the Z - direction and angular velocity about the axis O-y. I_y = moment of inertia of the system about the axis O-y, i.e. in the X - Z plane. The origin O of the parachute system axes is taken as the centroid of the representative sphere of which the parachute forms a hemisphere. R is the centre of pressure, the point through which the forces Np and Tp act.

The added mass components; α_{11}, α_{33}, are those associated with the; X - direction (Tangential) and Z - direction, (Lateral) respectively. The component α_{55} is the added moment of inertia about the Y - axis. The term α_{35} is the added mass coupling component for motion either along the Z - axis and about the Y - axis, or along the Y - axis and about the Z - axis. A full explanation of the origin of these terms is given by Cockrell and Doherr (10).

In the steady state condition i.e. at equilibrium, Doherr (43) has shown that $M = (\alpha_{11} - \alpha_{33}) \cdot u \cdot w$.

Thus when disturbed the term $(\alpha_{11} - \alpha_{33}) \cdot u \cdot v$, will no longer be present in equation 3.3.

Therefore at equilibrium all inertia terms vanish except; $(\alpha_{11} - \alpha_{33}) \cdot u \cdot w$. This term is already contained in the moment measured in steady-state in wind tunnel tests and may be cancelled by setting f = 0 in the moment equation, 3.3. The provision of this term 'f' arose from earlier disagreement about the nature of the term $(\alpha_{11} - \alpha_{33}) \cdot u \cdot w$ in equilibrium where the acceleration and rotational components of force are vanishing.

Neglecting the aerodynamic forces acting on the store, the external forces 'X' and 'Z' are written as;

$$Z = - N_p - mgSin\theta \qquad [3.4],$$

$$X = - T_p + mgCos\theta \qquad [3.5],$$

$$M = - N_p \cdot x_R - mg \cdot x_s \cdot Sin\ \theta \qquad [3.6].$$

Where; $N_p/[S_o \cdot (\rho/2) \cdot V_R^2] = C_N$, and $T_p/[S_o \cdot (\rho/2) \cdot V_R^2] = C_T$, V_R = the resultant velocity, which is at an angle α, with the parachute axis. α is the angle of attack. The expression for C_T, becomes that for C_D when the angle of attack $\alpha = 0$.

3.3. A Linearised Analysis.

By modelling the total force F acting on a parachute as a mean force F^* together with a fluctuating force $(F_a + F_s)$ writing;

$$F = F^* + (F_a + F_s),$$

where F_s is the stochastic force component, and F_a is the acceleration dependent force component. Doherr and Saliaris (4) & (23) accomplished two things; firstly a linearisation of Lester's equations of motion, and secondly a study of the stochastic nature of parachute motion. The following analysis is concerned with the first of their objectives.

3.3.1. Substitutions Employed.

Using Lester's equations Doherr and Saliaris represented the reference state corresponding to steady vertical descent by V_e. Perturbations in this motion are represented by ΔV_B, since V_B represents the velocity at the coordinate origin. To linearise Lester's equations C_N and C_T are assumed to comprise linear and constant functions of the angle of attack 'α', and 'α' is taken as equivalent to its sine and tangent values;

$$C_N = f(\alpha) \equiv [\partial C_N/\partial\alpha]\cdot\alpha = C_N'\cdot\alpha$$

and

$$C_D = \xi(\alpha) \equiv C_D' = \text{Constant.}$$

Also;

$$\tan(\alpha_R) = w_R/u_R = (w_B - qx_R)/u_B,$$
$$\tan(\alpha_B) = w_B/u_B.$$

Refering to the canopy diagram of Fig 3.3; α_B is the angle at the point B which is at O in the figure, between the parachute system axis (the X-direction), and the vector representing the resultant velocity of the components w_B and u_B. The angle α_R is the angle at the point R between the system axis and the vector representing the resultant velocity of the components w_R and u_B.

In linearising equations 3.1 to 3.6, the following substitutions are used:

$$V_B = V_e + \Delta V_B,$$

$$q = \theta', \ \dot{q} = \theta'',$$

$$u_B = (V_e + \Delta V_B)\cdot\cos(\alpha_B) \simeq V_e + \Delta V_B,$$

$$w_B = (V_e + \Delta V_B)\cdot\sin(\alpha_B) \simeq V_e\cdot\alpha_B,$$

$$\dot{u}_B = \Delta\dot{V}_B\cdot\cos(\alpha_B) - (V_e + \Delta V_B)\cdot\sin(\alpha_B)\cdot\dot{\alpha}_B \simeq \Delta\dot{V}_B,$$

$$\dot{w}_B = \Delta\dot{V}_B\cdot\sin(\alpha_B) + (V_e + \Delta V_B)\cdot\cos(\alpha_B)\cdot\dot{\alpha}_B \simeq V_e\cdot\dot{\alpha}_B,$$

$$V^2_R = (w_B - q\cdot x_R)^2 + u_B{}^2 \simeq V_e{}^2 + 2\cdot V_e\cdot\Delta V_B.$$

The normalization of time gives a dimensionless expression for time, independent of both the scale of the model and its velocity. For the model, the scaling factor l_B/V_e is chosen, where l_B is a typical length representative of the object, in this case the distance between the point B at the coordinate system origin and the rigging lines' confluence point. The term V_e is the representative velocity of the object. Therefore l_B/V_e is the time the object takes to travel a typical system dimension. By maintaining this as a value for all sizes of parachute, a time coefficient that allows easy changes of scale is obtained.

3.3.2. External Forces.

On substituting the expressions for C_N and C_T in N_p and T_p, equations [3.4] and [3.5], the external force in the Z-direction which is;

$$Z = -C_N\cdot S_o\cdot(\rho/2)\cdot V^2_R + mgSin\theta,$$

when linearised becomes;

$$Z = -C_N'\cdot S_o\cdot(\rho/2)\cdot V^2_e\cdot(\alpha_B - \theta\cdot x_R/V_e) + mg\theta \qquad [3.7].$$

For the X - direction, the external force which is;

$$X = -C_T' \cdot S_o \cdot (\rho/2) \cdot V^2_R + mg\cos\theta,$$

on linearisation becomes;

$$X = -C_T' \cdot S_o \cdot \rho \cdot V_e \cdot \Delta V_B \qquad [3.8].$$

The rotational component is M, given by;

$$M = -C_N' \cdot S_o \cdot (\rho/2) \cdot V^2_R \cdot x_R - mg \cdot x_s \cdot \sin\theta,$$

becomes;

$$M = -C_N' \cdot S_o \cdot (\rho/2) \cdot V^2_e \cdot x_R \cdot (\alpha_B - \theta \cdot x_R/V_e) - mg \cdot x_s \cdot \theta \qquad [3.9].$$

The expressions for the external forces and moments acting on the parachute canopy have now been linearised.

3.3.3. The Linearised Form of Lester's Equations.

Lester's equations can now be linearised. Refering to the substitutions in section 3.3.1. the resulting equations take the following form;

For the X-direction, from [3.1] the resulting equation of motion is;

$$\left[1 + \alpha_{33}/m\right] \cdot \alpha_B + \left[1 + \alpha_{11}/m\right] \cdot \theta' - \left[x_s/l_B - \alpha_{35}/ml_B\right] \cdot \theta'' - \ldots$$
$$\ldots - \left[\left[(C_N/C_T)(g/V^2_e)\right] \cdot \left[x_R\theta' + l_B\alpha_B\right]\right] - g \cdot l_B \cdot \theta/V^2_e = 0 \qquad [3.10].$$

For the Z - direction: linearising [3.2] the resulting equation of motion is;

$$\Delta V' + \left[2m/(m + \alpha_{11})\right] \cdot \left[gl_B/v^2_e\right] \cdot \Delta V = 0 \qquad [3.11].$$

Since α_B θ are both small their product is negligible and equation 3.11 is independent of α_{33}.

The rotational component, from [3.3] results in;

$$-\left[(x_s/l_B) - (\alpha_{35}/m\cdot l_B)\right]\cdot\alpha_B' +\ldots$$

$$\ldots+\left[\ [(\alpha_{11}-\alpha_{33})/m] - [\ (C_N/C_T)\cdot(x_R/l_B)\cdot(gl_B/V^2{}_e)\ ]\ \right]\cdot\alpha_B +..$$

$$\ldots+\left[\ [I_y(B) + \alpha_{55}(B)]/m\cdot l^2{}_B\ \right]\cdot\theta'' +\ldots$$

$$\ldots+\left[(x_s/l_B) - (\alpha_{35}/ml_B) + [(C_N/C_T)\cdot(x_R/l_B)^2\cdot(gl_B/V^2{}_e)]\right]\cdot\theta'$$

$$\ldots+\left[\ (x_s/l_B)\cdot(gl_B/V^2{}_e)\ \right]\cdot\theta = 0 \qquad [3.12].$$

3.4. Routh's Stability Criterion.

In the preceding section Lester's original equations of motion have been linearised, so that a set of equations is developed that can be examined using Routh's stability criterion. If the equations of motion for a system disturbed from equilibrium are linear or if, as in the case of the parachute, the non-linear equations are first linearised about their equilibrium value then Routh's stability criterion can be applied to them.

In the solution to the differential equations describing the motion each component will be proportional to the real part of some $\exp(\lambda t)$, where λ is the root of the auxiliary or determinental equation. If λ were real and positive, then over a period of time the component containing $\exp(\lambda t)$ would increase progressively, and this is an unstable condition. If the λ value were negative then displacement, velocity and acceleration would all be damped and the motion stable. If

the value of λ were zero, then the system would be in neutral equilibrium. Where λ is expressed in a complex form, say;

$$\lambda = \mu + i\omega,$$

then since the deviations from the equilibrium condition are proportional to $\exp(\mu t)\cdot\mathrm{Sin}(\omega t + \varepsilon)$, stability occurs for negative μ. Thus, the conditions for stability of a system are that all the real roots and all the real parts of the complex roots of the equations which describe its motion are negative. In such a case, the component;

$$\exp(\mu t)\cdot\mathrm{Sin}(\mu t + 1)$$

describes the exponential decay of sinusoidally varying motion. The differential equations are solved by use of a determinantal equation for which all the solutions need to be found. Since there are 'n' roots of a determinental equation of degree 'n' then the number of independent conditions required for complete stability is 'n'. For the present stability analysis, the complex eigenvalues;

$$\lambda_j = \sigma_j \pm i\omega_j$$

are required. The motion is dynamically stable when the real parts σ_j of these values are negative. There is a stability limit; the point of neutral stability, which occurs when $\sigma_j = 0$.

It was shown by Routh, that the conditions for complete

stability can be expressed as a set of 'n' inequalities to be satisfied by the coefficients of a determinental equation. Let the determinental equation be represented by $\Delta(\lambda)$.

Where;

$$\Delta(\lambda)=P_n\lambda^n + P_{n-1}\lambda^{n-1} + \ldots\ldots + P_1\lambda + P_o = 0.$$

Writing P_n as a positive number, then a necessary condition for stability is that all the coefficients of λ_n are positive. This is because a factorised form of $\Delta(\lambda)$ has for each λ_r a real factor $(\lambda - \lambda_r)$. For stability, all λ_r's are required to be negative. Therefore the coefficient of this real factor is positive.
1

The same argument applies to complex values of λ_r, for example; $\lambda_r = \mu_r + i\omega_r$. This gives rise to;

---

1 Illustrated by the principle of factorising Quadratic Equations.

i.e. $ax^2 + bx + c = 0$

Has solutions $x = -b \pm \sqrt{(b^2 - 4ac)/2a}$

$\therefore \left[x - (-b - \sqrt{[b^2 - 4ac]/2a}) \right]\cdot\left[x - (-b + \sqrt{[b^2 - 4ac]/2a}\right] = 0$

$\equiv (x - x_1)\cdot(x - x_2) = 0.$

Where x_1 and x_2 are required to be negative. Thus the coefficient of the other factor is positive. eg: (-(negative No) = positive No).

$$[\lambda - (\mu_r - i\omega_r)]\cdot[\lambda - (\mu_r + i\omega_r)]\cdot[\ldots]\cdot\ldots = 0.$$

Where (for stability; each ($\mu r \pm ir$) must be negative) a positive coefficient is obtained for each factor.

Given the polynomial $\Delta(\lambda)$;

$$\Delta(\lambda) = P_n\lambda_n + P_{n-1}\lambda^{n-1} + \ldots\ldots + P_1\lambda + P_o = 0$$

The following set of determinants used as test functions should be positive;

$$T_1 = P_{n-1}, \quad T_2 = \begin{vmatrix} P_{n-1} & P_n \\ P_{n-3} & P_{n-2} \end{vmatrix}, \quad T_3 = \begin{vmatrix} P_{n-1} & P_n & 0 \\ P_{n-3} & P_{n-2} & P_{n-1} \\ P_{n-5} & P_{n-4} & P_{n-3} \end{vmatrix}.$$

3.4.1. Application to the Linearised Analysis.

Returning to the stability analysis; and confining attention to the differential equations that are linear and homogenous; as in [3.10], [3.11], & [3.12],. These can be solved by appropriate choice of an exponential function. Equation [3.11] is solved by use of an integrating factor thus;

$$\Delta V = \Delta V_o \exp(\delta_1' \cdot \tau)$$

Where;

$$\delta_1' = \delta_1 l_B / V_e, \text{ and } \delta_1 = -2m\cdot g\cdot l_B/[(m + \alpha_{55})V_e^2].$$

This gives;

$$\Delta V = \Delta V_o \exp\left[-2mg\cdot l_B/[(m + \alpha_{55})\cdot V^2_e] \right]\cdot\tau \qquad [3.13].$$

Demonstrating the dependence of the exponential damping rate or decay factor on the ratio of mass/virtual mass. So, for [3.10], & [3.12]; setting:

$$\alpha = \alpha_o \cdot \exp(\lambda\tau) \quad \& \quad \theta = \theta_o \cdot \exp(\lambda\tau),$$

and substituting, gives:

$$(a_1\lambda + a_o)\cdot\alpha_o + (b_2\lambda^2 + b_1\lambda + b_o)\cdot\theta = 0 \qquad [3.14]\ ([3.12]),$$

$$(c_1\lambda + c_o)\cdot\alpha_o + (d_2\lambda^2 + d_1\lambda + d_o)\cdot\theta = 0 \qquad [3.15]\ ([3.10]).$$

Where; a_o, a_1, b_o, b_1, b_2, c_1, c_o, d_2, d_1, d_o, represent the coefficients of each λ^n, after substituting for 'θ' and 'α' in equations [3.10] & [3.12]). Equations [3.14], & [3.15] are only soluble if the determinant;

$$\begin{vmatrix} (a_1\lambda + a_o) & (b_2\lambda^2 + b_1\lambda + b_o) \\ (c_1\lambda + c_o) & (d_2\lambda^2 + d_1\lambda + d_o) \end{vmatrix} = 0,$$

or the determinant's equivalent polynomial $P(\lambda) = 0$. This is given by;

$$P(\lambda) = A_3\lambda^3 + A_2\lambda^2 + A_1\lambda + A_o = 0 \qquad [3.16].$$

Where:

$$A_3 = (a_1\cdot d_2 - b_2\cdot c_1) \equiv$$

$$\left[(m+\alpha_{33})/m\right]\left[\{I_y(B)+\alpha_{55}(B)\}/ml_B\right]-\left[(mx_s+\alpha_{35})/ml_B\right]^2\cdot\left[gl_B/V^2\right],$$

$$A_2 = (a_od_2 + a_1d_1 - b_2c_o - b_1c_1) \equiv$$

$$[C_N'/C_T]\cdot\left[Iy(B) + \alpha_{55}(B)+(m + \alpha_{33})\cdot x^2_R - 2x_R\cdot(mx_s +\alpha_{35})\right]/ml^2_B,$$

$$\ldots + [(mx_s - \alpha_{35})\cdot(\alpha_{11} - \alpha_{33})\cdot(f - 1)/m^2\cdot l_B]\cdot[V_e{}^2/g\cdot l_B].$$

$$A_1 = (a_1d_o + a_od_1 - b_1c_o - b_oc_1) \equiv$$

$$\left[(\alpha_{33}\cdot x_s - \alpha_{35})/ml_B\right] - \left[f[(\alpha_{11} - \alpha_{33})\cdot(m + \alpha_{11})]/m^2[V_e{}^2/gl_B\right] + \ldots$$

$$\ldots + [C_N/C_T]\cdot\left[[mx_s + \alpha_{35}] - [m + \alpha_{11}]\cdot x_R\right]/ml_B,$$

$$A_o = (a_od_o - b_oc_o) \equiv$$

$$[f(\alpha_{11} - \alpha_{33})/m] + [C_N/C_T]\cdot\left[(x_s - x_R)/l_B\right]\cdot gl_B/V_e{}^2.$$

The terms; $f(\alpha_{11} - \alpha_{33})$, α_{35} and α_{55} in the expressions for A_1, A_2, A_3, can be reduced to zero by an appropiate choice of coordinate system. The most suitable choice of coordinate system for a conventional parachute canopy is one in which the coordinate system origin is placed at the centre of pressure. The diagram of Fig 3.3 shows how these two points, R and B, almost coincide. The displacement in the X-direction; $-x_r$, between these points is assumed negligible.

For stability, all the coefficients; A_o, A_1, A_2, A_3, should satisfy Routh's criterion, that is;

A_o, A_1, A_2, A_3, > 0, and $(A_1A_2 - A_3A_o) > 0$.

The above equations show the significance of the term $k = C_N/C_T = [\partial C_N/\partial\alpha]\cdot[1/C_T]$, and of the added mass components α_{11} and α_{33}.

3.4.2. The Influence of $\partial C_N/\partial\alpha$ on the Stability Polynomial.

Due to its prominence in the equations, $k = C_N'/C_T$ can be separated out. To do this [3.16] is re-written as;

$$P(\lambda) = N(\lambda) + k\cdot z(\lambda)$$

$$= C_3\lambda^3 + C_2\lambda^2 + C_1\lambda + C_o + k\cdot(D_2\lambda^2 + D_1\lambda + D_o).$$

This gives a polynomial component $P(\lambda)$ which is independent of k. In the above components of $P(\lambda)$ the following substitutions apply;

$$C_3 = A_3,$$

$$C_2 = [(m\cdot x_s - \alpha_{35})\cdot(\alpha_{11} - \alpha_{33})\cdot(f - 1)]/m^2\cdot l_B\cdot[V_e^2/g\cdot l_B],$$

$$C_1 = [\alpha_{33}\cdot x_s + \alpha_{35}]/m\cdot l_B + [f(\alpha_{11}-\alpha_{33})\cdot(m+\alpha_{11})]/m^2\cdot V_e^2/gl_B,$$

$$C_o = f[\alpha_{11} - \alpha_{33}]/m,$$

$$D_2 = [I_y(B) + \alpha_{55}(B) + (m+\alpha_{33})\cdot x_R^2 - 2x_R\cdot(m\cdot x_s+\alpha_3^5)]/m\cdot l_B^2,$$

$$D_1 = [\alpha_{33}\cdot x_s + \alpha_{35} - (m + \alpha_{11})\cdot x_R + f(\alpha_{11} - \alpha_{33})\cdot x_R]/m\cdot l_B,$$

$$D_o = [x_s - x_R]\cdot g/V_e^2.$$

For $k = 0$; $P(\lambda) = N(\lambda)$. For $k \to \pm\infty$, then $P(\lambda) = Z(\lambda)$. The stability limit k^* of the motion, for which $\sigma = 0$, is obtained by setting $\lambda = i\omega$. This leads to;

$$(C_N'/C_T)^* = [\ -p \pm \sqrt{(p^2 - 4q)}\ ]/2.$$

Where;

$$p = (C_1 \cdot D_2 + D_1 \cdot C_2 - D_o \cdot C_3)/(D_1 \cdot D_2),$$
$$q = (C_1 \cdot C_2 - C_o \cdot C_3)/(D_1 \cdot D_2),$$
$$\omega^2(k^*) = C_1/C_3 + k^* \cdot D_1/D_2.$$

$P(\lambda)$ can have either three real roots or one real root and two complex roots. This is illustrated below by the stability diagram which has been produced by Doherr and Saliaris as a result of these derivations. Using a full scale personnel parachute as an example:

$$\partial C_N/\partial \alpha > 0,$$
$$\lambda_2 = \sigma_2 < 0,$$
$$\lambda_3 = \sigma_3 \pm \omega_3,$$
$$\lambda_4 = \sigma_4 \pm \omega_4.$$

The eigenvalue; λ_2 corresponds to damped aperiodic side-slip motion. The complex roots λ_3 and λ_4 correspond to oscillatory motion.

This oscillatory motion can either be damped, in which case the motion is dynamically stable, or undamped, in which case the motion is dynamically unstable. Routh's criterion is used to determine the stability state for the system.

Fig 3.4.2. Doherr and Saliaris's Stability Diagram.

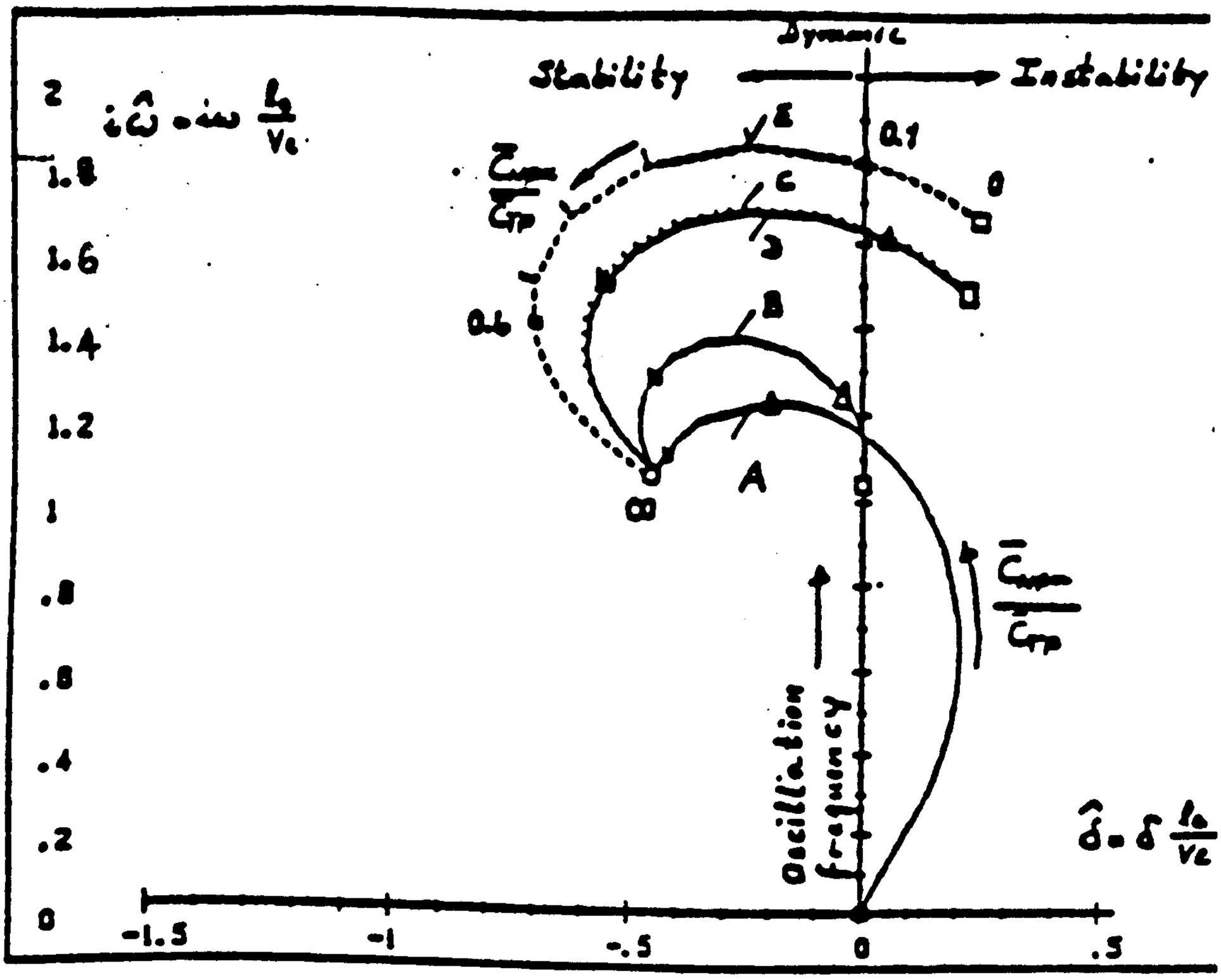

Notes for the above Diagram

The influence of the added masses indicated by their prominence in the stability coefficients A_o, A_1, A_2, A_3, in determining the stability of the parachute can be seen by their direct effect on the eigenvalues. This gives rise to the different graphs shown above. Table 3.4.2 gives the values of k_{11} and k_{33} which give rise to these different graphs.

A typical eigenvalue; $\lambda = \delta \pm i\omega$, has units of sec^{-1}. Multiplication by the factor l_B/V_e suitably changes these units for use in the complex plane. Thus, the axes have been made dimensionless, and make use of real numbers on the horizontal axis, and imaginary numbers on the vertical axis.

A large and positive C_N' or $\partial C_N/\partial\alpha$, represents a stable system, since any deviation from the equilibrium position by altering the angle of attack α is countered by a large lateral restoring force.

Table 3.4.2. Doherr and Saliaris's Added Mass Coefficient Values.

k_{ij}	A	B	C	D	E
$\alpha_{11}/(m_a)$	0.0	1.0	2.0	2.0	2.0
$\alpha_{33}/(m_a)$	0.0	1.0	1.0	1.0	1.0
$\alpha_{55}/(m_a l_B{}^2)$	0.0	0.0	0.0	0.05	0.05
$\alpha_{35}/(m_a l_B)$	0.0	0.0	0.0	0.0	-0.20

In the above table, the graphs on Fig 3.4.2 are represented by the letters A-E. The left hand column gives values of the added mass coefficients for these graphs. The coefficients k_{ij} are expressed as a measured mass α_{ij}, divided by the mass of fluid m_a contained in a representative hemispherical canopy. For α_{55} and α_{35} which are added moments of inertia, a factor of $l_B{}^2$ and l_B is placed in the denominator to give a dimensionless coefficient.

3.5. The Relevance of the Keulegan-Carpenter Number.

The linearisation of Lester's equations has demonstrated the influence added mass coefficient values k_{ij} have on parachute stability in pitching motion. The numerical values of these added mass coefficients depend on factors which are not represented in the linearised equations.

Added mass coefficients associated with parachute canopies could be assumed to be dependent on shape and Reynolds number. Thus;

$$k_{ij} = f\{ \text{Shape, Re} \} \qquad [3.17].$$

Where shape includes the canopy attitude α. Since added mass coefficients are detectable through inertial effects, the size of which are dependent on the strength of an oscillation, it is conceivable that added mass coefficients are also dependent on a dimensionless oscillation parameter, such as the Keulegan-Carpenter number, see Chapter 2.

Dimensional analysis for an object in unsteady fluid motion identifies certain groups of variables by a method known as the Buckingham-Pi theorem, Fox & Macdonald (40). The work of Keulegan and Carpenter (32) considers this oscillational parameter to be the Keulegan-Carpenter number K_C, where;

$$K_C = \hat{U} \cdot T/l \qquad [3.18].$$

Subsequently other workers such as Bearman et al (7), have verified that K_C influences the size of k_{ij}. The effects of varying K_C have also been discussed by Sarpkaya and Isaacson (5), from the study of wave forces which impinge on offshore structures. In this reference, one of the conclusions is that the size of added mass coefficients is influenced by the strength of an oscillation as determined by the value of K_C. So for oscillatory motion the dimensional expression of [3.17] is re-written;

$$k_{ij} = f\{\text{shape, Re, } K_C, \alpha\} \qquad [3.19].$$

Summary

Assuming Lester's equations are adequate to describe the motion of a parachute through a real fluid, the development of this model has demonstrated the influence of the static stability coefficient $\partial C_N/\partial\alpha$, and the added mass coefficients k_{11} and k_{33}, on the stability and hence the performance of a descending parachute. The need for experimental data to determine the numerical values of these coefficients and thus to identify an appropiate mathematical model has been emphasised by Doherr and Saliaris (4), (23). The work of Bearman (31), as well as Sarpkaya and Isaacson (5), has shown how the added mass coefficients vary with the oscillational Keulegan-Carpenter parameter for bluff bodies in real unsteady flow.

In addition to the work of those authors mentioned above the dimensional argument of section 3.5 emphasises the importance of extending these latter ideas to parachute canopies. Thus the remaining chapters of this report describe the experimental programme to determine how the added mass coefficients vary over a range of Keulegan-Carpenter numbers and how they may be influenced by this oscillational parameter for a variety of parachute canopy shapes.

CHAPTER 4

4. APPARATUS AND EXPERIMENTAL PROCEDURE

Introduction

The use of full scale parachute canopies can present problems in attempting to find and classify inertial effects and to determine the behaviour of force coefficients. Such problems arise for three main reasons; control of both the canopy under investigation and the surrounding environment, instrumentation and cost. Given particular aspects of parachute motion to be investigated which, in this case, depend on the inertial and velocity dependent drag coefficients, ideally experimentation should take place in a controlled environment. This allows greater control over the motion of the canopy permitting measurement of the instantaneous angle of attack. It results in less in time spent testing and in less cost than would be necessary for full scale experimentation. However in order to satisfy the functional expressions for aerodynamic and inertial forces, the conditions under which such testing is carried out should be similar to those for full scale, for example; similarity of angles of attack, of Reynolds number and of Keulegan-Carpenter number.

4.1. Apparatus Criteria.

The requirements for the equipment are that it should permit a standard of performance at which the data gained during testing, and subsequently employed for analysis, will be useful and relavent to the achievement of the objectives

set out in Chapter 2.

Parachutes undergoing steady descent execute an additional oscillatory pitching motion. The acceleration component of this motion as set out in Morison's equation will be influenced by the value of the added mass coefficient which itself is dependent upon factors such as the Keulegan-Carpenter number. The work of Sarpkaya and Isaacson (5) demonstrates that the added mass coefficients are influenced by the size of the unsteady component of the motion as defined by the Keulegan-Carpenter number. Thus, to investigate the nature of parachute added mass in unsteady motion, a series of simple harmonic motion oscillations imposed on the canopy provide a range of conditions of motion similar to the full scale case and thus appropiate for determining added mass coefficients over a range of Keulegan-Carpenter (K_C) numbers and angles of attack.

Generally, during full scale parachute descent, the parachute and its attached store oscillate and as such may be observed to follow an arc type of movement. Under these conditions the store swings as a pendulum underneath the canopy. The rotational symmetry of a typical conventional canopy shape allows the simplifying assumption that such oscillations occur in two dimensions. Therefore it may be assumed such arc type oscillations of a full scale descending parachute consist of two components of unsteady motion; one in the lateral direction and one in the axial direction. In addition to the movement of a parachute in this way it has

been shown by Cockrell et al (21), that under certain conditions; where it may be assumed that the origin of the body axes is coincident with the centre of pressure, the two most influential added mass coefficients relavent to a parachute's motion are the axial coefficient, k_{11}, and the lateral coefficient, k_{33}.

In attempting to investigate k_{11} and k_{33}, it is not a requirement that these arc type oscillations need be strictly modelled. To determine the nature of the added mass coefficients for these two component directions sufficient conditions are provided by imposing axial and lateral oscillations independently. The apparatus therefore has the facility for imposing simple harmonic motion on the canopy under test in either the axial or the lateral direction.

As stated in Chapter 3, it is assumed the added mass coefficients k_{ij}, for the canopy are dependent on a number of variables such as; canopy shape, Reynolds number, Keulegan - Carpenter number K_C, and angle of attack α. Thus;

$$k_{ij} = f\{ \text{Shape}, \text{Re}, K_C, \alpha \} \qquad [4.1].$$

The apparatus therefore, has the facility for easy variation of oscillatory amplitudes, frequencies, and the angle of attack. These variables also affect the velocity-dependent aerodynamic force coefficients; C_D in the axial direction and C_N in the lateral direction. The variables on which the added mass coefficients k_{ij} depend are

directly related to the oscillatory motion which during testing is imposed upon the steady forward motion. For steady state testing only the constant forward velocity of the parachute canopy is considered, so the mechanism which imparts the oscillatory motion is not used. In this case the coefficients to be gained from subsequent analysis are the velocity dependent drag coefficient C_T (C_D at $\alpha = 0°$), and the coefficient of the lateral aerodynamic force C_N. This is obtained at discrete angles of attack and thus yields $\partial C_N/\partial\alpha$ at the equilibrium angle of attack, this being the static stability coefficient in pitch.

4.2. The Ship Tank.

A ship testing tank containing still water as used for the testing of ship models, provides a facility which from the above standpoints is well suited for testing parachute models.

4.2.1. Advantages.

The advantages of employing the ship tank facility are;

(i) Control of Environmental Factors.

Conditions within the tank help to achieve this more readily than in the atmosphere, or even in a wind tunnel. Atmospheric tests are highly susceptible to air currents and random gusting. The assumption that the atmosphere through which the parachute is descending may be still, is an over

simplification since gusting can change a canopy's shape and its angle of attack, thus altering the aerodynamic forces developed on it. For a wind tunnel, the presence of turbulence and unsteadiness due to the fan driving the air also affect the flow past the canopy, thus introducing uncertainties in the measured forces. The water in a ship tank is static and these uncertainties are avoided. Also its density results in much greater forces than those which are developed in air at the same velocity for a given size of canopy.

(ii) Control of the Canopy.

When using the ship tank, the canopy model under test can be towed through the water at a predetermined, constant velocity and at any required angle of attack. The facility to repeat ship tank tests is also advantageous for testing the validity of a particular experimental procedure, or if a particular test run should be aborted due to such problems as bad inflation or rigging line entanglement.

Instrumentation is easier to implement when control over both the environment, and the canopy geometry is accomplished. A parachute descending through the atmosphere will execute both rotational and translational unsteady motion about a trajectory relative to earth bound axes. Although this can be detected from the ground, there is considerable difficulty in measuring simultaneously the instantaneous motion of the canopy relative to the parachute's body axes and the instantaneous aerodynamic

forces which are developed. For the execution of tests in the ship tank an instrumented mounting or sting was used to locate the flying position of the canopy, and since it also carried strain gauges and an accelerometer, measurements of both forces and accelerations relative to the parachute body axes were made.

(iii)

There are also economic advantages in the use of a ship tank. An air launched test facility, for example an aircraft, taking off and landing for a limited number of parachute drops, is not required. With the ship tank there is no great mass of fluid to be set in motion and driven as there is with a wind tunnel. The energy required to accelerate and drive the towing carriage which supports the model is likely to be far less than that which would be required to accelerate and drive the water contained within the ship tank, at an equivalent velocity. Since the ship tank contains water whose density is three orders of magnitude greater than that of air, inertial forces are much easier to measure than they would be in air due to their dependence on the density of the medium.

(iv) Advantages in Test Facility Scale

The particular ship tank used has a large cross-sectional area of 1.83 x 3.66 m^2. Access to a similar size wind tunnel facility, in which for the size of the model under test the blockage constraints are so small, is limited.

4.2.2. Disadvantages.

When considering the constraints of any test facility such as a water tank compared to the free atmosphere, some disadvantages are apparent. Two disadvantages of the ship tank are the blockage which its walls impose on the flow around the parachute canopies and the constraint imposed by the presence of its free surface, see reference 42. Also the porosity of a parachute canopy in water will be different from its corresponding value in air.

(i) Blockage.

When a model is tested in a bounded zone of finite dimensions such as a wind tunnel or a water tank, due to the area it presents perpendicular to the flow, the model effectively reduces the cross sectional area of this bounded zone. The presence of the bounds to this zone affects the shape of the streamlines produced by the model at and near to these bounds. In the case of the ship tank such a zone is bounded by its walls and by the free water surface. This results in the local velocity at points around the body being higher than it would be if the ship tank were unbounded.

This effect causes aerodynamic forces which are larger than they would be in the free atmosphere. The velocity of the towing carriage as measured over a timed distance does not correctly describe the flow velocity about the object in the presence of blockage. Therefore when the towing carriage

velocity is used to obtain parameters such as the Reynolds number R_e, and the velocity dependent force coefficient C_D corrections must be made to the values obtained.

The inconsistencies due to the channel boundary interfering with the flow around the body are known as blockage effects. For a bluff body such as a parachute canopy, according to Maskell (28), blockage effects become significant when the test model blocks the testing section of a tunnel or tank by approximately 5% of that section's cross sectional area. Maskell's equations for correcting C_T or C_D values, as expressed by Cockrell (41), are;

$$\Delta C_D/C_D = -2.77 \cdot C_D \cdot S_p/A \qquad [4.2].$$

$$C_D^* = C_D - \Delta C_D \qquad [4.3].$$

Where: C_D^* = the corrected value for C_D; C_D = the measured velocity dependent force coefficient at $\alpha = 0°$; ΔC_D = the correction factor applied to C_D; A = the cross-sectional area of the test section of the ship tank; S_p = the Canopy projected area.

The first batch of tests performed in April 1986 was made with canopies that characteristically blocked the water tank by approximately 1% of its cross-sectional area. The second batch of tests were performed in April 1987 with canopies which blocked the cross-sectional area of the ship tank by approximately 4 %. The final series of tests in January 1988

was performed with two sets of canopies, both large and small, having the same specifications as those used in the earlier 1986 and 1987 tests.

No blockage correction was applied to the smaller set of canopies used during these tests. According to Maskell's criterion shown in equations 4.2 and 4.3, correction for blockage of the results obtained is unnecessary since they only blocked the tank by approximately 1% of its cross-sectional area. However, the aerodyamic drag coefficient values (C_D), for the large set of canopy models, in both steady and unsteady flow have been corrected.

(ii) Free Surface Effects.

The tests performed in the ship tank were conducted at a depth below the water surface of approximately 720mm, this being the depth measured from the axis of the parachute up to the water surface. The water surface in the tank presents a free surface, giving rise to surface waves generated from flow around the submerged canopy. Proximity of the free surface to a test model can result in an incorrect interpretation of the data, if the data is analysed assuming the effect of an unbounded or infinite fluid. According to Srokosz (29), the depth at which the effect of a free surface significantly changes the added mass coefficient from that value expected in an infinite fluid is when the ratio of the radius of a submerged body, to the depth at which it is submerged is greater than a given ratio. For a sphere the ratio quoted is 1/3, but no appreciable change is experienced

until the ratio is greater than 1/2. Thus, using Srokosz'z model and assuming the flow around the inflated hemispherical parachute canopy is comparable to that of a sphere the ratios in these tests ranged from 1/4 in the case of the small canopy models, to 1/2 in the case of the large canopy models. The relative sizes, in terms of D_o, compared to the depth at which canopies were flown in the tests considered presents no difficulty in the determination of the added mass coefficients with regard to the ship tank free surface effect.

4.2.3. Specifications.

Tests were conducted at the ship tank at The Southampton Institute Of Higher Education, Southampton, England. The tank measures 61m in length, with a cross sectional area of 3.66m x 1.83m. A railway guided towing carriage is situated above the tank. This experimental platform from which the tests were conducted was essentially similar to that used for earlier parachute experiments, and a full description of this test facility is given by Yavuz (11).

4.3. The Test Sting.

This is used for mounting the parachute canopy in a flying orientation within the tank. Any force experienced by the parachute during a test run produces a bending moment acting on the sting. The strain gauges which are firmly attached to the body of the sting are deformed by these moments and these deformations change the resistance of the gauges. Since the strain gauges form parts of bridge circuits, any changes in their output voltages can be amplified and recorded, in both analogue and digital form. The changes in output voltages from the bridge circuit are first amplified, then passed to both an analogue recorder, and an analogue to digital (A/D) converter. The analogue recorder produces a chart recording. The output from the A/D converter is passed via the microprocessor to a disc file.

The test sting is illustrated in Figs 4.1.(a) and (b). It is constructed of 32mm diameter steel tube. The vertical member measures 940mm in length, and the horizontal member 296mm in length. To prevent fluid dynamic forces being developed on the sting's vertical member it is enclosed within an aluminium shroud the diameter of which is 64mm. Thus the bending moments developed on the sting are caused wholly by the aerodynamic and inertia forces developed on the model canopies which are attached to the sting.

4.3.1. Calibration Procedure.

The strain gauged force channels for the sting were calibrated by attaching weights to the end of the horizontal member. The range of forces and moments over which the calibrations were conducted are:

Tangent channels I & II; 0 → +90 Newtons.

Normal channels I & II; -60 → +60 Newtons.

Moment channels I & II; -12 → +12 Newton-metres.

A computer program was written for the purpose of calibrating the sting. The output from the strain gauges was first amplified and then passed to the computer. The value in Newtons, of the weight hung from the sting for a particular strain gauge output was also entered into the computer via its keyboard. This procedure was followed for each particular weight hung from the sting. The following diagram shows the schematic plan for the strain gauges which were attached to

the sting.

Fig. 4.1.(a). Coordinate System for Strain Gauges.

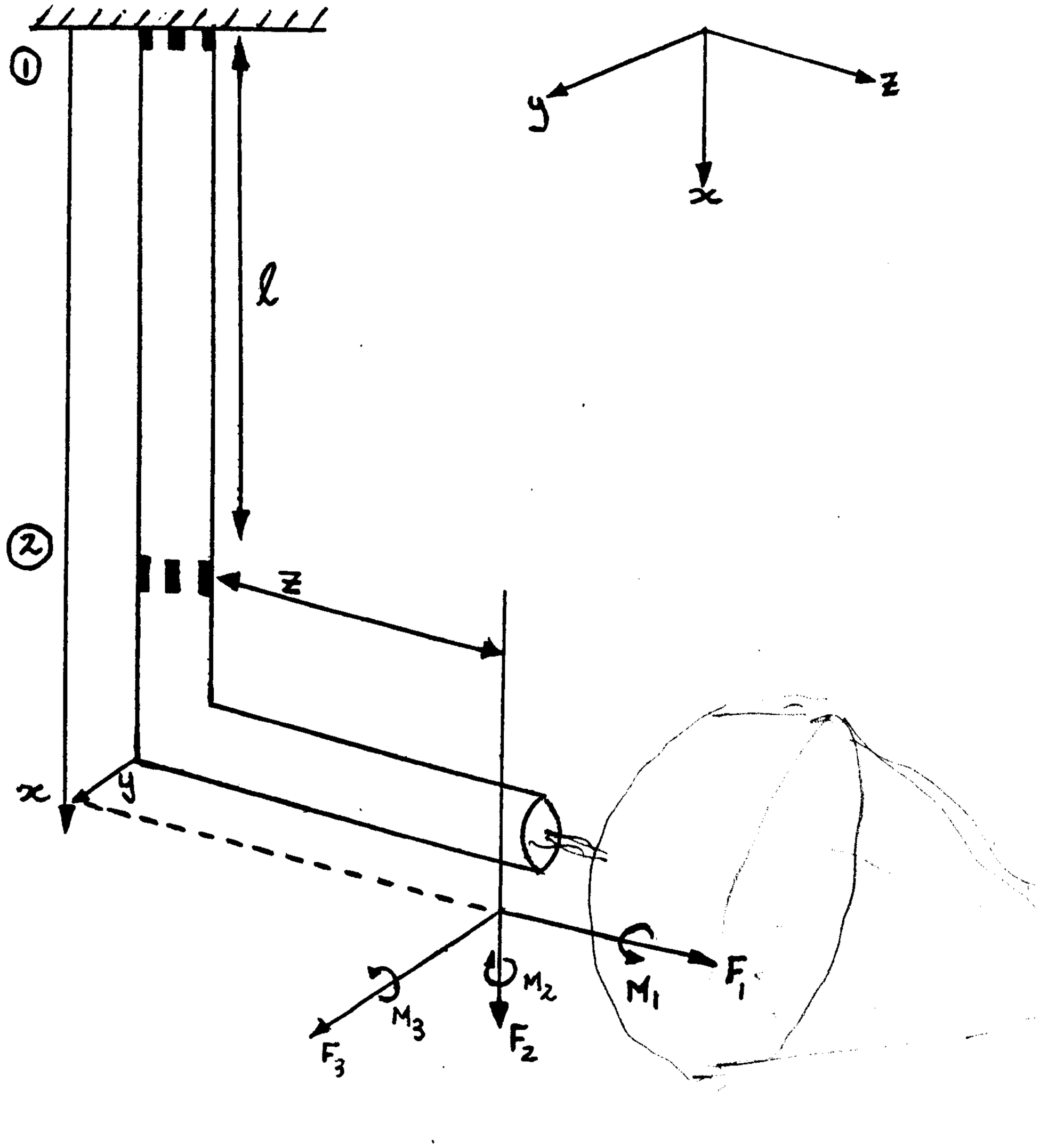

Fig. 4.1.(b). Sting and Shroud Assembly.

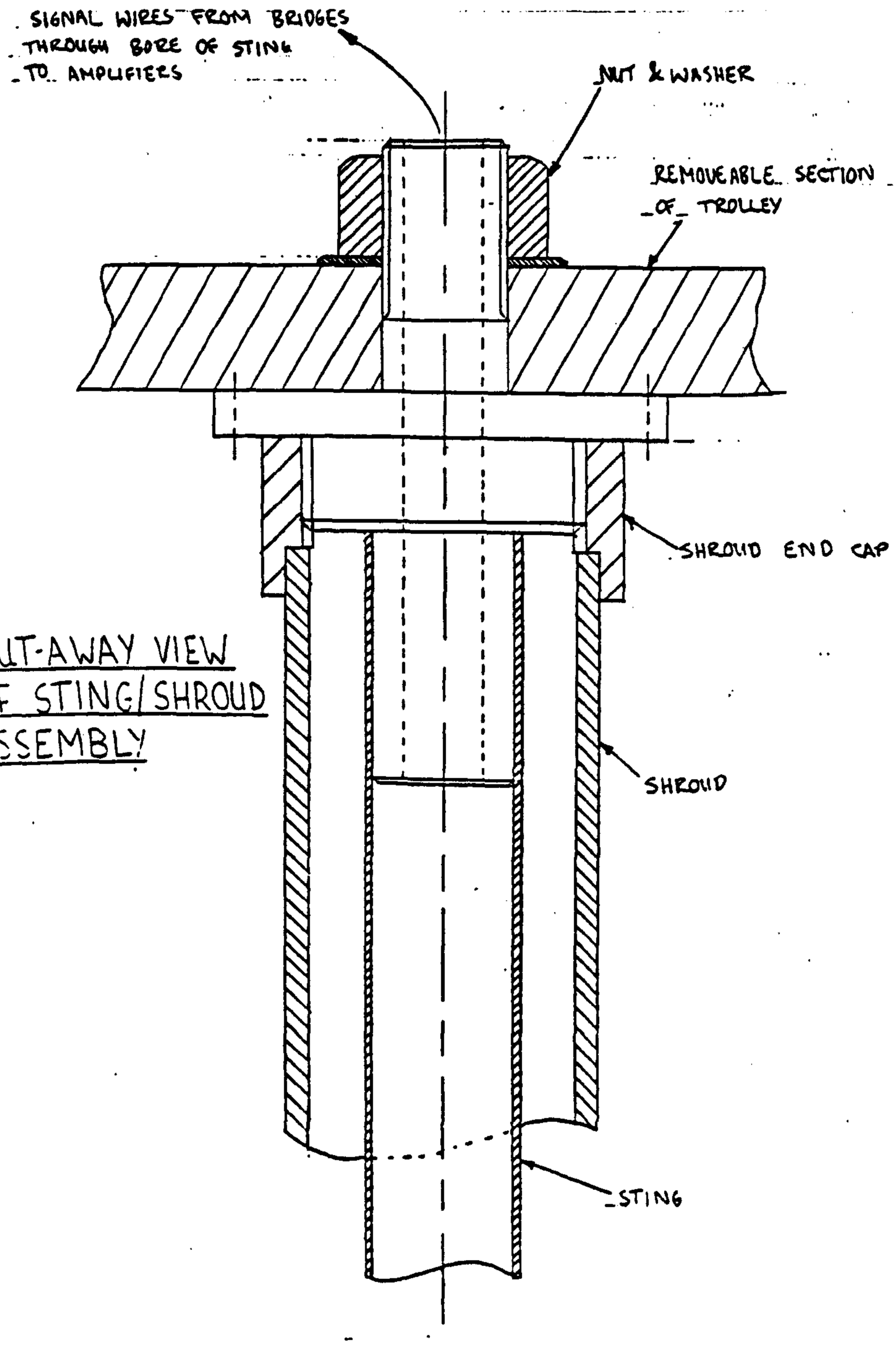

CUT-AWAY VIEW OF STING/SHROUD ASSEMBLY

Referring to Fig 4.1, the two strain gauge stations, indicated by positions 1 and 2, can measure moments about the X, Y, Z axes. Thus for the top set of strain gauges at position 1:

$$M_y = F_1 \cdot x - F_2 \cdot z + M_3 = \text{Moment about the Y-axis},$$
$$M_z = F_2 \cdot y - F_3 \cdot x + M_1 = \text{Moment about the Z-axis},$$
$$M_x = F_3 \cdot z - F_1 \cdot y + M_2 = \text{Moment about the X-axis}.$$

For the bottom set of strain gauges at position 2:

$$m_y = F_1 \cdot (x - 1) - F_2 \cdot z + M_3,$$
$$m_z = F_2 \cdot y - F_3 \cdot (x - 1) + M_1,$$
$$m_x = F_3 \cdot z - F_1 \cdot y + M_2.$$

For the purposes of this analysis torque and moment have the same effect, and may be measured at any height. Thus, M_x the moment about the X-axis at the top strain gauge station is equal to m_x, the moment as measured from the bottom strain gauge station.

Generally torque and moment may be distinguished as dynamic and static representations respectively, of the same phenomenon.

The origin of the coordinate system may be placed at any point; x, y, and z indicate displacements parallel to their respective directions. The displacement 'y' from the end of the sting is required, to account for forces and moments arising at a point away from the axis of the parachute

system, for example forces caused by vortex shedding from the canopy hemline.

During the calibration process of hanging the weights, the computer program provided a graphic display of force versus strain gauge output on the terminal screen. For this graphic display the horizontal axis had units in Newtons for the range of forces as entered from the keyboard, and the vertical axis had units indicating the 'count', which represents the value assigned by the computer to a particular strain gauge output as produced by hanging a weight. A graphic display in the form of a linear response to the addition of weights, indicated an acceptable calibration. Thus, if a hanging weight was wrongly recorded, for example entering ten Newtons at the keyboard for a weight equivalent to twenty Newtons as hung from the sting, a stray point would appear on the calibration graph relative to the correctly recorded points. This graph also indicated a non-linear response, if for example the strain gauges were to fail, an event that may not be immediately apparent if the only output from the computer was that provided via the resulting calibration parameters.

On completion, the calibration provided a set of parameters for each strain gauged force and moment channel.*

During testing the sting was subjected to cyclic variation of forces. Before such tests were conducted, this process was expected to affect the calibration parameters obtained since

*see p.79

the sting, strain gauges, and ancillary equipment might change their characteristics, during testing. Therefore the calibration process was performed at the beginning and end of each programme of tests, and at intervals during each programme. Thus the equipment was re-calibrated once every fifty to sixty test runs along the ship tank. It was unnecessary to re-calibrate after each test run along the tank because there was only a slight variation of the order of 2 to 3% in the calibration parameters between batches of approximately fifty tests.

Parameters were displayed by the computer which defined the slope and intercept of the calibration graph. Subsequently these were used during analysis by a separate analysis program. Typical calibration parameters for force and moment channels are given in the analysis program, a listing of which is given in Appendix II.

4.4. The Oscillation Test Rig.

The top of the sting's vertical member is attached to a sliding block mechanism. This mechanism is located in the oscillation rig and is free to move along two parallel rails. Motion is imparted to the sliding block via an electric motor which transmits power through a gearbox. A piston and crank mechanism transforms the gearbox output into simple harmonic motion. This mechanism has a variable amplitude and the gearbox provides a variable speed output. Thus the sliding block and hence the sting may be driven at a range of

oscillatory frequencies and amplitudes. The motor, gearbox, rails and sliding block are mounted on a turntable within the outer frame of the oscillation rig as shown in Figs. 4.2.(a) & (b).

From p.77, re: Sting Calibration

Subsequent testing required unsteady motion and thus dynamic calibration of the test sting. The natural frequency of the sting was excited by hitting it gently with a soft hammer. An analogue chart recording of the strain gauge outputs showed it to take on a value of approximately 12-13Hz, and the sting itself to be heavily damped. Fortunately this frequency was out of the range of unsteady test oscillations.

In the absence of a parachute canopy the sting may be treated as a bluff body. Thus the inertial effect of the sting can be found by testing and analysing the sting using the same method as for a canopy under test. By subtracting the inertial effect of the sting (without canopy) from that of tests performed with canopies, the inertial effect of the sting is accounted for. Ideally sting-alone tests should be performed after each test run. However, time constraints and the consistency of the static calibrations meant that such tests were performed only when changes in test parameter were made, e.g: for each change in K_C.

Fig. 4.2.(a). Circular Turntable Mounted in the Outer Frame of the Oscillation Rig.

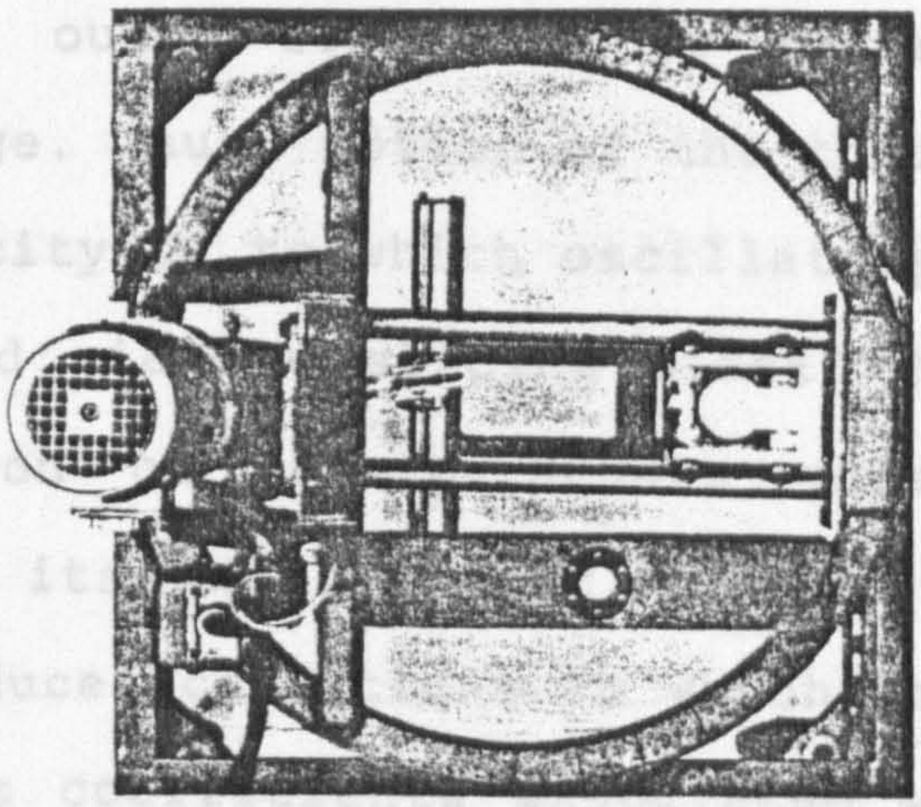

Fig. 4.2.(b). Schematic Plan of Simple Harmonic Motion Mechanism.

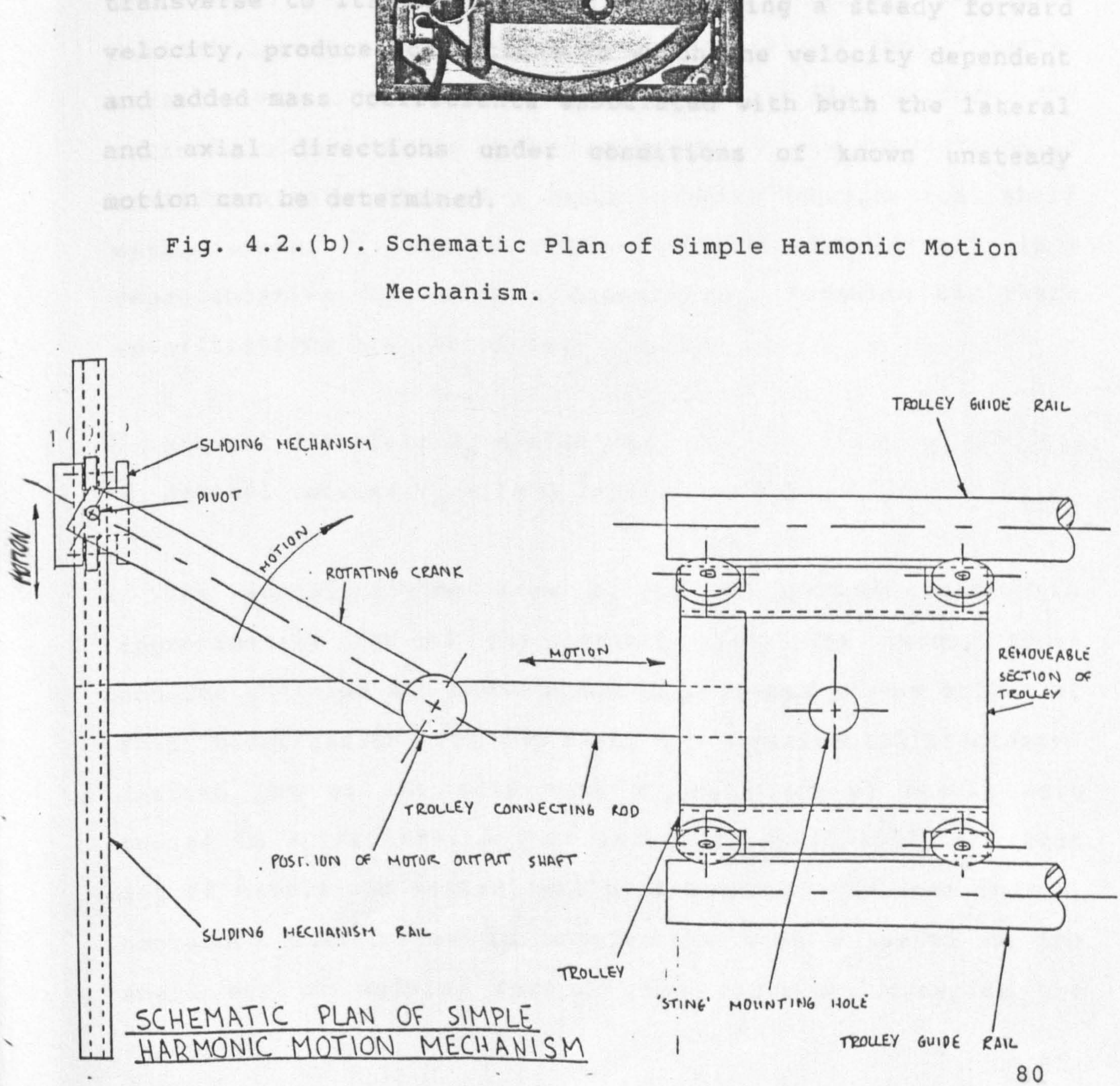

Since the turntable allows rotation through 90 degrees, simple harmonic motion may be imparted in the lateral or the axial directions or at any known intermediate setting.

The entire outer framework is bolted to the ship tank towing carriage. Thus, motion of the towing carriage produces a steady velocity on to which oscillatory motion to the sting can be imposed via the sliding block. The ability to impose unsteady motion on the parachute model, either along or transverse to its axis, whilst maintaining a steady forward velocity, produces conditions in which the velocity dependent and added mass coefficients associated with both the lateral and axial directions under conditions of known unsteady motion can be determined.

4.5. Parachute Canopy Models.

Introduction.

In the following section conventional canopy specifications are given. Different canopies may have different flying shapes. For example the shape of a deployed hemispherical parachute may appear flatter than that of a deployed ribbon canopy. Thus, a standard form of specification has been adopted which is based on the canopy nominal diameter D_o. The nominal diameter is that diameter measured when the canopy is spread out on a flat surface. The nominal volume of the inflated canopy V_o is conventionally considered to be that of a representative hemispherical shell with diameter D_o, similarly the nominal surface area S_o is a representative disc with a diameter D_o. Formulae for these specifications are therefore:

Nominal diameter; $D_o = \sqrt{(4S_o/\pi)}$,

Nominal volume; $V_o = (\pi D_o^3/12)$.

The actual flying area S_p of a deployed canopy is approximately 70% of the nominal area. The canopy types considered below are those which were agreed at the outset of this investigation. For the first two experimental programmes carried out at the ship tank a small set of models were tested in April 1986. A year later, in April 1987, a larger set of models was tested, which although of the same design, contained differences in manufacture when compared to the small set of models. For all the cruciform canopies the

smallest had rigging lines of thin circular cord, the large models had rigging lines made of flat ribbon. The method of construction adopted for the cruciform canopies differed according to their size; the large parachute models were made by sewing together two crossed strips of material, the small models were made by cutting a cross shape from one piece of fabric. This difference may have influenced the performance of the porous cruciform canopies, since for the large models the double layer of fabric at the crown would affect canopy porosity in this region.

4.5.1. Hemispherical Canopies.

Four of these canopy models were employed: two small models; one used in 1986 and another in 1988, and two large models; one used in 1987 and the other in 1988. With the exception of the 1987 model these canopies were constructed from gores, or panels. The particular models tested were manufactured to have twelve panels. The large canopy used in the 1987 test programme was constructed from one piece of flat circular material from which a sector had been removed and the remaining edges sewn together. All four hemispherical canopy models were made from imporous fabric.

The 1986 and 1987 models have been used in two configurations, both with and without drive slots. For the small canopy in 1986 the drive slots were 85mm long by 7mm wide, each cut centrally in a panel and separated from one another by one uncut panel. For the large canopy used in 1987 they measured 170mm x 15mm.

Drive slots were cut because they are often used to obtain

greater directional control when used in a personnel carrying role. It was considered that the presence of these slots and the consequent redistribution of the airflow could affect the added mass compared to the same canopy without slots. Drive slots were not incorporated in the canopies used in the 1988 tests.

4.5.2. Cruciform Canopies.

A cruciform parachute makes use of a cross shaped canopy. The ratio for the width to length of the crossed arms together with the porosity of the fabric from which they are manufactured, and the ratio of suspension line length to nominal diameter, define the type of canopy employed.

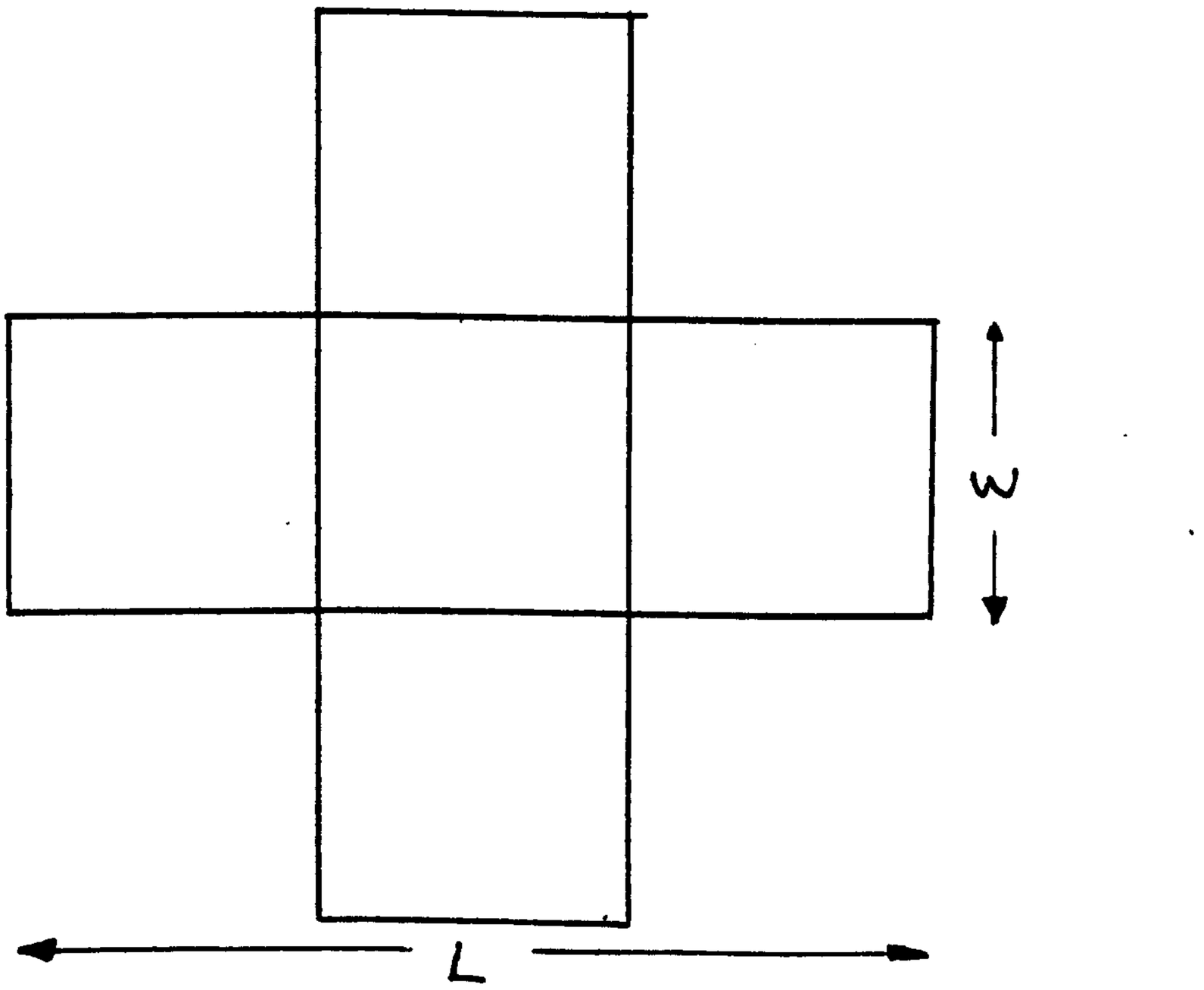

Fig. 4.3. Cruciform Canopy Plan. L = Length, W = Width.

Two sets of cruciform canopies were used during these

tests, one set consisting of 3:1 arm ratio models (i.e. L/W = 3) and the other set consisted of 4:1 arm ratio models (i.e. L/W = 4). For each set of arm ratios there were two sizes of canopy model. Small models of both 3:1 and 4:1 arm ratio had a nominal diameter (D_o), of 367mm. The nominal diameter of the large models of both types of arm ratio was 734mm.

For the 3:1 arm ratio canopies a range of fabric porosites were used, details of which are contained in tables 4.5.1. and 4.5.2. With the exception of the 1987 models, each cruciform canopy model was constructed from one piece of rip-stop nylon fabric, cut into a cross shape. The cruciform canopies used in 1987 were each constructed from two separate strips of rip-stop nylon fabric, sewn together into a cross shape.

For the small canopies used in 1986 and 1988 the arms for the 3:1 arm ratio models measured 437mm x 147mm, & the arms of the 4:1 arm ratio models measured 490mm x 124mm. The large cruciform models used in 1987 and 1988 measured 714mm x 394mm for the 3:1 arm ratio models, and 980mm x 248mm for the 4:1 arm ratio models.

4.5.3. Ribbon Canopies.

These were constructed from ribbons sewn in a series of concentric circles, centred on the apex of the canopy. These ribbons were sewn in place to radial ribbons which converged at the apex. Among other applications this design is commonly applied to braking parachutes for aircraft. A schematic plan of the small Ribbon Canopy used during these tests is shown

in Fig 4.4. The large Ribbon Canopy was made to the same specifications, except all linear dimensions were increased by a factor of two.

Fig. 4.4. Ribbon Canopy Plan.

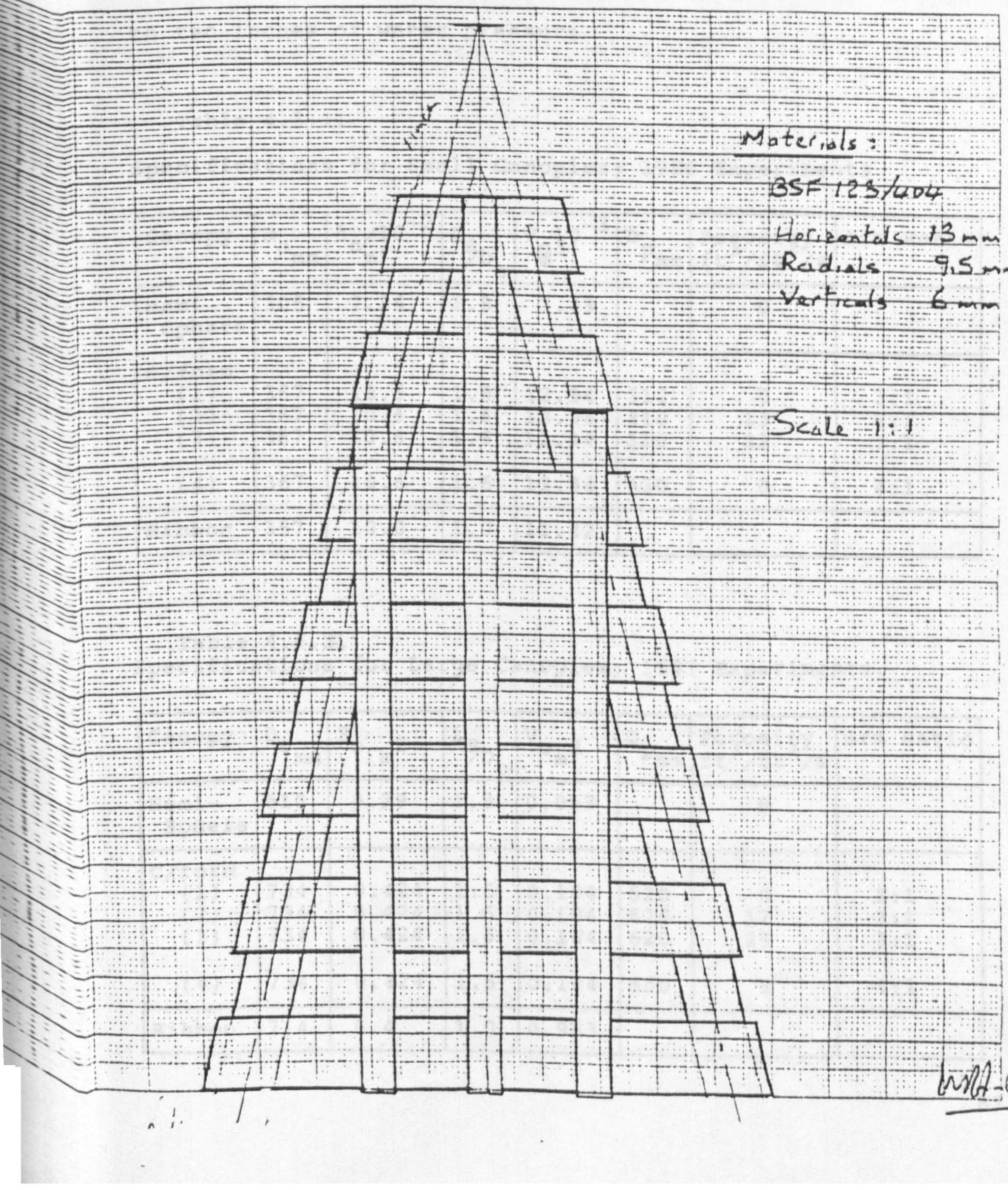

4.5.4. Canopy Specifications.

In the following tables the porosity units are given in Imperial measurement as; cubic feet per square foot per second. This is the rate at which air permeates the fabric when the pressure difference across the fabric is equivalent to ten inches of water pressure.

Table 4.5.1.

Specifications for Small Canopies; 1986 Experiments.

Canopy	D_o mm	$S_o/m^2 10^{-2}$	L_R/D_o	$V_o/m^3 10^{-3}$	D_p mm	Porosity $ft^3/ft^2/s$	Arm Ratio
Hemi-Sphere	305	7.26	1.8	7.43		0	
C/form							
(1)	367	10.6	1.6	12.94	310	0	3:1
(2)	367	10.6	1.6	12.94	310	13	3:1
(3)	367	10.6	1.6	12.94	310	23	3:1
(4)	367	10.6	1.6	12.94	330	0	4:1
Ribbon	357	10.0	1.0	11.22			

Table 4.5.2.
Specifications for Large Canopies; 1987 Experiments.

Canopy	D_o mm	S_o m^2	L_R/D_o	V_o m^3	D_p mm	Porosity $ft^3/ft^2/s$	Arm Ratio
Hemi-Sphere	610	0.29	1.8	0.059		0	
C/form							
(1)	734	0.424	1.6	0.104	620	0	3:1
(2)	734	0.424	1.6	0.104	620	12	3:1
(3)	734	0.424	1.6	0.104	620	25	3:1
(4)	734	0.424	1.6	0.104	660	0	4:1
Ribbon	714	0.4	1.0	0.953			

In the 1988 test programme the models shown in tables 4.5.1 & 4.5.2 were replaced by a new complete set of both small and large canopies having similar specifications. Small differences arose between the large canopies as used in 1987 with those used in 1988. These occured as a result of differences in manufacture leading to different types of rigging line and canopy gore being used for the same canopy specification. These differences are described in sections 4.5.1, 4.5.2, and 4.5.3.

4.6. Recording Experimental Data.

Data signals were transmitted from their respective source along eight channels.

There were four force channels, two moment channels, and one accelerometer channel, the eighth channel catered for a wheel interrupt signal.

The force channels consisted of two for recording tangential force, and two for recording normal force. The channels were duplicated in this way to ensure no loss of data in the event of channel failure. Similarly there were two moment channels for recording moments acting in the X - Z plane.

Data were recorded in two forms; analogue form on a chart recorder, and also in a digital form for subsequent analysis. For any test condition the analogue recording gave an immediate indication of the size and variation of the aerodynamic forces. This was particularly useful if the

forces produced were sufficient to overload the computer input.

The accelerometer detected the oscillatory acceleration imposed by the simple harmonic motion mechanism shown in Fig 4.2. During subsequent analysis this signal was integrated to provide the oscillatory velocity.

The wheel interrupt device consisted of a reed switch fixed to the towing carriage and activated by a magnet attached to one of its wheels. Thus the computer registered an impulse once for every wheel rotation. Only the force channels were recorded in an analogue form, but all channels were recorded digitally.

4.6.1. Analogue Recording.

Analogue recordings were accomplished using a multichannel chart recorder. Typical forces recorded in this form are illustrated in Fig 4.5.

4.6.2. Digital Recording.

The analogue signals from strain gauges, accelerometer, and wheel interrupt were converted into a digital form, and stored for subsequent analysis in a file on floppy discs using an RM 380 Z microprocessor.

Fig. 4.5. Chart Recording of Analogue Signal.

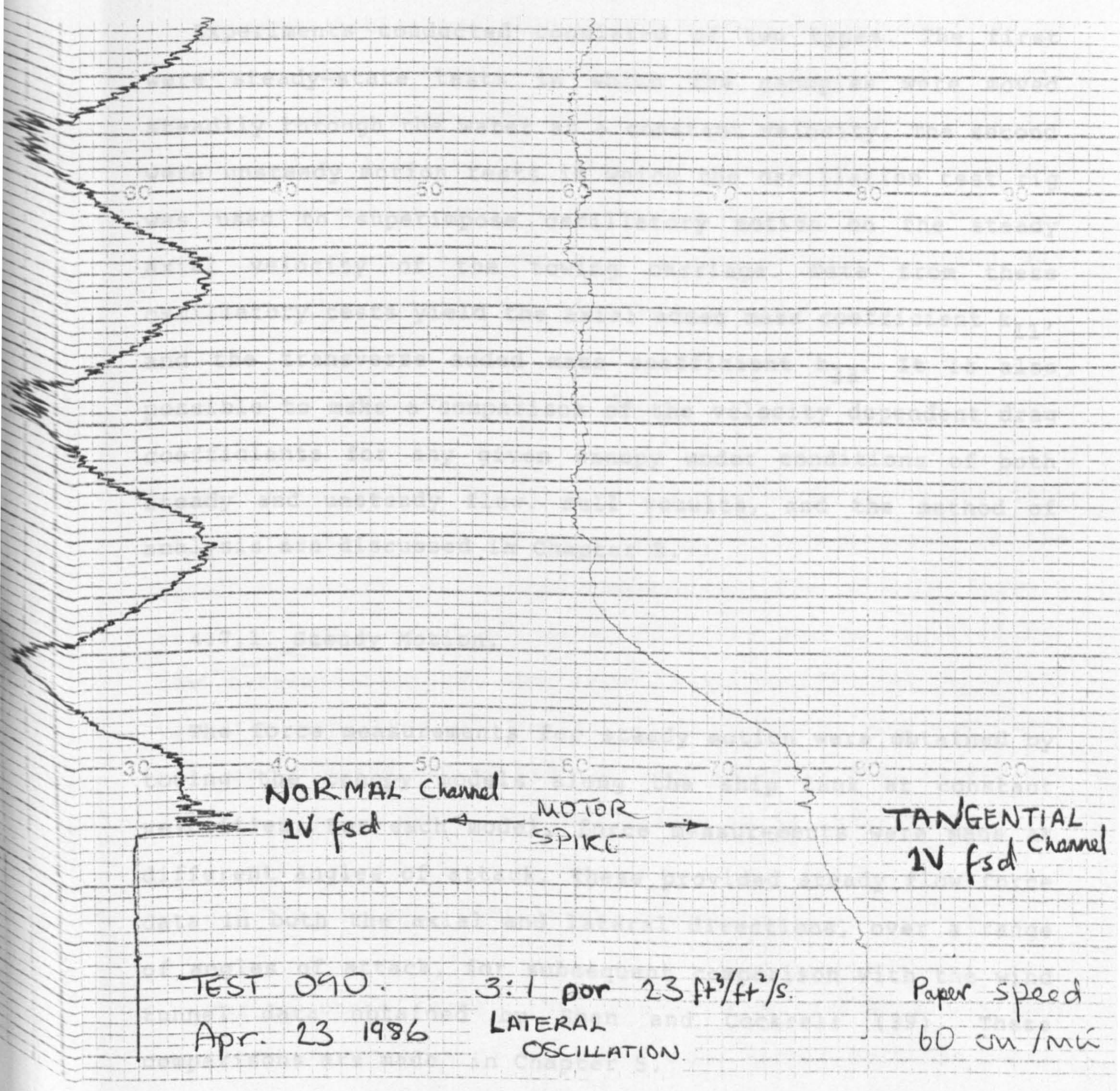

4.7. Experimental Procedure.

Experiments conducted consisted of two types. The first were steady-state tests in which the canopies were moved steadily through the water at a constant velocity. The second were unsteady motion tests in which the oscillation test rig was used to superimpose oscillatory motion on the steady axial velocity of the towing carriage. Data from these oscillatory tests yield the axial added mass coefficient k_{11}, and the transverse added mass coefficient k_{33}. It is also possible to make a comparison of the velocity dependent drag coefficients for any given canopy under conditions of both steady and unsteady flow. Full results, and the method of analysis are discussed in Chapter 5.

4.7.1. Steady Motion.

The force measurements for steady motion were obtained by towing the canopy models along the ship tank at constant velocities. For each model, force measurements were made at different angles of attack. These provided steady flow force data in both the axial and lateral directions, over a range of angles of attack, for subsequent comparison with the wind tunnel data obtained by Shen and Cockrell (39). These comparisons are made in Chapter 5.

4.7.2. Unsteady Motion.

Unsteady motion was obtained by superimposing oscillatory motion on the canopy's constant axial velocity as it was moved steadily along the tank. The axis of the canopy was maintained parallel to the length of the ship tank throughout an unsteady motion test. In order to determine the two added mass coefficients k_{11} and k_{33}, simple harmonic motion was applied either axially or laterally.

4.7.2.1. Axial Oscillatory Motion.

For this purpose the test model was towed along the tank in a direction parallel to its axis. Oscillations in the axial direction were superimposed on the steady forward velocity. This provided the oscillatory motion required for the determination of the added mass coefficient k_{11}. The velocity amplitude of the oscillatory motion was such that the canopy possessed no net rearward velocity when in motion. In this way the canopy was maintained in an inflated state.

4.7.2.2. Lateral Oscillatory Motion.

During these tests, the axis of the parachute was held parallel to the axis of the ship tank. Simple harmonic motion was applied perpendicular to the parachute system's axis and therefore transverse to the tank. This provided the necessary motion for the determination of the added mass coefficient

k_{33} over a range of angles of attack, similar to that in the steady state tests. The oscillatory lateral force is dependent upon both the oscillatory acceleration and the oscillatory velocity. It also depends on the angle of attack which is constantly changing. The following diagram illustrates how the angle of attack α changes. Where V_u is the unsteady component of velocity, V_s is the steady velocity and the resultant velocity is given by V_R.

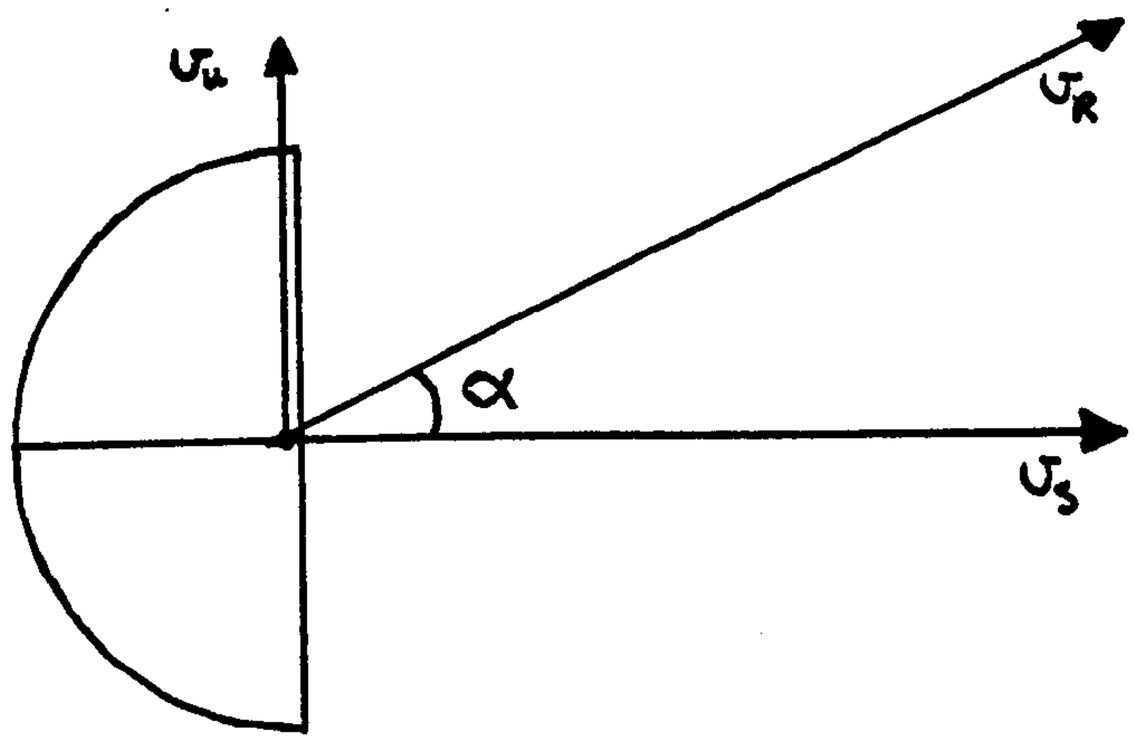

Fig. 4.6. The Angle of Attack α Arising From V_R.

4.8. Reynolds Number: $Re = \rho \cdot V \cdot D_o / \mu$.

The Reynolds number Re is defined as above, where; ρ = Fluid Density, $kg \cdot m^{-3}$; V = Relative Flow Velocity, $m \cdot s^{-1}$; D_o = Canopy Nominal Diameter (a typical system dimension), m; μ = Viscosity of the fluid, $m^{-1} \cdot s^{-1} \cdot Kg$.

For the tests performed during the experimental programme, Re was in the range; 3×10^5 to 4×10^5. This is low when compared to the typical full scale values of the order of 10^7 associated with steadily descending parachutes subject to

imposed oscillations. Jorgenson (37), produced a graph which demonstrated there is no substantial dependence of C_D on Reynolds numbers above 3×10^5. Thus, the drag coefficients obtained at test Reynolds numbers are relavent to full-scale parachutes.

During the steady state tests, the Reynolds number was determined using the value of the steady velocity component and the canopy nominal diameter. For oscillatory motion a mean Reynolds number was assumed, based on the steady relative velocity.

CHAPTER 5

5. ANALYSIS AND RESULTS

Introduction

In this chapter the need for a modelling procedure is discussed based on what is known about bluff body motion, with respect to both velocity dependent and acceleration dependent aerodynamic forces. The methods which were used for data analysis are presented, with a description of how the coefficients; C_T, $\partial C_N/\partial\alpha$, k_{11}, and k_{33}, are obtained. These results are then presented in tabular form. The relationship between dynamic forces and the Keulegan-Carpenter number K_C is discussed, and the possible significance of K_C is considered, given the results of the tests.

5.1. Data Analysis.

The adoption of a modelling procedure for the forces acting on a parachute canopy is necessary, since in addition to the velocity dependent force component there exists an inertial force component encompassing added mass, which makes a contribution to the total aerodynamic force.

$$F(t) = a \cdot v^2(t) + b \cdot dV/dt \qquad [5.1].$$

The modelling procedure is to use the force, acceleration and velocity data for a particular canopy as tested in the ship tank, and substitute this data into Morison's equation [5.1] above, for which at this stage 'a' and 'b' exist as two

unknown parameters. However, this method can be used to determine the mean values of both these parameters 'a' and 'b' which then yield the velocity dependent and added mass coefficients respectively. The determination of an added mass coefficient in addition to the velocity dependent coefficient provides a model which is capable of describing aerodynamic forces developed by the body.

The experimental data which were stored digitally on a magnetic disc exist in a form suitable for analysis on the microprocessor which was used for data logging the test measurements. An analysis program was written for the data and is described and listed in appendix II. During each test run, signals from force, moment, and acceleration channels were logged from the instant the towing carriage started to move along the tank until it stopped.

5.1.1. General Method.

A typical ship tank test was analysed using the microprocessor. The process of "sampling" refers to the transfer of data from the file which is stored on the magnetic disc.

A data file was opened, and sampling of the data began. To overcome initial inflation effects a starting point for the analysis was found in the data file, equivalent to a distance of approximately six metres of towing carriage travel along the tank. This was achieved by monitoring signals from the wheel interupt device. Analysis was witheld until this point

because equation [5.1] may not be valid during the inflation process.

The wheel interupt device was intended initially to provide the data from which the towing carriage velocity could be computed. However, the average towing velocity could be determined independently from the time taken to cover a measured distance during each run and this was used instead. The wheel interupts could therefore be interpreted as data markers which identified particular points in the the test run data file. This made the process of analysis more efficient since it provided a route into the data file which did not require the large scale sampling of force channel data.

Analysis took place for blocks of data points representative of a period of oscillation. The aerodynamic force coefficient values were noted for each data block, and then a further block was sampled. This process was repeated during the history of the run. The resulting values for the parameters 'a' and 'b' for each block were collected and used to obtain a mean value for the force parameters 'a' and 'b' for the whole test run. The way in which these parameters subsequently yielded values for the coefficients; C_T, $\partial C_N/\partial\alpha$, k_{11} and k_{33}, is described in the following section.

5.1.2. Unsteady Motion.

The first analysis of the results for these unsteady motion experiments took place during 1986, the first year of this research programme. The results obtained together with a discussion on them are contained in a paper published that same year by Cockrell, et al (3). A method which has been described by Sarpkaya and Isaacson (5) was used by which average values per cycle of the aerodynamic force coefficients C_T, $\partial C_N/\partial\alpha$, k_{11} and k_{33} were determined.

(i) The Method of Average Values.

Average values of the components 'a' and 'b' were calculated by forming a product of the governing equation [5.1], with either the instantaneous velocity V(t), or the instantaneous acceleration dV(t)/dt. The functions in [5.1] which describe force F(t), acceleration dV/dt, and velocity V(t) were replaced with the actual data measurements of these functions. Subsequent integration with respect to time over a cycle of period T yielded average values for 'a' and 'b'.

By forming a product of the governing equation with the the velocity of the canopy as recorded from the data, then integrating the resulting equation, a mean value for 'a' over one cycle is obtained. Since the integration takes place with respect to time, the resulting integrand terms are all divided by the period of the cycle.

Hence 5.1 becomes:

$$1/T\int_0^T F\cdot V(t)\cdot dt = 1/T\int_0^T a\cdot V^3(t)\cdot dt + 1/T\int_0^T b\cdot \dot{V}(t)\cdot V(t)\cdot dt \quad [5.2].$$

In sinusoidal motion the functions describing velocity and acceleration are orthogonal, thus the term containing 'b' consisting of the product of V(t) and dV(t)/dt, becomes zero, for

$$1/T\int_0^T \dot{V}(t)\cdot V(t)\cdot dt = 0 \quad [5.3].$$

Thus the average value of the velocity-dependent force parameter 'a' is given by;

$$\bar{a} = \frac{1/T\int_0^T F(t)\cdot V(t)\cdot dt}{1/T\int_0^T V^3(t)\cdot dt} \quad [5.4].$$

The average value of the inertial parameter 'b' is obtained similarly by multiplying each term of the governing equation by the acceleration dV/dt, and subsequently integrating it over a cycle, The orthogonality of the functions of velocity and acceleraton in sinusoidal motion cause the term containing 'a' to become zero, i.e.

$$1/T \int_0^T a \cdot v^2(t) \cdot \dot{v}(t) \cdot dt = 0 \qquad [5.5].$$

This results in an expression for the average value of 'b' of the form:

$$\bar{b} = \frac{1/T \int_0^T F \cdot \dot{v}(t) \cdot dt}{1/T \int_0^T \dot{v}(t) \cdot \dot{v}(t) \cdot dt} \qquad [5.6].$$

By this method, it is possible to extract average values of both parameters 'a' and 'b' from the single equation 5.1. Although the values of 'a' and 'b' may themselves vary as Sarpkaya and Isaacson (5) has shown, it is a convenient technique to employ, since a constant parameter is more readily applicable to an engineering problem than one which varies over a period.

However, this method has disadvantages; it is not possible to determine the degree to which the instantaneous values of the parameters 'a' and 'b' vary during a cycle of data, or to observe the scatter in the data. Additionally there is the problem of determining the two unknowns 'a' and 'b' from one equation as in [5.1], for the instantaneous aerodynamic force F(t). Yavuz (11), in his solution for instantaneous values of 'a' and 'b', reduced the number of unknowns to one by first assuming the velocity dependent parameter 'a' was equal to

its steady state value during unsteady motion and offered no evidence for this assumption.

(ii) The Least Squares Method.

A second method of data analysis was used, in which the governing equation [5.1], was first written in terms of two components so that a least squares technique could be employed for the simultaneous determination of average values for both the velocity dependent and inertial parameters 'a' and 'b'.

Division by the acceleration term V(t) in equation [5.1] results in an equation consisting of two variables. i.e.

$$F(t) = a \cdot V^2(t) + b \cdot \dot{V}(t) \qquad [5.1].$$

$$\rightarrow \qquad F/\dot{V}(t) = a \cdot V^2(t)/\dot{V}(t) + b \qquad [5.6].$$

This equation can be applied to lateral and longitudinal oscillatory force data and is essentially of the form;

$$Y_i = a \cdot X_i + b.$$

Where the 'i' subscript refers to individual sets of data, represented by the variables $F/V(t)$ and $V^2(t)/V(t)$. A least squares analysis gives values of 'a' and 'b', representative of slope and intercept for the best straight line fit to these data. The application of such a method may be justified by inspection of a graph obtained in this way and shown in Fig 5.1.

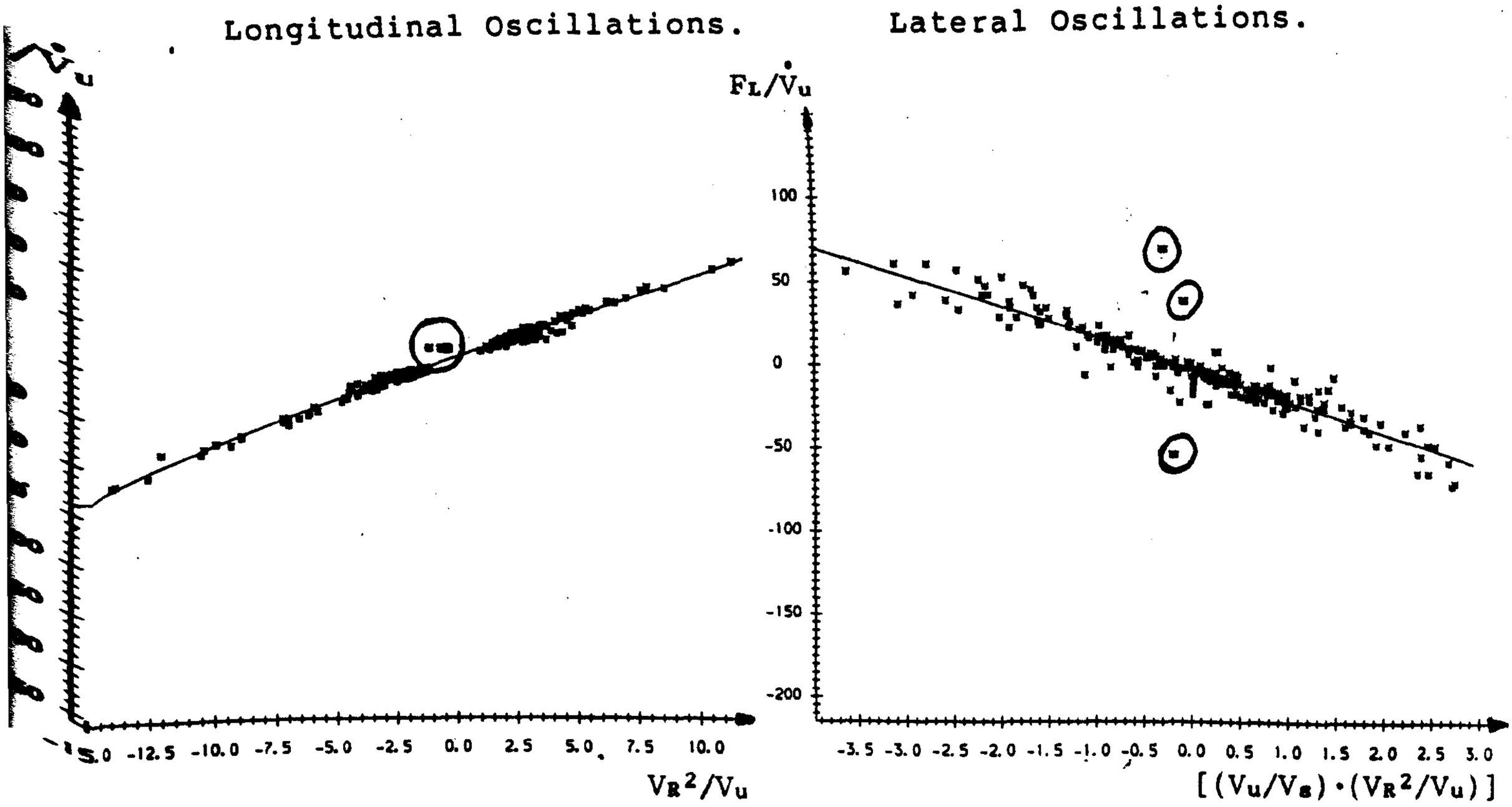

Fig 5.1. Representative Experimental Data Presented in the

Form:

$$F/\dot{V}(t) = a\cdot V^2(t)/\dot{V}(t) + b \qquad \text{(equation 5.6).}$$

For longitudinal oscillations in which the angle of attack $\alpha = 0°$ and the parachute canopy is oscillated along its axis, equation [5.6] becomes;

$$F_T/\dot{V}_u = a\cdot V_R^2/\dot{V}_u + b \qquad [5.7].$$

Where: F_T = Total tangential force,

V_s = steady velocity,

V_u = oscillatory velocity,

$V_R = V_s + V_u$, hence $\dot{V}_u$ = Acceleration $\equiv \dot{V}_R$,

$a = (1/2)\cdot\rho\cdot S_o\cdot C_T$,

and $b = \rho\cdot\upsilon\cdot k_{11}$.

Thus [5.7] becomes;

$$F_T/\dot{V}_u = (1/2)\cdot\rho\cdot S_o\cdot C_T\cdot(V_R^2/\dot{V}_u) + \rho\cdot k_{11}\cdot\upsilon \qquad [5.8].$$

The values of S_o, υ, ρ, & V_s, are known. Both F_T & $\dot{V}_u$ can be measured. V_R or V_u is obtained by integration of an accelerometer signal. The analysis yields C_T the velocity dependent force coefficient, and k_{11} the axial added mass coefficient.

For lateral oscillations where the parachute is oscillated transverse to its axis, and hence to the steady forward velocity of the towing carriage, equation [5.6] becomes;

$$F_L/\dot{V}_u = aV_R^2/\dot{V}_u + b \qquad [5.9].$$

Where; $V_R = \sqrt{[V_s^2 + V_u^2]}$,

$\dot{V}_u = dV_u/dt$,

F_L = Total lateral force,

$b = \rho \cdot \upsilon \cdot k_{33}$,

$a = (1/2) \cdot \rho \cdot S_o \cdot (\partial C_N/\partial \alpha) \cdot \alpha$.

In this analysis the coefficient of the velocity dependent component of lateral force C_N is assumed to be a linear function of the angle of attack α. Hence;

$$C_N = (\partial C_N/\partial \alpha) \cdot \alpha, \text{ and } C_N = 0 \text{ when } \alpha = 0.$$

For a small range of angles of attack 'α' representative of the full scale case: $\alpha = V_u/V_s$.

Thus;

$$a = (1/2) \cdot \rho \cdot S_o \cdot (\partial C_N/\partial \alpha) \cdot V_u/V_s.$$

Hence [5.9] becomes;

$$F_L/\dot{V}_u = (1/2) \cdot \rho \cdot S_o \cdot (\partial C_N/\partial \alpha) \cdot [(V_u/V_s) \cdot (V_R^2/\dot{V}_u)] + \rho \cdot \upsilon \cdot k_{33} \qquad [5.10].$$

The values of V_s, υ, S_o, & ρ are known. F_L & $\dot{V}_u$ are experimental data and integration of $\dot{V}_u$ yields V_u. The values of $\partial C_N/\partial\alpha$, and k_{33} are determined by a least squares analysis on data represented in the two component form by $F_L/\dot{V}_u$ and $[(V_u/V_s)\cdot(V_R^2/\dot{V}_u)]$.

The graphs shown in Fig 5.1 describe the relationship between $F/(dV/dt)$ and $V^2/(dV/dt)$ as in equation 5.6, e.g.

$$F/\dot{V}(t) = a\cdot V^2(t)/\dot{V}(t) + b \qquad \text{(equation 5.6)}.$$

This method yields values for the dynamic force parameters 'a' and 'b' in a way similar to the method of average values discussed in Section 5.1.2 (i). It also enables the variations for 'a' and 'b' during the cycle to be observed and to be determined statistically. Hence the uncertainty in the value of the slope and intercept and thus in the values gained for C_T, $\partial C_N/\partial\alpha$, k_{11}, and k_{33} can be assessed. The stray points encircled have been found to have been caused by electrical interference from the wheel interupt mechanism with the force measurement signals and have been disregarded in the data analysis.

5.1.3. Steady Motion.

Steady state analysis consisted of the determination of C_R in the following form of equation [5.1];

$$F = 1/2 \cdot \rho \cdot S_o \cdot C_R \cdot V^2 \qquad [5.11].$$

The coefficient C_R may represent C_T in the case of axial tests ($C_D = C_T$ when $\alpha = 0°$), or C_N for tests in which the angle of attack 'α' is varied and the lateral aerodynamic force F is considered.

Analysis followed the method of examining blocks of data. For each data block, a value of C_T or C_N was obtained. Generally, ten such values per run would be obtained, from which a mean value for the particular model under test could be determined.

5.2. Results.

Introduction

The following tables; 5.2.1 to 5.2.4, contain the results from the first two batches of tests performed in 1986 and 1987. Tables 5.4.1. to 5.4.12. contain the results for the tests performed in January 1988. The parachute canopies which were tested are those described in section 4.5.4.

Results are presented according to the type of motion which gave rise to them and each group of tables deals with a specific type of motion. Similar tests were performed on two sets of canopy models which although of the same design, differed in the scale of their linear dimensions. Thus, for each type of parachute canopy which was tested there were two different models; one set of models having twice the linear dimensions of the other set. To maintain consistency of Reynolds number between the sets in each batch of experiments both the oscillational and steady components of velocity were reduced by a factor of two for the larger sets of models tested.

In the following, D_o is the nominal diameter of the parachute canopy model and P_o is the fabric porosity measured in cu.ft/sq.ft/sec of air at a pressure difference equivalent to a ten inch head of water. Where relevant the data uncertainty listed in the Table was determined.

5.2.1. Results For Steady Motion at $\alpha = 0$.

1986 and 1987 Tests.

Results obtained from equation [5.11] for the velocity dependent drag coefficient C_D, C_T at an angle of attack $\alpha = 0°$. Correction for blockage is signified by C_D^*, and where necessary is applied according to Maskell's (28) formula, see Section 4.2.2. (i).

Table 5.2.1

(i) Hemispherical Canopies.

Unslotted

D_o/mm	C_D ± %	C_D^*
305	0.61 ± 4	-
610	0.76 ± 5	0.69

Slotted

D_o/mm	C_D ± %	C_D^*
305	0.57 -	-
610	0.82 -	0.74

(ii) Ribbon Parachutes

D_o/mm	C_D ± %	C_D^*
357	0.51 ± 4	-
714	0.51 ± 4	0.47

(iii) Cruciform Parachutes of Arm ratio 3:1

D_o = 367mm.

P_o	C_D ± %
0	0.64 ± 10
13	0.71 ± 5
23	0.66 ± 4

D_o = 734mm.

P_o	C_D ± %	C_D^*
0	0.66 ± 10	0.58
12	0.74 ± 5	0.65
25	0.74 ± 4	0.64

(iv) Imporous Cruciform Parachutes of Arm Ratio 4:1

D_o/mm	C_D ± %	C_D^*
367	0.77 ± 6	-
734	0.81 ±10	0.69

5.2.2. Steady Motion at Discrete Angles of Attack.

1986 and 1987 Tests.

In these tests the rate of change of lateral force coefficient C_N with angle of attack α at $\alpha = 0°$ was determined using equation 5.11. The data were obtained from tests conducted at discrete angles of attack of: +5°, 0°, -5°. The value of $\partial C_N/\partial\alpha$ at $\alpha = 0°$ was assumed to be that developed over the range from -5° to +5°, over which C_N was considered to be a linear function of the angle of attack, α.

Table 5.2.2

(i) Hemispherical Canopies.

Unslotted

D_o/mm	$\partial C_N/\partial\alpha$
305	-0.26
610	-0.28

Slotted

D_o/mm	$\partial C_N/\partial\alpha$
305	0.02
610	-0.32

(ii) Ribbon Parachutes

D_o/mm	$\partial C_N/\partial\alpha$
357	0.06
714	0.31

(iii) Cruciform Parachutes of Arm ratio 3:1

D_o = 367mm

Porosity	$\partial C_N/\partial\alpha$
0	-0.19
13	0.00
23	0.46

D_o = 734mm

Porosity	$\partial C_N/\partial\alpha$
0	-0.53
12	0.04
25	0.14

(iv) Imporous Cruciform Parachutes of Arm ratio 4:1

D_o/mm	$\partial C_N/\partial\alpha$
367	0.52
734	-0.20

5.2.3. Axial Unsteady Motion.

1986 and 1987 Tests.

This section describes results obtained from tests in which an oscillatory component of motion in the axial direction was superimposed on steady motion, therefore the angle of attack; $\alpha = 0°$. The values of C_D and k_{11} are obtained from analysis which used equation [5.8].

Table 5.2.3

(i) Hemispherical Parachutes.

Unslotted

D_o/mm	C_D ± %	k_{11} ± %
305	0.64 ± 5	1.1 ± 30
610	0.91 ± 10	0.49 ± 15

$C_D^* = 0.81$, for $D_o = 610$mm.

Slotted

D_o/mm	C_D	k_{11}
305	0.57	1.0
610	1.02	0.25

$C_D^* = 0.90$, for $D_o = 610$mm.

(ii) Ribbon Parachutes

D_o/mm	C_D ± %	k_{11} ± %
357	0.52 ± 5	1.0 ± 13
714	0.51 ± 6	0.18 ± 8

$C_D^* = 0.47$, for $D_o = 714$mm.

(iii) Cruciform Parachutes of Arm ratio 3:1

$D_o = 367$mm

P_o	C_D ± %	k_{11} ± %
0	0.68 ± 7	2.4 ±10
13	0.70 ± 7	0.78 ±15
23	0.67 ± 5	0.80 ±15

$D_o = 734$mm

P_o	C_D ± %	k_{11} ± %	C_D^*
0	0.82 ±20	0.25 ±30	0.70
12	0.68 ±25	0.12 ±25	0.60
25	0.80 ± 6	0.10 ±20	0.68

(iv) Imporous Cruciform Parachutes of Arm ratio 4:1

D_o/mm	C_D ± %	k_{11} ± %	C_D^*
367	0.76 ± 9	1.6 ±15	-
734	0.78 ± 5	0.17 -	0.67

5.2.4. Lateral Unsteady Motion.

1986 and 1987 Tests.

This section describes the results obtained from tests in which an oscillatory component of motion was applied perpendicular to the direction of the steady motion. The values for $\partial C_N/\partial\alpha$ at $\alpha = 0°$, and k_{33} are average values, obtained in accordance with equation [5.10], for 'α' in the range -12° to +12°, over which C_N was considered to be a linear function of the angle of attack.

Table 5.2.4

(i) Hemispherical Canopies.

Unslotted

D_o/mm	$\partial C_N/\partial\alpha$ ± %	k_{33} ± %
305	0.05 * ±15	0.17 ±20
610	-0.23 * ±20	0.02 ±20

Slotted

D_o/mm	$\partial C_N/\partial\alpha$ ± %	k_{33} ± %
305	0.06 -	0.48 -
610	-0.11 -	0.03 -

(ii) Ribbon Parachutes;

D_o/mm	$\partial C_N/\partial\alpha$ ± %	k_{33} ± %
357	0.12 ± 8	0.17 ±10
714	0.16 ±30	0.07 ±20

(iii) Cruciform Parachutes Arm ratio 3:1;

D_o = 367mm

P_o	$\partial C_N/\partial\alpha$ ± %	k_{33} ± %
0	0.13 ± 15	0.26 ± 8
13	0.25 ± 6	0.21 ±10
23	0.41 ± 5	0.08 ±15

D_o = 734mm

P_o	$\partial C_N/\partial\alpha$ ± %	k_{33} ± %
0	0.10 ± 20	0.20 ±15
12	0.10 ± 65	0.11 ±40
25	0.14 ± 55	0.06 ±40

(iv) Imporous Cruciform Parachutes of Arm ratio 4:1.

D_o/mm	$\partial C_N/\partial\alpha$ ± %	k_{33} ± %
367	0.43 ± 9	0.11 ±15
734	0.27 ± 45	0.15 ±20

* A probable explanation of this is the different build standard, previously discussed on P.83, which occurs between the large and small canopies.

5.3. The Keulegan-Carpenter Number K_C.

In the results presented in Tables 5.2.1 - 5.2.4, there is a difference between the values of force coefficients obtained for the small-sized canopies and those obtained for the larger canopies, even though the Reynolds numbers at which these tests were conducted were broadly similar. However, the two test programmes were conducted at different Keulegan-Carpenter numbers K_C and equation [4.1] (see Chapter 4, section 4.1.) indicates that average aerodynamic force coefficients may be K_C dependent. i.e.

$$k_{ij} = f\{ \text{Shape, Re, } K_C, \alpha \} \qquad \text{Equation [4.1].}$$

In 1988 a third series of tests was conducted in the Southampton ship tank. The purpose of this test programme was to examine the dependence if any, of the added mass coefficient k_{11} on Keulegan-Carpenter number K_C. Thus, a schedule was planned in which a range of K_C numbers would be considered.

5.4. Results of The 1988 Test Programme.

During the 1988 test programme a range of both large and small canopy models was used in which there were no manufacturing differences all models were produced in the same batch. Specifications are given in section 4.5.4. The following Tables: 5.4.1. to 5.4.12 show the variation of k_{11}

and C_D with K_C for each canopy model tested.

5.4.1. Small Canopy Models.

Table 5.4.1. Hemispherical Imporous. D_o = 305mm.

K_C	k_{11} ± %	C_D ± %
1.15	- -	0.59 ± 10
1.62	0.6 ± 30	0.60 ± 10
2.12	0.54 ± 40	0.61 ± 10
2.62	0.79 ± 20	0.60 ± 5
3.11	1.45 ± 35	0.61 ± 9
3.60	1.1 ± 30	0.61 ± 5
4.10	1.62 ± 30	0.60 ± 6

Table 5.4.2. 3:1 Cruciform Imporous. D_o = 367mm.

K_C	k_{11} ± %	C_D ± %
0.96	-	0.55 ± 7
1.35	-	0.52 ± 6
1.76	-	0.54 ± 8
2.17	-	0.52 ± 13
2.59	0.45 ± 75	0.56 ± 7
3.00	1.13 ± 60	0.58 ± 7
3.40	0.86 ± 40	0.57 ± 8

Table 5.4.3.3:1 Cruciform Medium Porosity; P_o = 12 $ft^3/ft^2/sec.$ D_o = 367mm.

K_C	k_{11} ± %	C_D ± %
0.96	-	0.62 ± 10
1.35	-	0.58 ± 15
1.76	-	0.55 ± 12
2.17	0.43 ± 45	0.53 ± 6
2.59	0.72 ± 65	0.53 ± 8
3.00	1.18 ± 35	0.52 ± 7
3.40	0.82 ± 35	0.57 ± 9

Table 5.4.4.3:1 Cruciform High Porosity; P_o = 25 $ft^3/ft^2/sec.$ D_o = 367mm.

K_C	k_{11} ± %	C_D ± %
0.96	-	0.49 ± 10
1.35	-	0.51 ± 7
1.76	0.1 ± 65	0.52 ± 7
2.17	0.55 ± 25	0.54 ± 6
2.59	0.73 ± 40	0.52 ± 7
3.00	0.90 ± 25	0.52 ± 6
3.40	0.83 ± 35	0.53 ± 6

Table 5.4.5. 4:1 Cruciform Imporous. D_o = 367mm.

K_C	k_{11} ± %	C_D ± %
0.96	-	0.65 ± 9
1.35	-	0.65 ± 5
1.76	-	0.69 ± 15
2.17	-	0.65 ± 6
2.59	0.38 ± 50	0.65 ± 6
3.00	0.81 ± 20	0.65 ± 6
3.40	0.81 ± 45	0.66 ± 6

Table 5.4.6. Ribbon Canopy. D_o = 357mm.

K_C	k_{11} ± %	C_D ± %
0.99	-	0.43 ± 5
1.39	-	0.43 ± 10
1.81	0.26 ± 50	0.43 ± 6
2.24	0.24 ± 55	0.44 ± 6
2.66	0.65 ± 30	0.44 ± 6
3.08	0.76 ± 25	0.43 ± 6
3.50	1.00 ± 25	0.44 ± 6

5.4.2. Large Canopy Models.

Table 5.4.7. Hemispherical Imporous Canopy. D_o = 610mm.

K_C	k_{11} /10^{-2} ± %	C_D ± %	C_D^*
0.58	-0.45 ± 300	0.48 ± 20	0.45
1.3	-1.54 ± -	0.63 ± 15	0.58
2.05	8.45 ± 200	0.70 ± 25	0.64

Table 5.4.8. 3:1 Cruciform Imporous. D_o = 734mm.

K_C	k_{11} /10^{-2} ± %	C_D ± %	C_D^*
0.48	-4.5 ± 90	0.67 ± 30	0.59
1.1	-3.2 ± -	0.63 ± 30	0.56
1.7	-23 ± 120	0.94 ± 30	0.78

Table 5.4.9. 3:1 Cruciform Medium Porosity; P_o = 12 $ft^3/ft^2/sec$. D_o = 734mm.

K_C	k_{11} /10^{-2} ± %	C_D ± %	C_D^*
0.48	-8 ± 200	0.80 ± 18	0.69
1.1	-20 ± 120	0.79 ± 30	0.68
1.7	-36 ± 65	0.98 ± 30	0.81

Table 5.4.10. 3:1 Cruciform High Porosity; P_o = 25 $ft^3/ft^2/sec.$ D_o = 734mm.

K_C	k_{11} /10^{-2} ± %	C_D ± %	C_D^*
0.48	-4.1 ± 150	0.69 ± 10	0.61
1.1	0.68 ± 270	0.59 ± 30	0.53
1.7	-26 ± 130	1.01 ± 30	0.83

Table 5.4.11. 4:1 Cruciform Imporous. D_o = 734mm.

K_C	k_{11} /10^{-2} ± %	C_D ± %	C_D^*
0.48	-3.9 ± 75	0.82 ± 15	0.70
1.1	-12 ± 85	0.79 ± 20	0.68
1.7	-17 ± 140	0.84 ± 25	0.72

Table 5.4.12. Ribbon Canopy. D_o = 714mm.

K_C	k_{11} /10^{-2} ± %	C_D ± %	C_D^*
0.5	-2.3 ± 140	0.43 ± 20	0.40
1.1	-7.5 ± 200	0.55 ± 25	0.50
-	-	-	-

5.5. Errors and Uncertainties.

Introduction

During a run, data for force and acceleration were recorded in a coded format on a magnetic disc file. This coded format is a data equivalent number known as a "count" which, according to the output level of the strain gauge or accelerometer, is assigned by the computer to the data file. The process of transforming the count, equivalent to force and acceleration data into physical units of Newtons and $m \cdot s^{-2}$, occurs when the data is retrieved for analysis. During this analysis a measure of the forces and accelerations imposed on the canopy-sting system can be identified.

5.5.1. Types of Uncertainty.

Generally, two types of uncertainties are encountered during experiments. These are random uncertainties and systematic uncertainties.

(i) Random Uncertainty.

Random uncertainties have an equal chance of being positive or negative. These can be caused by:

(a) the sensitivity of the measuring instruments;

(b) a particular measurement not being reproducible by repetition of the experiment;

(c) scatter in the data; e.g. external interference.

Such uncertainties may be revealed by repeated observation of a particular quantity. This procedure also helps to reduce its effect.

(ii) Systematic Uncertainties.

These uncertainties cause a set of measurements to be spread about a value other than a true value. They are caused by:

(a) instruments having an uncertainty about their zero reading;

(b) incorrect calibration;

(c) the observer persistently performing a wrong action during experimentation, e.g. continually starting a stopclock five seconds late.

Systematic uncertainties are not revealed by repeated measurement, but may be eliminated or corrected by:

(i) varying the conditions of the measurement;

(ii) suitable treatment of the observations.

The uncertainties in the values of the tabulated coefficients; C_D, $\partial C_N/\partial\alpha$, k_{11}, and k_{33}, are revealed by the two processes of measurement and analysis. Uncertainties in the process of measurement depend on the accuracy with which equipment has been calibrated, in particular the strain

gauges and accelerometer. Uncertanties which arise during analysis depend on the amount by which data are scattered. Such scatter may be due to external interference.

5.5.2. Uncertainties due to Measurement

During the process of data retrieval the data equivalent count is transformed into a measurement of force expressed in Newtons, and acceleration expressed in $m \cdot s^{-2}$. This transformation involves the use of calibration factors. These are obtained during calibration of the sting and accelerometer by the method described in section 4.3.1.

A given set of strain gauge calibration parameters determined after a particular batch of tests may be different to the strain gauge parameters which were determined immediately before that batch of tests commenced. This is because the sting and strain gauges may change their characteristics through use.

Thus, for test runs conducted between calibrations, it is not known if the data obtained are relavent to the state of the sting and strain gauge system associated with calibration parameters obtained prior to such tests, or calibration parameters obtained after such tests. Therefore, during analysis of such batches of tests, a mean value of the initial and final calibration parameters is employed. The standard deviation of these calibration parameters, is used as a measure of their associated uncertainty. This particular uncertainty is classed as systematic for the purposes of the

current work. Later in this section using the symbol δf, it will be treated according to the occurrance of the force term in Morison's equation.

The data provided by the accelerometer when subjected to analysis provided both an acceleration signal, and in its integrated form, a velocity signal. The measurement of velocity by this method corresponded to independent measurement of the unsteady velocity according to the pre-determined oscillational parameters for period and amplitude.

Over the entire test programme the characteristics of the accelerometer were consistent. However, the velocity signal during initial analytic trials was observed to steadily decrease throughout a run. This reduction in the velocity did not coincide with other independent measurements of both the oscillation test rig and towing carriage velocities. Apart from faulty manufacture or damage during use, a possible reason for this negative trend in the velocity data may be that the accelerometer mounting was inclined to the vertical. This would have the effect of introducing a correspondingly small component of gravity. Such an effect may be classified as a systematic error. As a result of this systematic uncertainty, the trend which occured in the velocity measurement was equivalent to approximately 1/2 % of 'g', corresponding to less than one degree of error in the accelerometer mounting, which was required to be at ninety degress to the vertical. The computer program used in

analysis, listed in Appendix II, corrected the accelerometer signal for this systematic effect before analysis commenced.

5.5.3. Uncertainties in Analysis due to Scatter.

The data obtained from these tests was done so in an environment prone to electrical noise and mechanical vibration.

In similar tests conducted by Polpitiye (26), electrical interference was experienced, which manifested itself in the form of spikes in graphs of the data. Thus, during the present series of test programmes all electrical leads used screened cable for conducting signals between strain gauges, the accelerometer, and their respective amplifiers. Once amplified, force and acceleration signals were less susceptible to interference from electrical sources, but were nevertheless passed from the amplifier to the computer along a further length of screened cable.

The only significant interference of an electrical nature to occur during these tests was that of the wheel interupt signal with the force channels. Once detected the resulting spikes were removed from the data prior to analysis.

The biggest source of interference giving rise to noise and hence scatter in the data was mechanical vibration.

Mechanical vibration of the sting mechanism causes extraneous effects which are detected by the strain gauges. Sting vibration is at its strongest when no canopy is attached. When the canopy is stable in pitch fitting it to

the sting is observed during testing to dampen sting vibrations. Small porous canopies in steady motion perform best in this respect tending to have a small amount of vibration present in the sting compared to that occuring when large imporous canopies are flown. The highest amount of sting vibration is observed to occur when large canopies are flown, this is due to using a longer sting which requires extra stiffness to reduce vibration to the same levels as the shorter stings used with the small canopies.

Mechanical vibration of the towing carriage as it travels along the ship tank causes jolting which is detected by the accelerometer. This is mainly due to the steel wheels running over joints in the railway, and to a lesser extent interference is also caused by operation of the oscillation mechanism during unsteady motion tests.

The result of these extraneous sources of vibration is a signal which, in the case of acceleration, is scattered about a locus describing the sinusoidal motion, and in the case of force data, a signal which is generally a smooth curve but prone to occasional spikes, and mild deviations. When converted to a two-parameter form of Morisons equation the spikes present in the force signal are clearly visible, as clusters of data points. These, shown in Fig. 5.1, have been found to be caused by the interference of the wheel interupt signal and were removed prior to analysis.

5.5.4. Processing Uncertainties

(i) Unsteady Motion

The following statistical analysis to determine possible uncertainties due to noise was performed.

During analysis data were examined in batches, ten batches per run yielding ten pairs of force parameters.

A further statistical analysis was performed on the resulting ten pairs of slope and intercept parameters. This provided the mean coefficient values, either C_D and k_{11} for axial motion or $\partial C_N/\partial\alpha$ and k_{33} for lateral motion. The resulting standard deviation was used to measure the uncertainty in values gained for the force coefficients due to scatter. These random uncertainties were then combined with the sytematic uncertainties due to measurement to give the overall figure as listed in the results tables of Chapter 4.

The scatter calculated using the least squares method was a root-mean-square measure of the scatter of data from the best fit straight line, expressed in units of the vertical axis in Fig 5.2 representing F/V. Therefore, this is the standard-deviation associated with the intercept on the vertical axis. This intercept is the parameter which yields the added mass coefficient and is shown in Fig 5.1.

The deviation in the value of the parameter defining slope, from which the coefficients C_D and $\partial C_N/\partial\alpha$ may be obtained, was determined by finding possible maximum and

minimum values of the slope according to the value of the standard deviation associated with the intercept parameter. This meant that most of the data could be enclosed within an area bounded by these possible lines defined by the maximum and minimum values of slope.

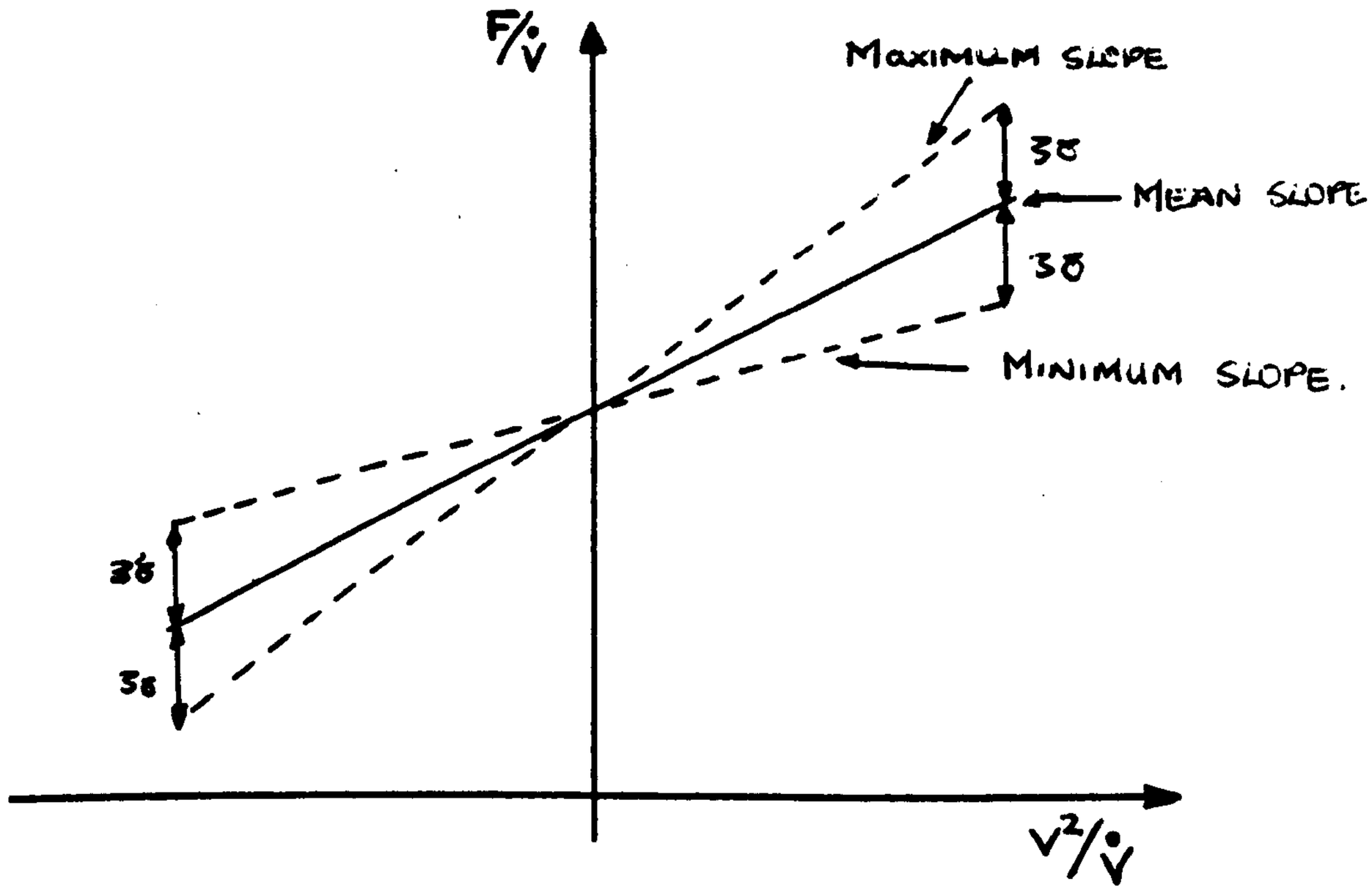

Fig 5.2. Scatter Enclosed by Maximum and Minimum Slopes.

The difference between the mean slope and both the maximum and minimum slopes was found, and this difference provided a value for the deviation in the slope and thus the velocity dependent force coefficient, for each individual batch of data. The process of determining deviations in the slope and intercept for the data was repeated for each batch of data analysed for each run.

This consistently produced low deviations characteristically 2% for velocity dependent force coefficients, but high deviations characteristically 30% for added mass coefficients.

(ii) Steady Motion

Since the equation for steady state motion does not

involve the determination of two independent parameters, the data for steady state motion was not subjected to a least squares analysis. For steady motion, ten blocks of data per run were analysed, from which were obtained ten values of velocity dependent force coefficient, either C_D or C_N for axial or lateral forces respectively. An analysis was then performed on these values to determine their mean values and their standard deviations. The systematic uncertainties associated with the equipment were combined with the uncertainty due to scatter as for the unsteady motion.

Systematic uncertainties associated with the various pieces of equipment were estimated and are tabulated below.

Table 5.5.1. Systematic Uncertainties.

Source	Uncertainty	Symbol
Sting System.	≃ 3 %	δf
Accelerometer.	≃ 1/2 %	δa
Oscillatory - Amplitude.	≃ 1 %	-

Consistent values were obtained for the velocity dependent force parameter yielding C_D and $\partial C_N/\partial\alpha$, for both unsteady and steady motion. For unsteady motion the acceleration dependent force parameter 'b' which yields k_{11} or k_{33} gave relatively inconsistent sets of values. There is a greater amount of scatter present in the data as exhibited by the least squares method when determining the added mass coefficients and this reflects the approximate nature of equation 5.1, on which the analysis is based.

5.5.5. Formulae.

The combining of uncertainties in accordance with the form in which Morison's equation was applied, is set out below. The formulae used in the determination of the least squares fit and the subsequent deviations due to scatter for both slope and intercept, are detailed in Appendix I.

Given the governing equation of motion:

$$F(t) = a \cdot V^2 + b \cdot dV/dt,$$

where the velocity 'V' is a function of time and the parameters 'a' and 'b' are to be determined; the systematic uncertainties associated with the force F and the acceleration dV/dt are expressed as δF and δa respectively. The function describing unsteady velocity is obtained by integration of the acceleration data, thus:

$$V = \int [\ \dot{V}\ ] \cdot dt.$$

Inclusion of the uncertainty from the accelerometer measurement introduces δa;

$$V = \int [\ \dot{V} + \delta a\ ] \cdot dt = \int [\ \dot{V}\ ] \cdot dt + \int [\ \delta a\ ] \cdot dt.$$

The uncertainty 'δa' in the accelerometer which gave rise to the trend in the velocity signal was eliminated during analysis. Since this trend was small yet still detectable, being equivalent to 1/2 % of 'g', it may be assumed that any

further systematic error in the accelerometer was negligible.

The main source of uncertainty in these tests which affected the accelerometer signal arose from mechanical vibration which caused scatter and hence random uncertainty in the results. The sting and its attached strain gauges are also affected by mechanical vibration. Combining systematic uncertainties and those due scatter produces an overall uncertainty '$\Sigma\delta$' as shown below.

Given the two parameter form of Morison's equation;

$$F/\dot{V} = a \cdot V^2/\dot{V} + b,$$

there are systematic uncertainties δF present in the force signal and random uncertainties due to scatter which give;

$$\Sigma\delta. = \delta f + \text{Scatter}.$$

The figure $\Sigma\delta$, is that displayed in the Tabulated Results. It varies from 10% to 40% for the added mass coefficients, and from 5% to 25% for the velocity dependent coefficients, depending on the size of the canopy. See section 5.2.

Summary

This chapter has described the method of data analysis, the results obtained from these tests, and the cause and treatment of uncertainties that arise from the analysis.

The largest cause of uncertainty has been that due to mechanical vibration. Thus, results were subject to relatively large amounts of random uncertainty compared to systematic uncertainties associated with the experimental equipment.

For the large canopy models the results show a marked increase in random uncertainty over those for the small canopies. This is caused mainly by scatter as a result of the increased vibration of the canopy mounting.

Trends in the results indicate relations between both the axial added mass coefficient k_{11} and the velocity dependent force coefficient C_D in unsteady motion with the Keulegan-Carpenter number K_C. This and other observations will be discussed further in the following chapter.

CHAPTER 6

6. DISCUSSION OF RESULTS

Introduction

This chapter contains a discussion of the results obtained from the test programme, and their implications. A comparison is made betweeen the results of the experiments which the author conducted in 1986 and 1987. The necessity for testing the relationship between the axial added mass coefficent k_{11} and the Keulegan-Carpenter number K_C for a range of parachutes is then discussed, based on the results of the tests performed in 1986 and 1987. This was the subject of investigation in the 1988 test programme, the results of which are represented graphically with relavent points inserted for the corresponding values obtained previously, during 1986 and 1987.

Comparison is then made between steady-state results obtained from this programme of research and results obtained from wind-tunnel work conducted by Shen and Cockrell (39), and the analytical model put forward by Frucht (36).

Recommendations for any future research which might continue from this work are made. Conclusions are then presented.

6.1 The Velocity Dependent Axial Force Coefficient C_D.

With the exception of the Medium Porosity Cruciform Canopy in unsteady motion and the Ribbon Canopy in steady motion, the results for the velocity dependent drag coefficient C_D from the 1986 and 1987 test programmes demonstrate that values for C_D are consistently higher in the 1987 tests in which large canopies were used, for both steady and unsteady motion. The amount by which these values are greater varies.

For steady-state tests C_D is 25% higher in the case of the Hemispherical Canopies, around 10% for the Cruciform Canopies and there is no difference for the Ribbon Canopies. See Table 5.2.1.

For the unsteady motion tests C_D is as much as 50% greater for the large Hemispherical Canopy compared to its value for the small Hemispherical Canopy; it is approximately 20% greater for the large Cruciform Canopies; and virtually no different for the Ribbon Canopies. See Table 5.2.3.

That the above effects may be due to blockage of the ship-tank would explain the consistently higher C_D values for the large canopy tests. Blockage has been corrected for in the tabulated results, see section 5.2. In the case of the larger canopies the blockage is four times greater at approximately 4% of the ship-tank cross-sectional area, than that of the small canopy models which block the ship-tank by approximately 1% of its cross sectional area.

To account for the effects of blockage, for the tests on large canopies as used in 1987 and 1988, correction was applied to C_D values for these canopies, and is denoted by C_D^* in Table 5.2.1. Maskell's formula (28), shown in equations [4.2] and [4.3] of Chapter 4, was used for this purpose. The small canopies did not block the ship-tank test section significantly. Thus, it has been assumed un-necessary to correct the C_D values for the small canopies as used in 1986 and 1988.

Under conditions of steady motion the velocity dependent force coefficients; C_D without blockage correction, e.g. small canopies, and C_D^* with blockage correction, e.g. large canopy models, show a tendency to remain consistent within the bounds of experimental uncertainty. See Table 5.2.1.

Under conditions of unsteady motion, there is a trend for the velocity dependent force coefficient C_D to decrease with decreasing Keulegan-Carpenter number K_C. This is not a substantial effect, but is consistent over the range of K_C numbers for the small canopies tested. See Tables 5.4.1, and 5.4.6.

For the large canopy models in unsteady motion, mechanical vibration and blockage tend to affect the accuracy with which the velocity dependent force coefficient is determined. However the values for C_D^* in Tables 5.4.7 to 5.4.12 suggest, as is the case for small canopies, that increasing the Keulegan-Carpenter number K_C, causes the velocity dependent

force coefficient, in this case C_D^*, to increase as well.

Table 6.1. A Comparison of the Velocity Dependent Force Coefficient C_D in Conditions of Both Steady and Unsteady Motion. For uncertainties and porosities see Tables 5.2.1 and 5.2.3.

Canopy	Size	C_D (Unsteady)	C_D (Steady)
Hemispherical Imporous	Small Large	0.64 0.81	0.61 0.69
Ribbon	Small Large	0.52 0.47	0.51 0.47
Cruciforms Arm Ratio 3:1			
Imporous	Small Large	0.68 0.70	0.64 0.58
Medium Porosity	Small Large	0.70 0.60	0.71 0.65
High Porosity	Small Large	0.67 0.68	0.66 0.64
Cruciform Arm Ratio 4:1 Imporous	Small Large	0.76 0.67	0.77 0.69

Using the definition of Keulegan-Carpenter number K_C where;

$K_C = \hat{U}T/D_o$, and '$\hat{U}$' the oscillatory amplitude is given by;

$$\hat{U} = \omega \cdot R = (2\pi/T) \cdot R,$$

then the expression for K_C reduces to:

$$K_C = 2\pi R/D_o.$$

Thus unsteady motion may be denoted by a finite value of K_C for which the amplitude of oscillation 'R' also has a finite value, steady motion occurs without oscillation for which 'R' is equal to zero, and thus $K_C = 0$.

Table 6.1 above shows that values of C_D obtained from unsteady motion tests are generally higher, when compared to their equivalent coefficients obtained from steady motion tests.

6.2 The Stability Parameter $\partial C_N/\partial\alpha$.

To determine values for the stability parameter $\partial C_N/\partial\alpha$, at zero angle of attack $\alpha = 0°$ under conditions of both steady and unsteady flow, measurements of lateral force with variation in angle of attack α, were recorded. Comparison of the values for this parameter across the range of both steady-state and unsteady-state experiments conducted during 1986 and 1987 presents anomalies. These are apparent when comparing the values in Table 5.2.2 with those in Table 5.2.4, and may be due to the reasons outlined below.

(i). The range over which the angle of attack α varied was different, according to whether the motion was unsteady or steady.

For unsteady motion, α was typically in the range -12° to +12°. For this range an average value of $\partial C_N/\partial\alpha$ at $\alpha = 0°$, is obtained. Under steady flow conditions, the results for $\partial C_N/\partial\alpha$ about $\alpha = 0°$ were obtained for α in the range -5° to

+5°. This is the value for the slope in this range in the graph of steady state motion shown below; Fig 6.1. Assuming this graph describes the variation in the lateral force

Fig 6.1. Velocity Dependent Lateral Force Coefficient C_N vs. Angle of Attack α. Data points obtained from steady state tests. See Table 5.2.2.

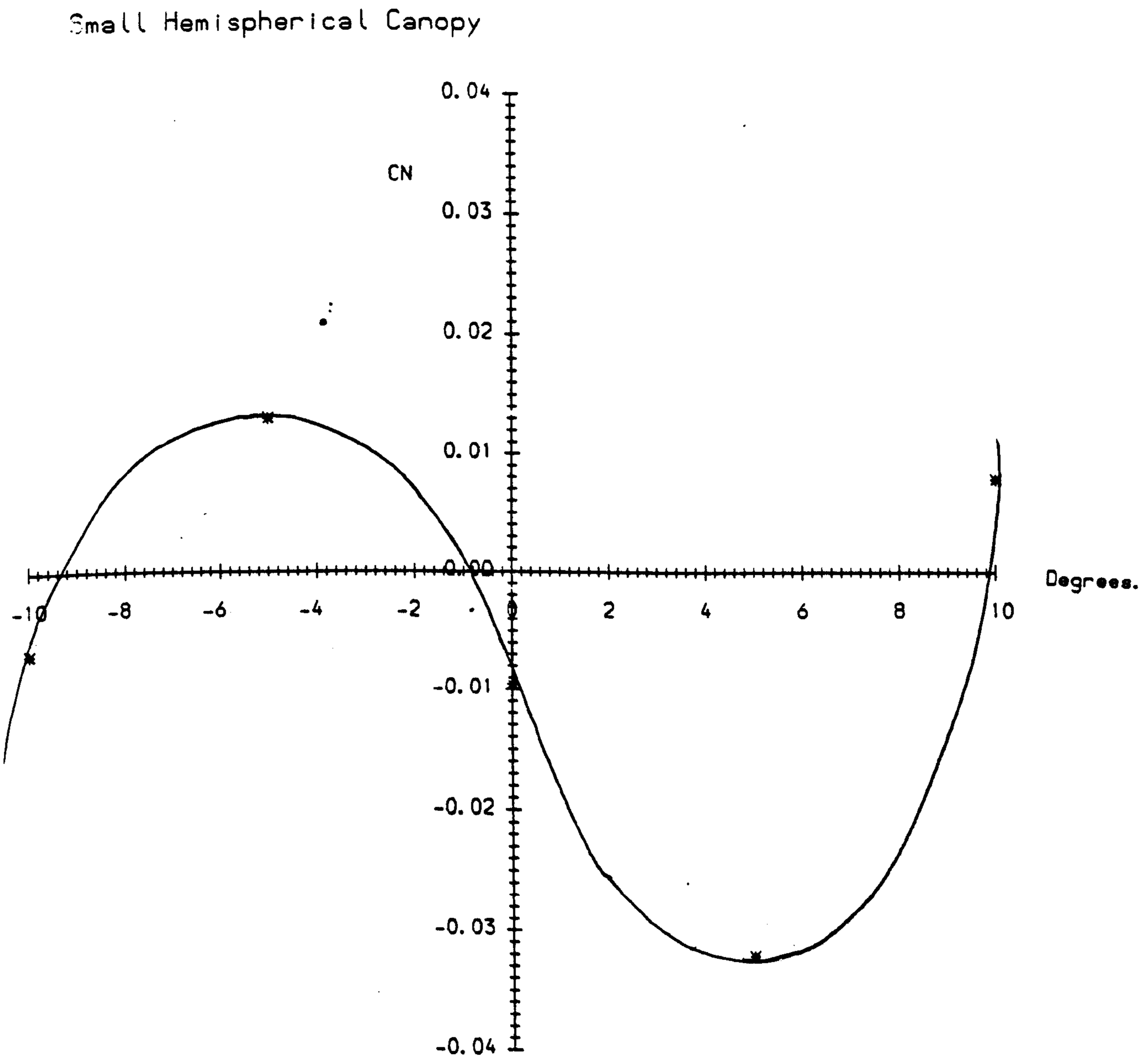

coefficient for unsteady tests as well, then, it shows how a mean value for $\partial C_N/\partial\alpha$ in the range -5° to +5° is different to that obtained for the range -12° to +12°.

(ii). An inflated cruciform canopy may vary its flying orientation as a result of rotation during a test run, or there may be inconsistencies occuring in orientation as a result of attaching the model to the sting at the beginning of each run. Variation in rotational orientation of the cruciform canopies can result in different lateral forces. The size of the lateral forces due to this effect depends on whether the arms of the canopy, or the gap between arms, was present in the plane of oscillation.

During tests in the ship tank cruciform canopies were observed to rotate, leading to random differences in the lateral forces.

The two reasons (i) and (ii) above may account for the inconsistencies in results for $\partial C_N/\partial\alpha$ at $\alpha = 0°$, between different canopies in conditions of both steady and unsteady motion.

Similarly application of these results may prove incorrect when considering a full scale cruciform parachute during descent, undergoing variation in pitch, since it is also subject to rotation. However prevention of cruciform canopy rotation is difficult to achieve, both for full-scale flight and for model tests.

6.3. The Axial Added Mass Coefficient k_{11}.

The values of the axial added mass coefficient k_{11}, shown in Table 5.2.3, are consistently smaller for the large model canopies tested in 1987, compared to the values obtained for the smaller model canopies tested in 1986. Typically this difference amounts to the k_{11} values from the 1986 test programme being approximately eight times larger than k_{11} values obtained in 1987. Since k_{11} is a coefficient, it is improbable this anomally is due to the larger dimensions of the canopies tested in 1987 when compared to those of the canopies tested in 1986. This is demonstrated by the dimensional dependence statement of Chapter 4, equation [4.1], where;

$$k_{ij} = f\{ \text{Shape, Reynolds Nº} \}.$$

The independence of the added mass coefficient on canopy dimensions is also demonstrated by the expression for the added mass coefficient k_{ij} as used during analysis, which accounts for the nominal volume V_o of the canopy, which contains a mass α_{ij} of fluid of constant density ρ;

$$k_{ij} = \alpha_{ij}/\rho \cdot V_o.$$

Similarly it is unlikely that the minor structural differences between models, such as construction and variation of rigging line type would have such an effect on

the size of k_{11}. The Reynolds number did not vary substantially, neither did the C_D values between both steady and unsteady flow. This evidence indicates that anomalies in the values of k_{11} may have been due to some dimensionless parameter associated with the unsteady motion. The results of the 1988 test programme show this parameter to be the Keulegan - Carpenter number K_C. See Tables 5.4.1, to 5.4.6, and Tables 5.4.7, to 5.4.12.

6.4. The Lateral Added Mass Coefficient k_{33}.

The lateral added mass coefficient k_{33} in Table 5.2.4, also exhibits differences between the two sets of canopies tested in 1986 and 1987. For the rotationally symmetric models such as the Hemispherical and Ribbon Canopies, the results obtained from 1986 using small canopy models are respectively ten and three times greater than the results subsequently gained in 1987 using equivalent larger canopy models. The Cruciform Canopies of both three and four to one, arm ratios do not show an equivalent trend in their values for k_{33}. Thus, the trend for cruciform canopies is for there to be little difference in k_{33} values when testing different sized canopies in conditions of unsteady lateral motion.

When examining the results for the cruciform canopies, it may be that the value assumed by k_{33} is dependent on canopy orientation. Thus, results for unsteady motion may be different and difficult to apply to full scale descent for the same reasons that results for $\partial C_N/\partial\alpha$ about $\alpha = 0°$ differ.

The results obtained for k_{33} may also be difficult to apply. However tests performed on the rotationally symmetric canopy models i.e. the Hemispherical and Ribbon canopies, are not subject to the variations in k_{33} which are experienced with Cruciform Canopies as a result of random rotation, and thus may provide more reliable data for this type of test.

Comparison of the two different added mass terms indicates that the values for k_{33}, presented in Table 5.2.3, are consistently smaller than those for k_{11}, presented in Table 5.2.4. The application of Lester's equations and of their linearisation by Doherr and Saliaris (23) will be influenced by these values. Doherr and Saliaris stated the importance of identifying appropiate values for k_{33} and k_{11} since for canopies for which $\partial C_N/\partial\alpha$ at $\alpha = 0°$ is small the relative value of these coefficients has a strong effect on the canopy's dynamic stability characteristics.

The Leicester Parachute Performance Prediction Program described by Cockrell (38), can be used to predict the performance of a full scale canopy during descent. This is dependent on the values which are input for the added mass and force coefficients k_{11}, k_{33}, C_T, and C_N. In order to apply this program knowledge of these in unsteady motion is required for the range of canopy types that have been tested.

6.5 GRAPHS OF RESULTS.

6.5.1. Variation of Axial Added Mass Coefficient k_{11} with Keulegan-Carpenter number K_C.

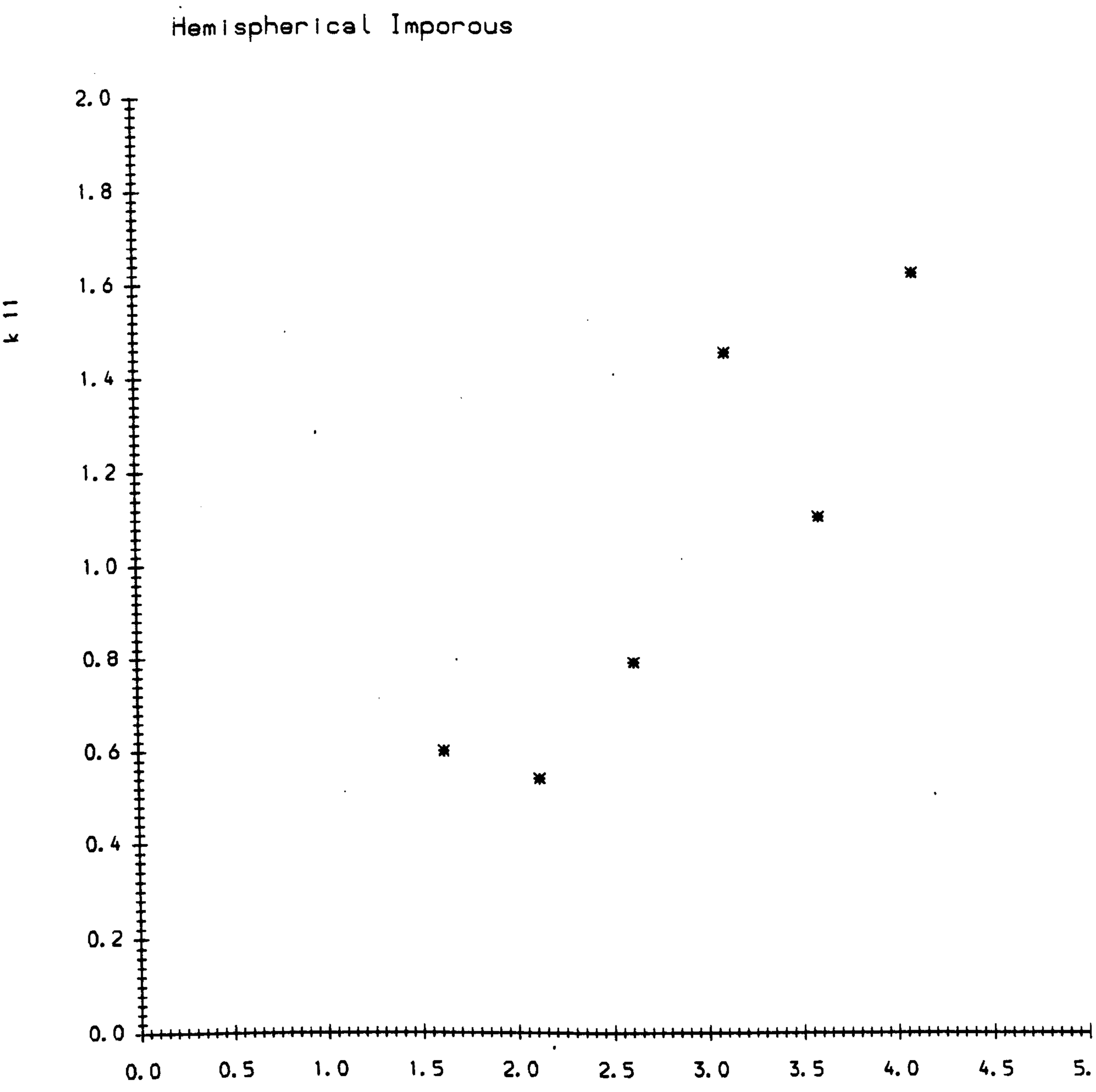

6.5.2. Variation of Axial Added Mass Coefficient k_{11} with Keulegan-Carpenter number K_C.

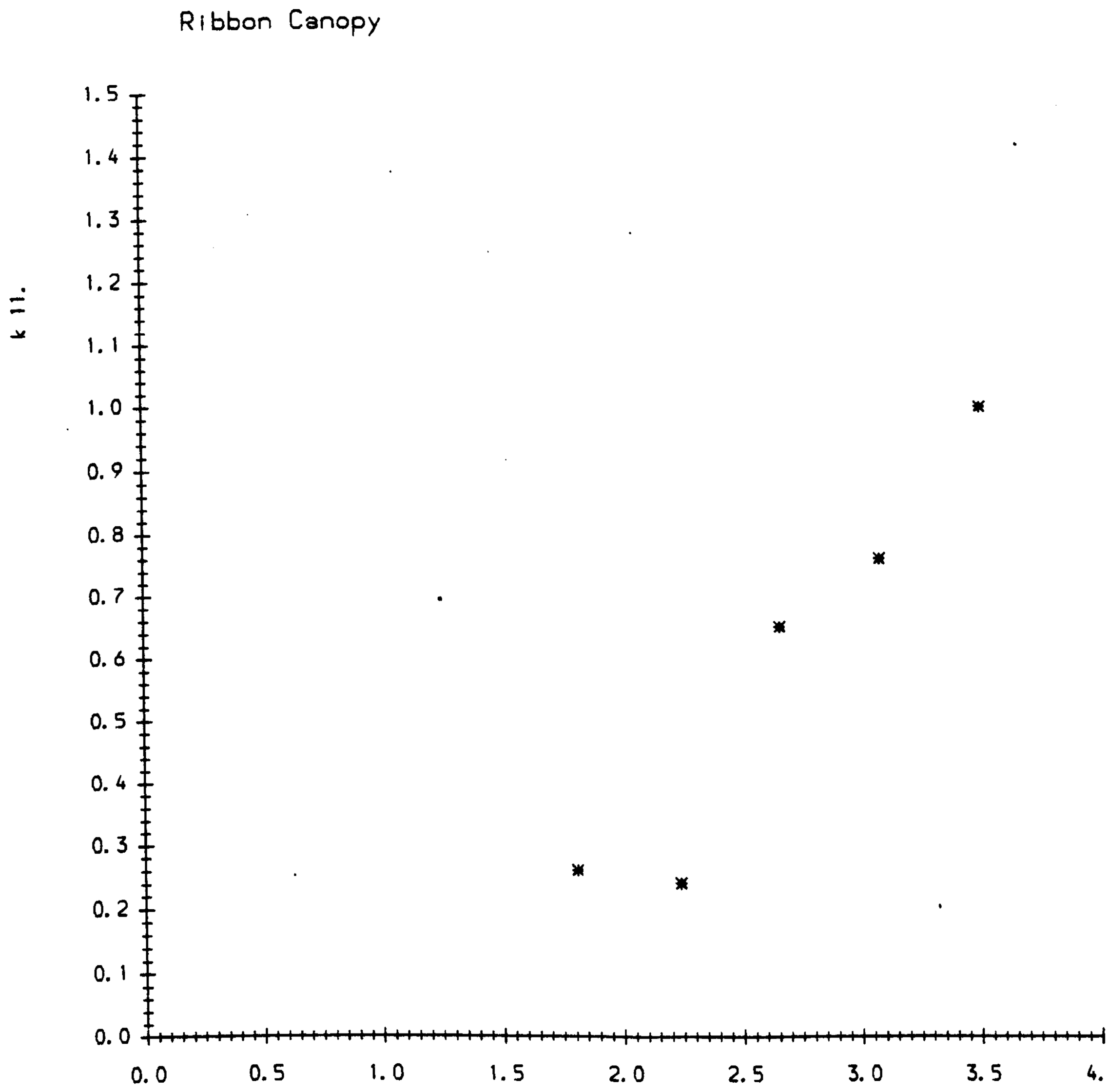

6.5.3. Variation of Axial Added Mass Coefficient k_{11} with Keulegan-Carpenter number K_C.

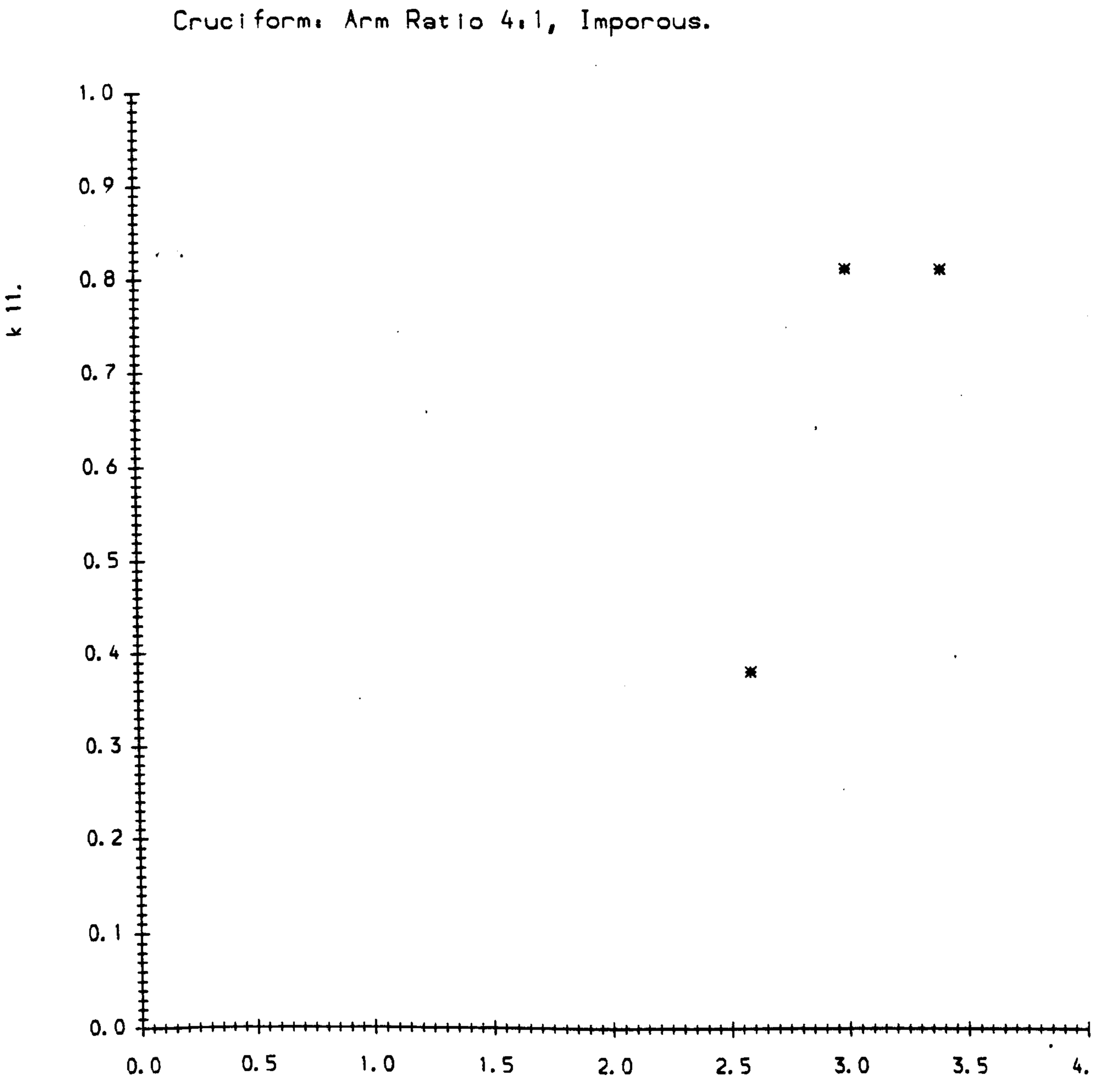

6.5.4. Variation of Axial Added Mass Coefficient k_{11} with Keulegan-Carpenter number K_C.

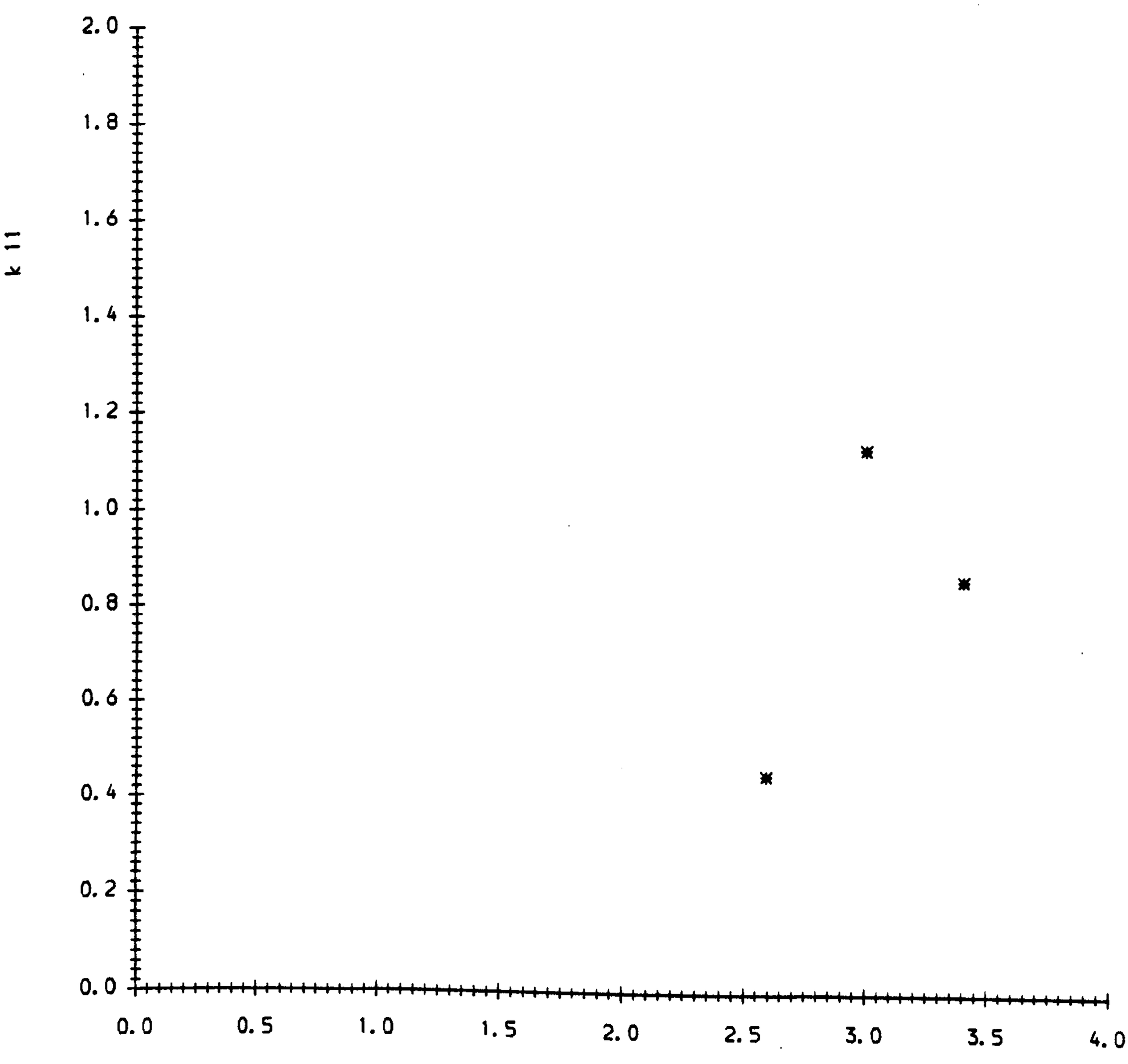

6.5.5. Variation of Axial Added Mass Coefficient k_{11} with Keulegan-Carpenter number K_C.

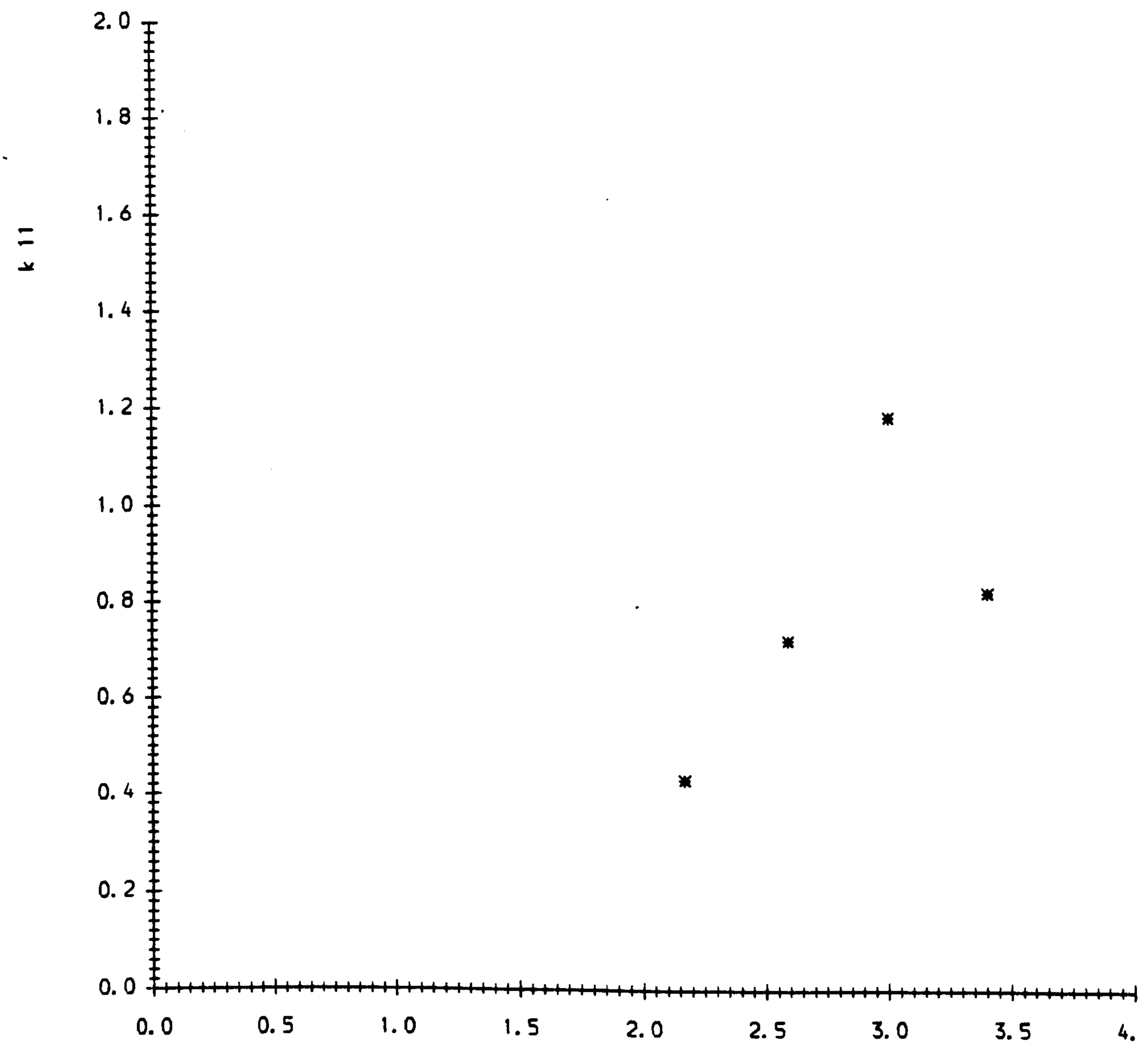

6.5.6. Variation of Axial Added Mass Coefficient k_{11} with Keulegan-Carpenter number K_C.

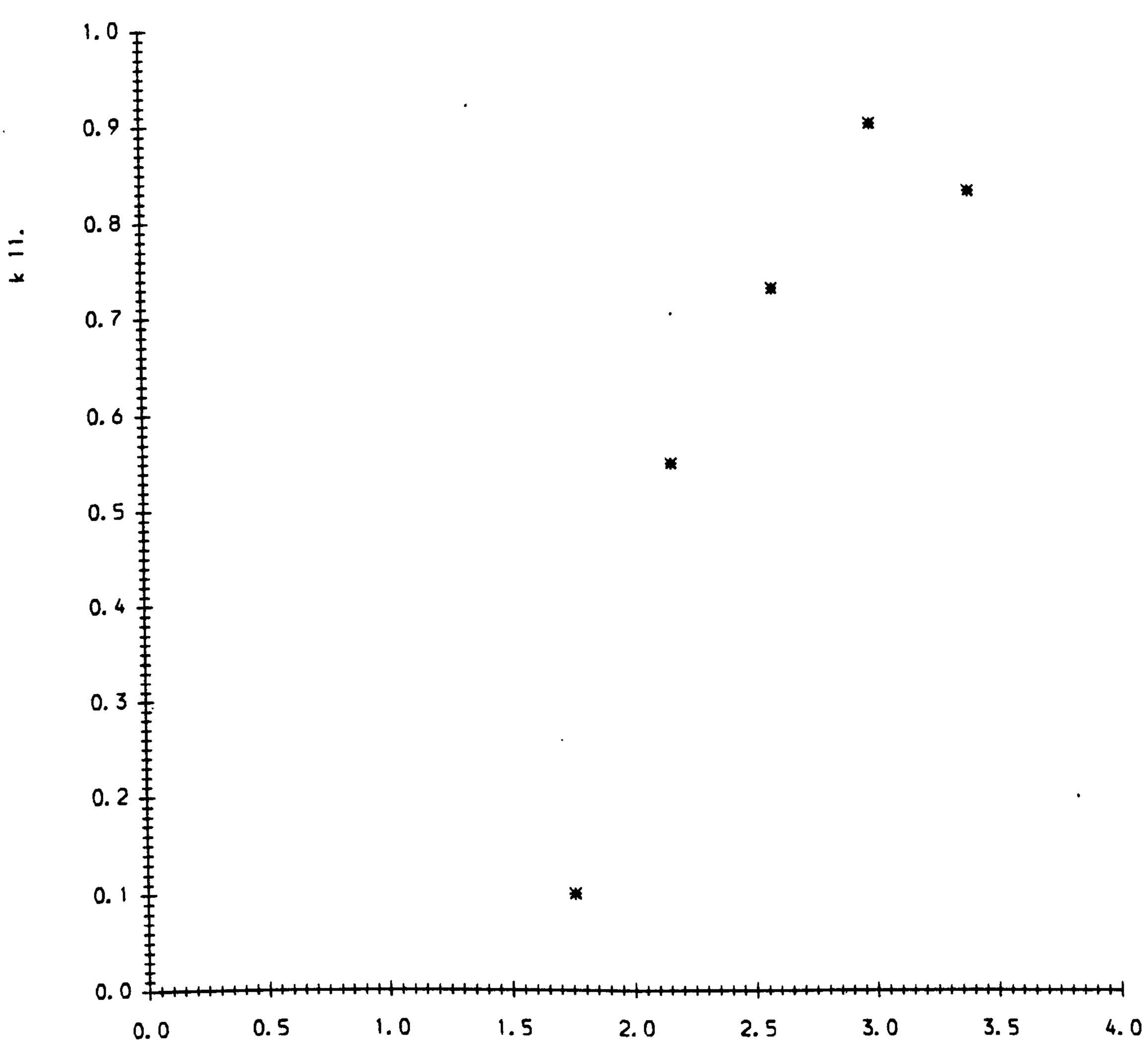

6.5.7. Variation of Axial Force Coefficient C_T with Angle of Attack $\alpha°$ for Steady-State Tests.

Large Ribbon Canopy.

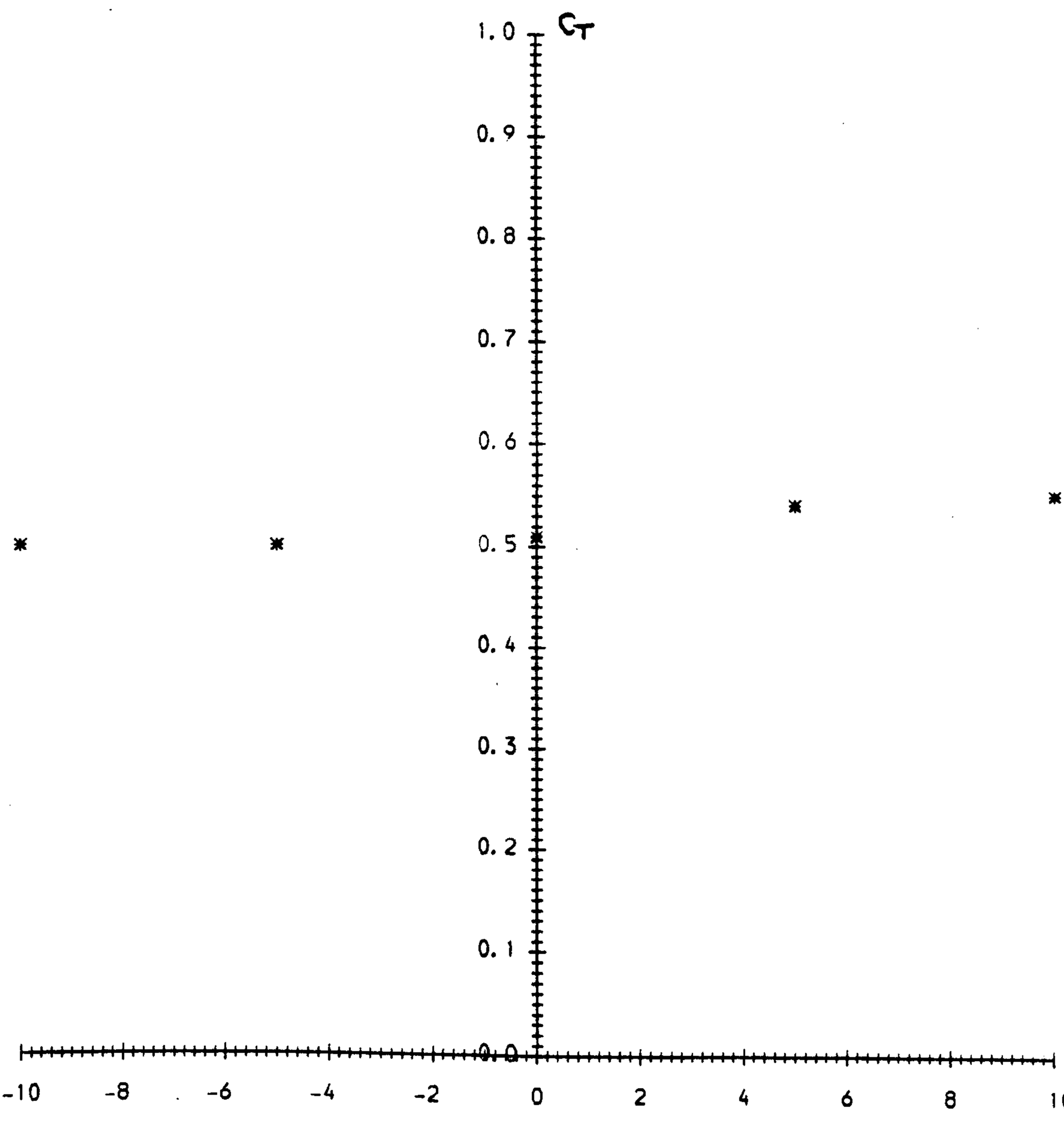

6.5.8. Variation of Axial Force Coefficient C_T with Angle of Attack $\alpha°$ for Steady-State Tests.

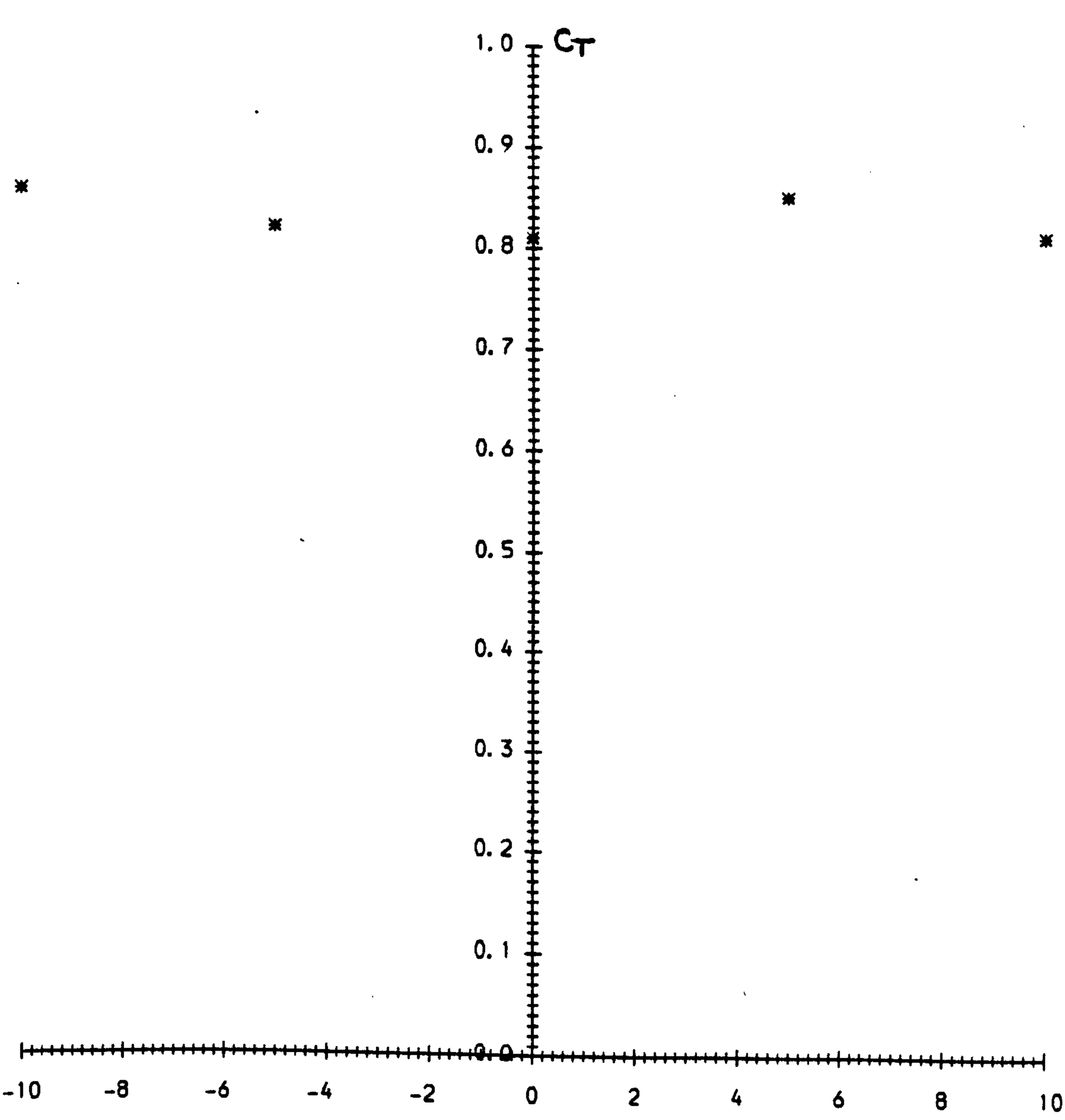

6.5.9. Variation of Axial Force Coefficient C_T with Angle of Attack $\alpha°$ for Steady-State Tests.

Large Cruciform Canopy, 3:1 Arm Ratio. High Porosity.

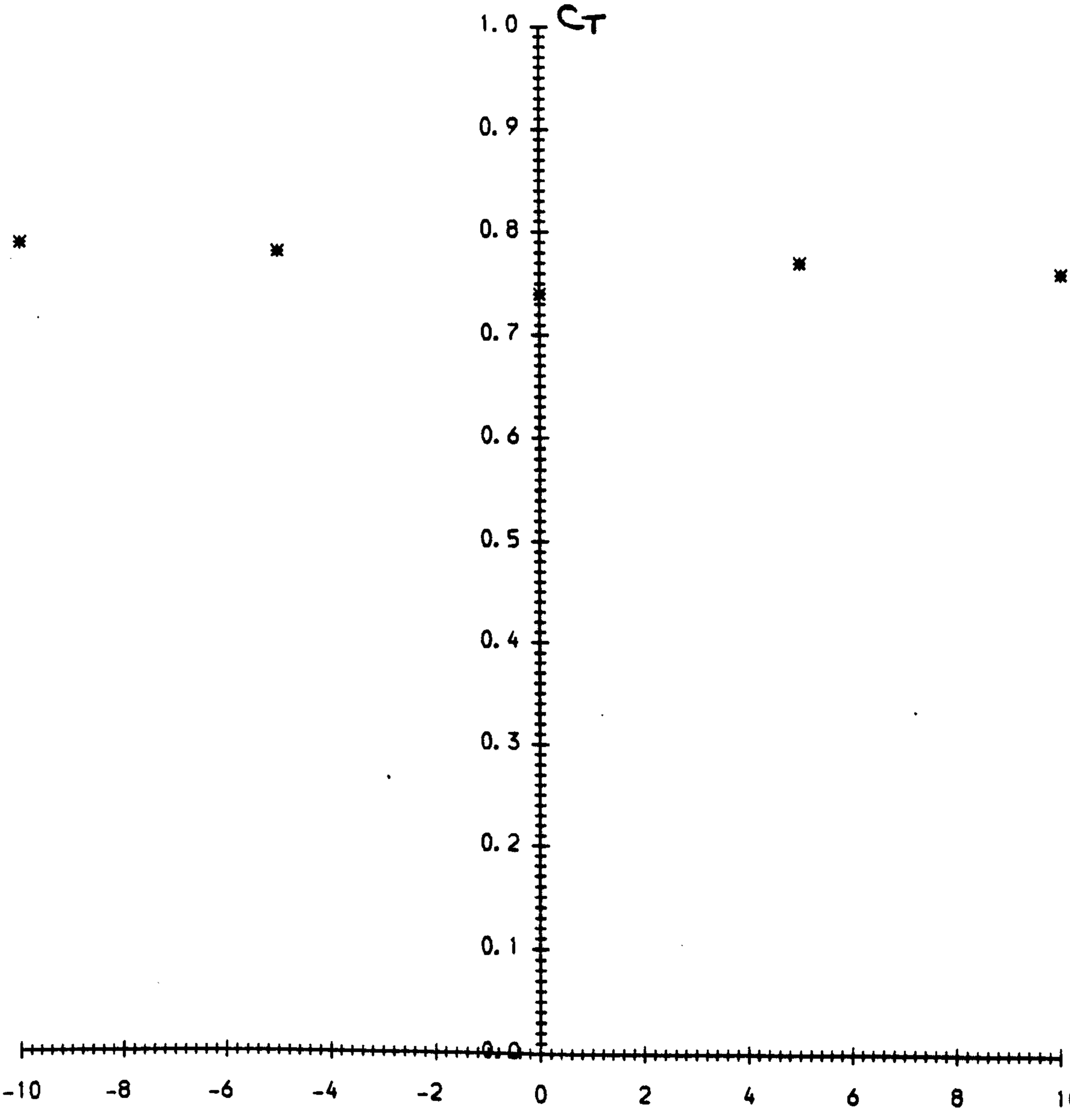

6.5.10. Variation of Axial Force Coefficient C_T with Angle of Attack $\alpha°$ for Steady-State Tests.

Large Cruciform Canopy, 3:1 Arm Ratio. Medium Porosity.

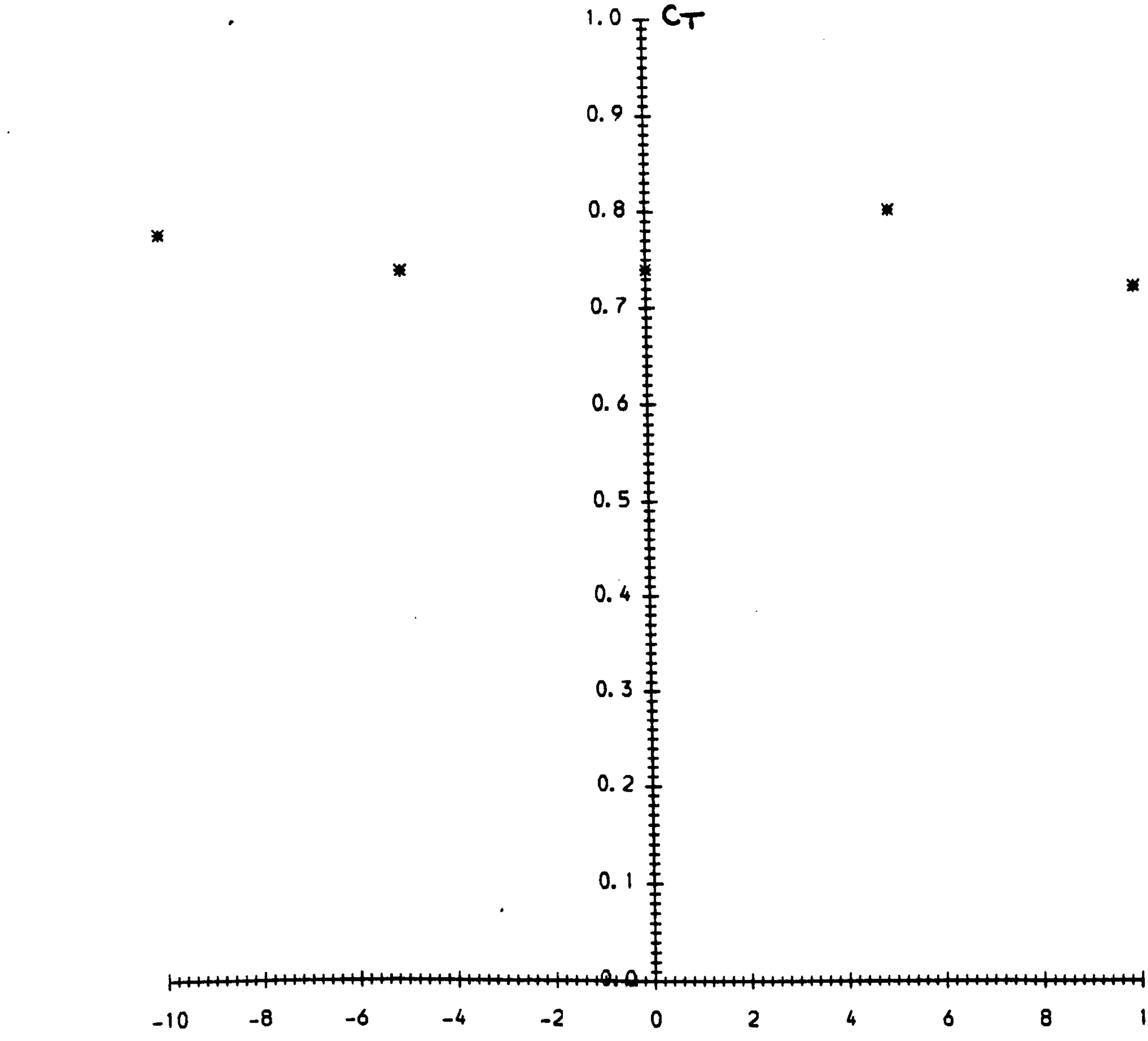

6.5.11. Variation of Axial Force Coefficient C_T with Angle of Attack $\alpha°$ for Steady-State Tests.

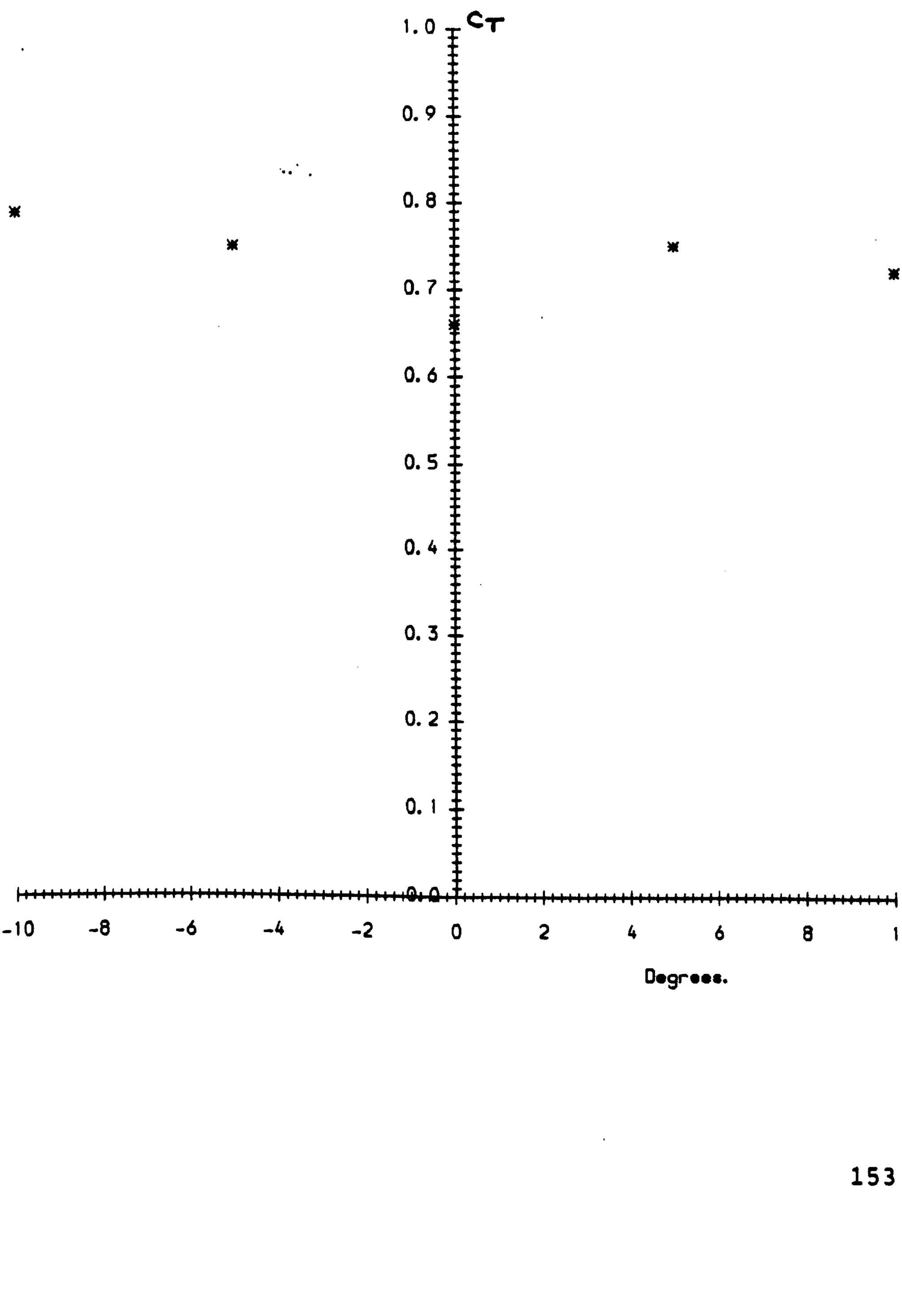

6.5.12. Variation of Axial Force Coefficient C_T with Angle of Attack $\alpha°$ for Steady-State Tests.

Large Hemispherical Canopy. Imporous.

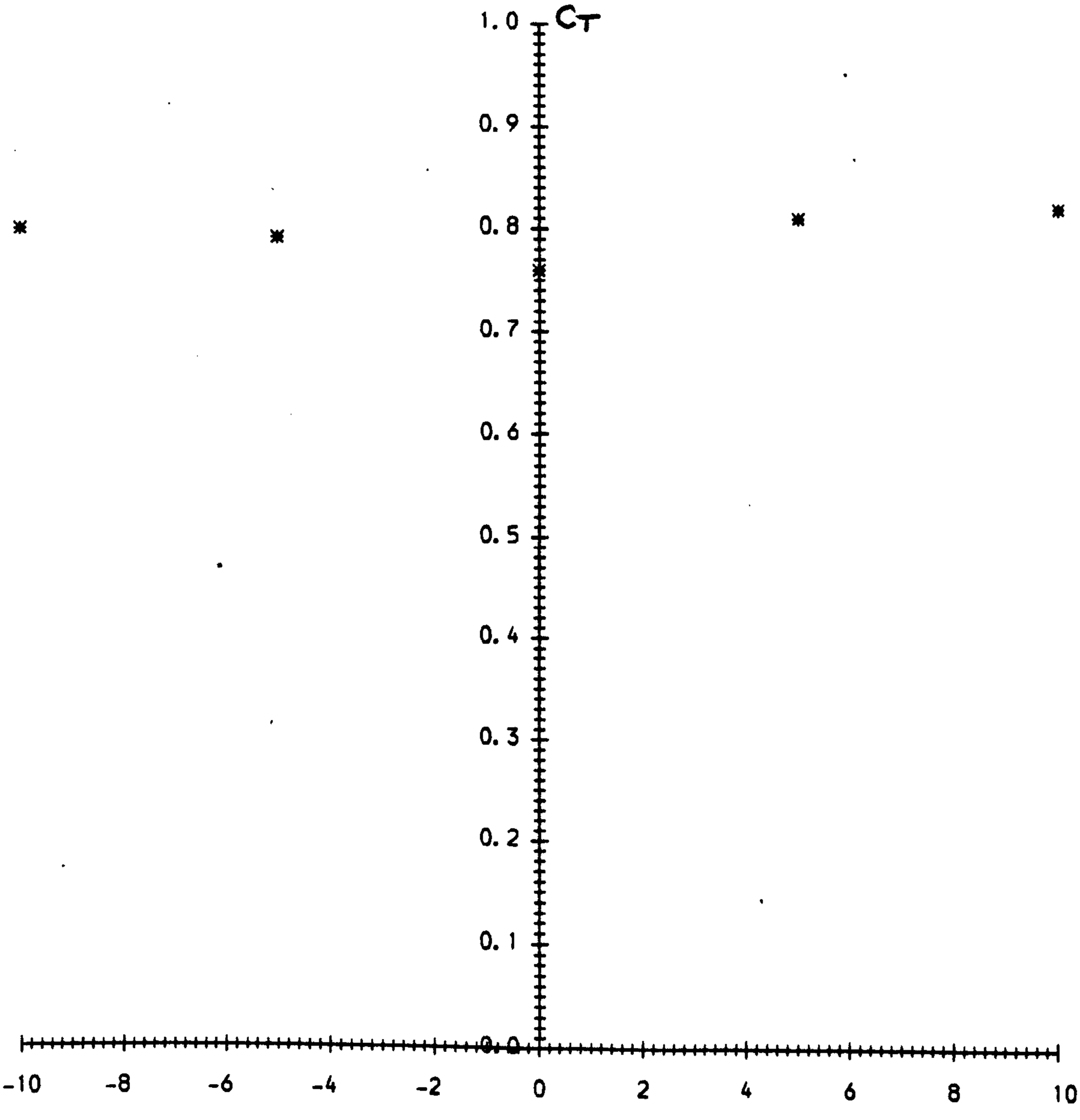

6.5.13. Variation of Axial Force Coefficient C_T with Angle of Attack $\alpha°$ for Steady-State Tests.

Small Ribbon Canopy.

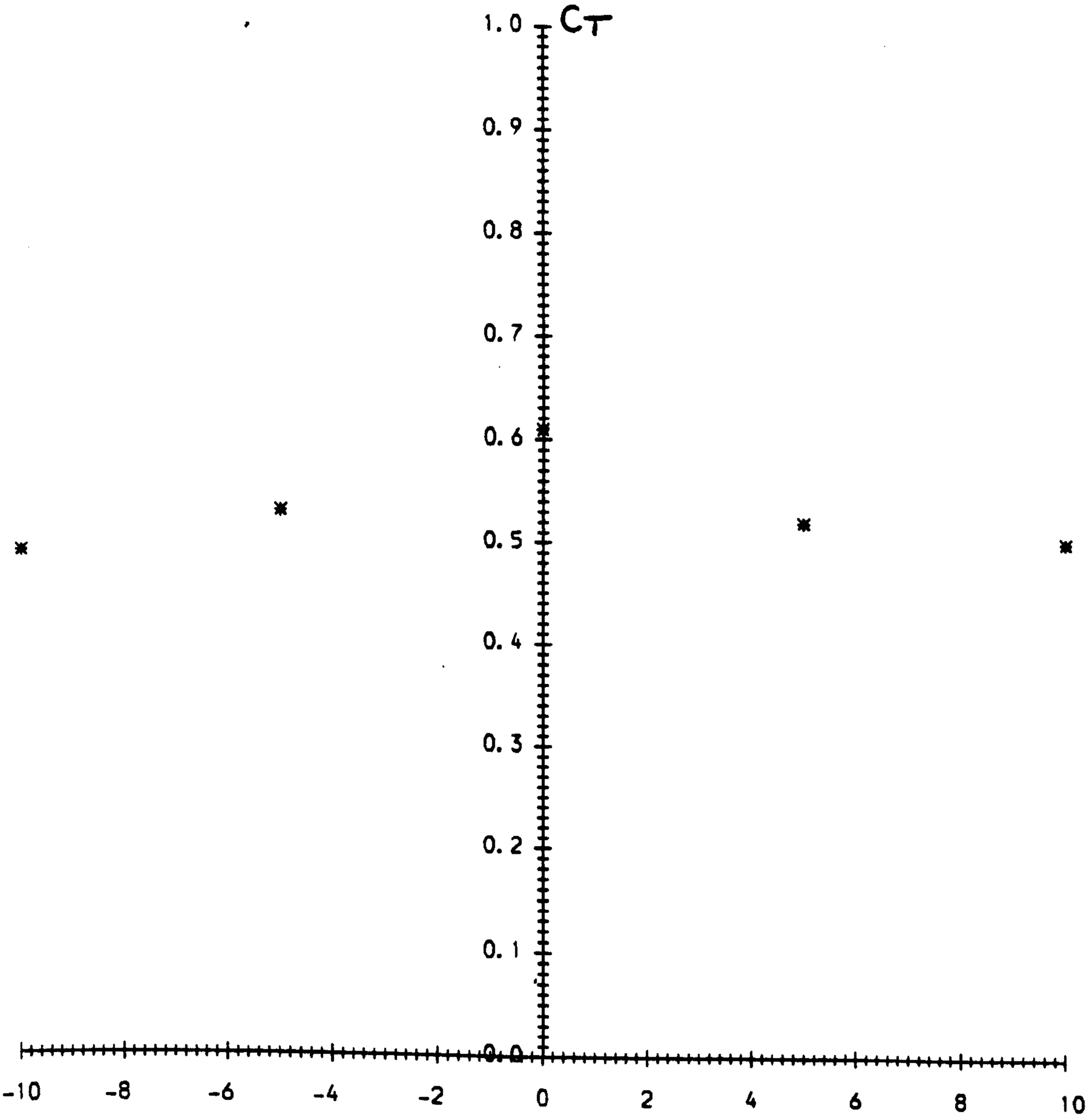

6.5.14. Variation of Axial Force Coefficient C_T with Angle of Attack $\alpha°$ for Steady-State Tests.

Small Cruciform Canopy, 4:1 Arm Ratio. Imporous.

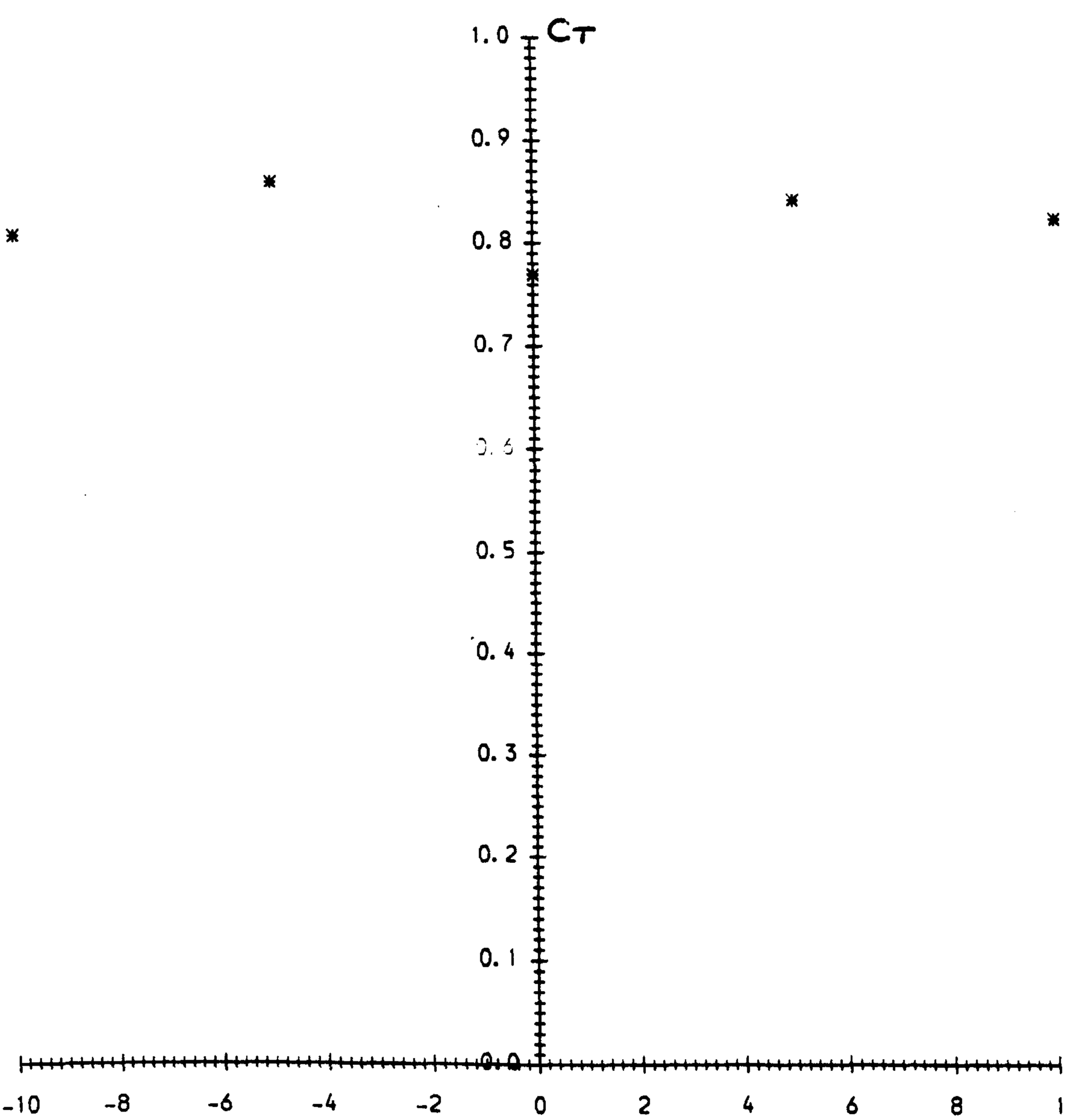

6.5.15. Variation of Axial Force Coefficient C_T with Angle of Attack α° for Steady-State Tests.

Small Cruciform Canopy, 3.1 Arm Ratio. High Porosity.

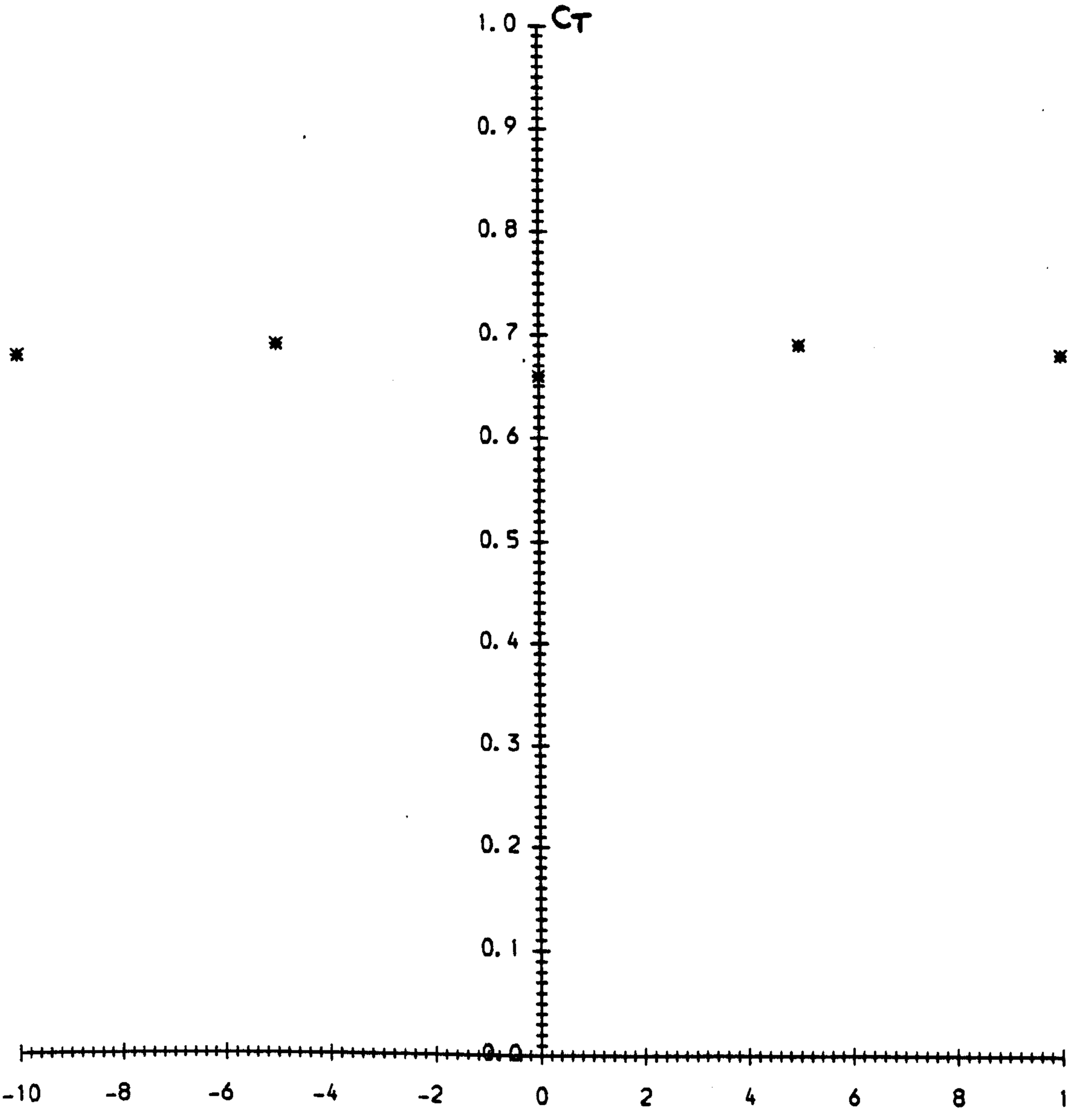

6.5.16. Variation of Axial Force Coefficient C_T with Angle of Attack $\alpha°$ for Steady-State Tests.

Small Cruciform Canopy, 3.1 Arm Ratio. Medium Porosity.

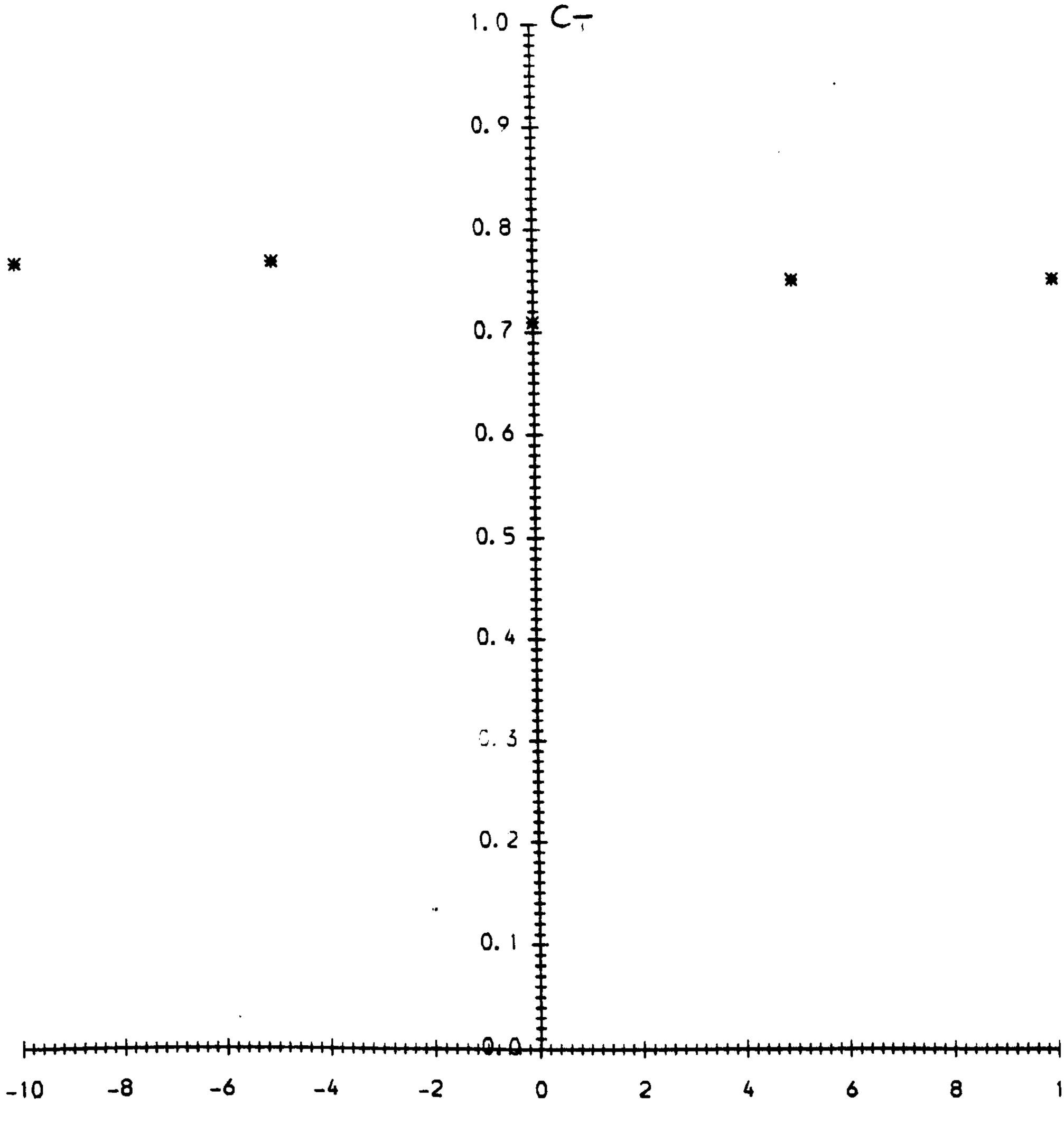

6.5.17. Variation of Axial Force Coefficient C_T with Angle of Attack $\alpha°$ for Steady-State Tests.

Small Cruciform Canopy, 3.1 Arm Ratio. Imporous.

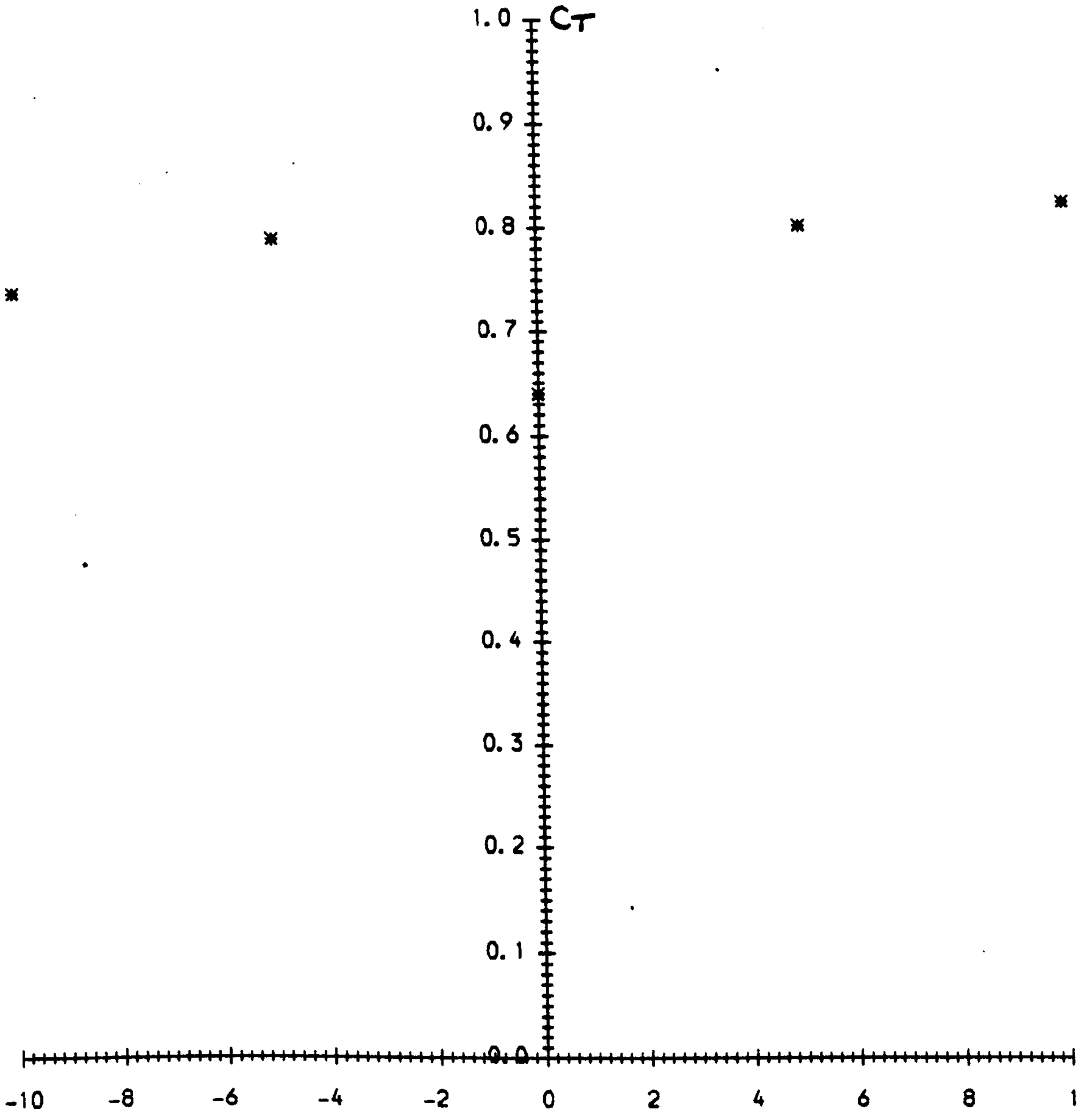

6.5.18. Variation of Axial Force Coefficient C_T with Angle of Attack α° for Steady-State Tests.

Small Hemispherical Canopy. Imporous.

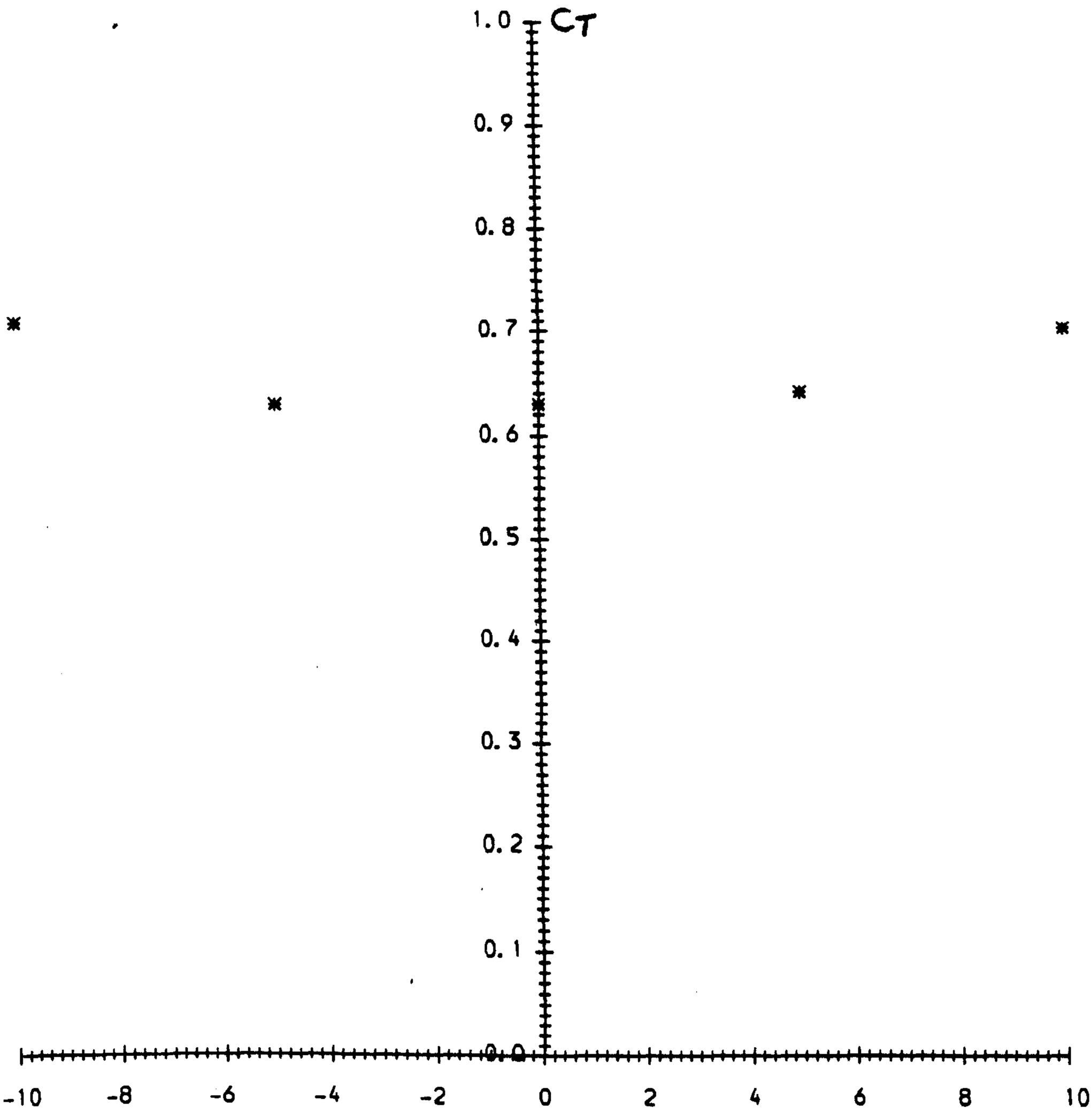

6.5.19. Variation of Normal force Coefficient C_N with Angle of Attack $\alpha°$ for Steady-State Tests.

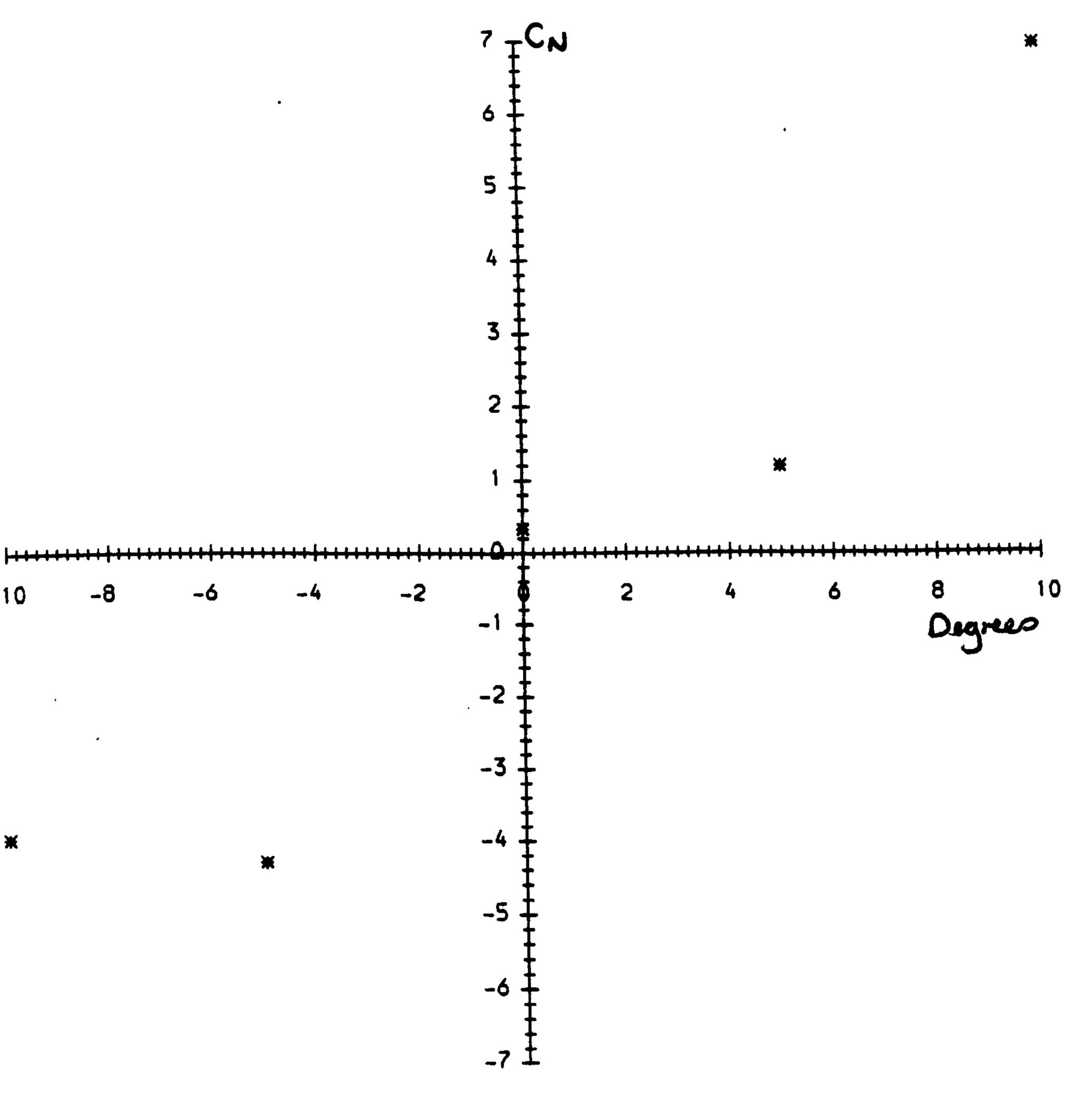

6.5.20. Variation of Normal force Coefficient C_N with Angle of Attack $\alpha°$ for Steady-State Tests.

Large Cruciform Canopy, 4:1 Arm Ratio. Imporous.

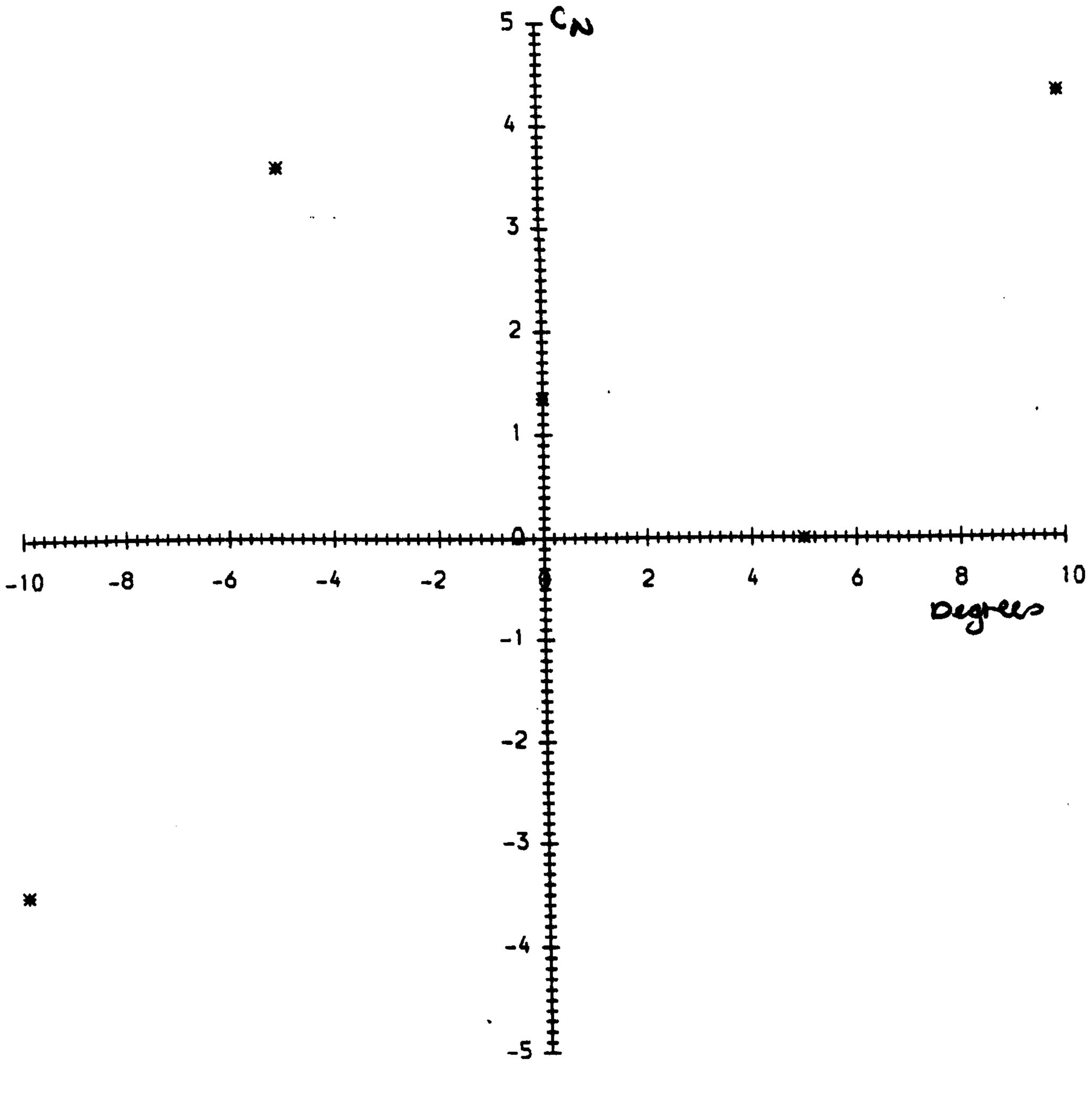

6.5.21. Variation of Normal force Coefficient C_N with Angle of Attack $\alpha°$ for Steady-State Tests.

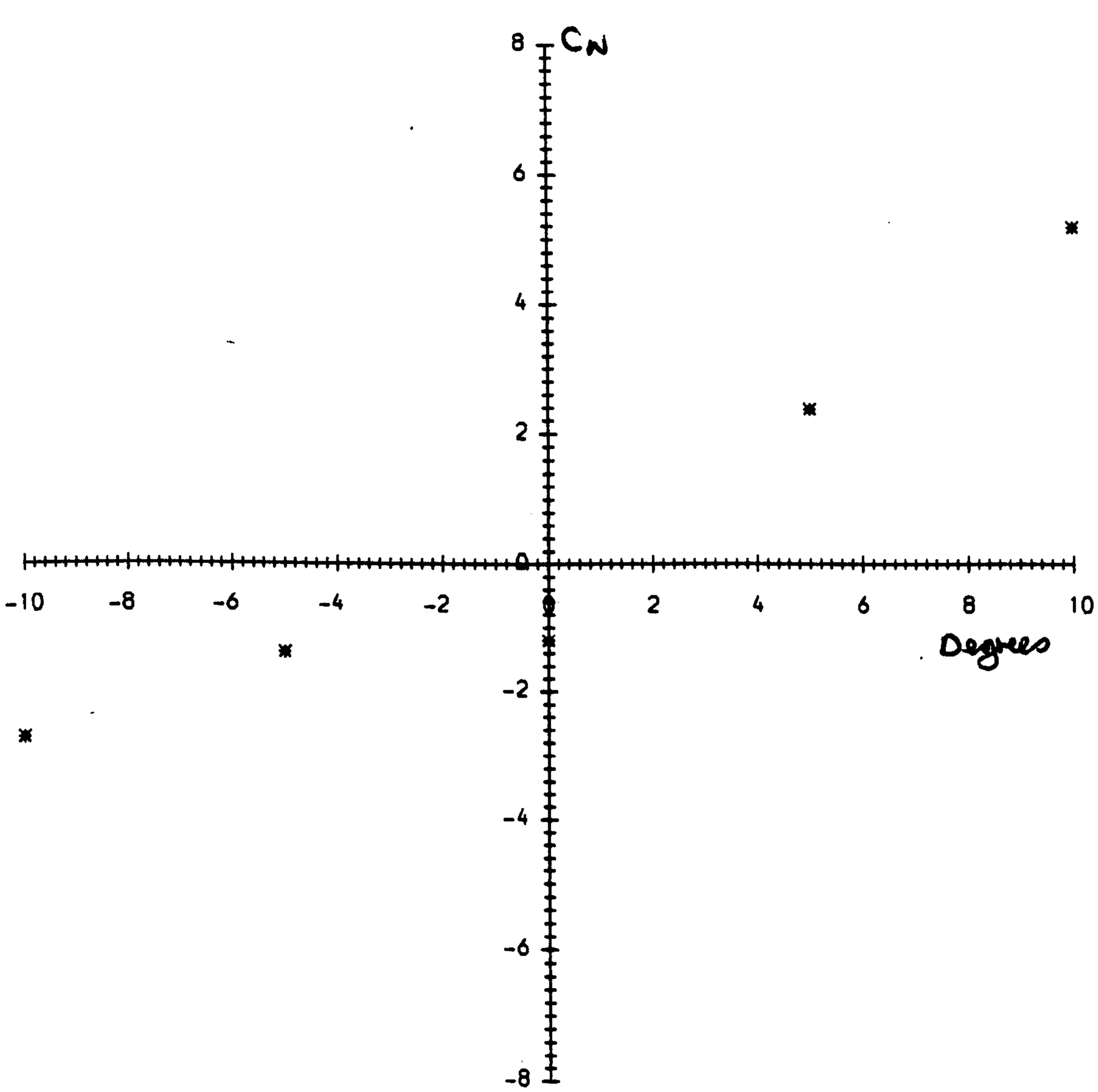

6.5.22. Variation of Normal force Coefficient C_N with Angle of Attack $\alpha°$ for Steady-State Tests.

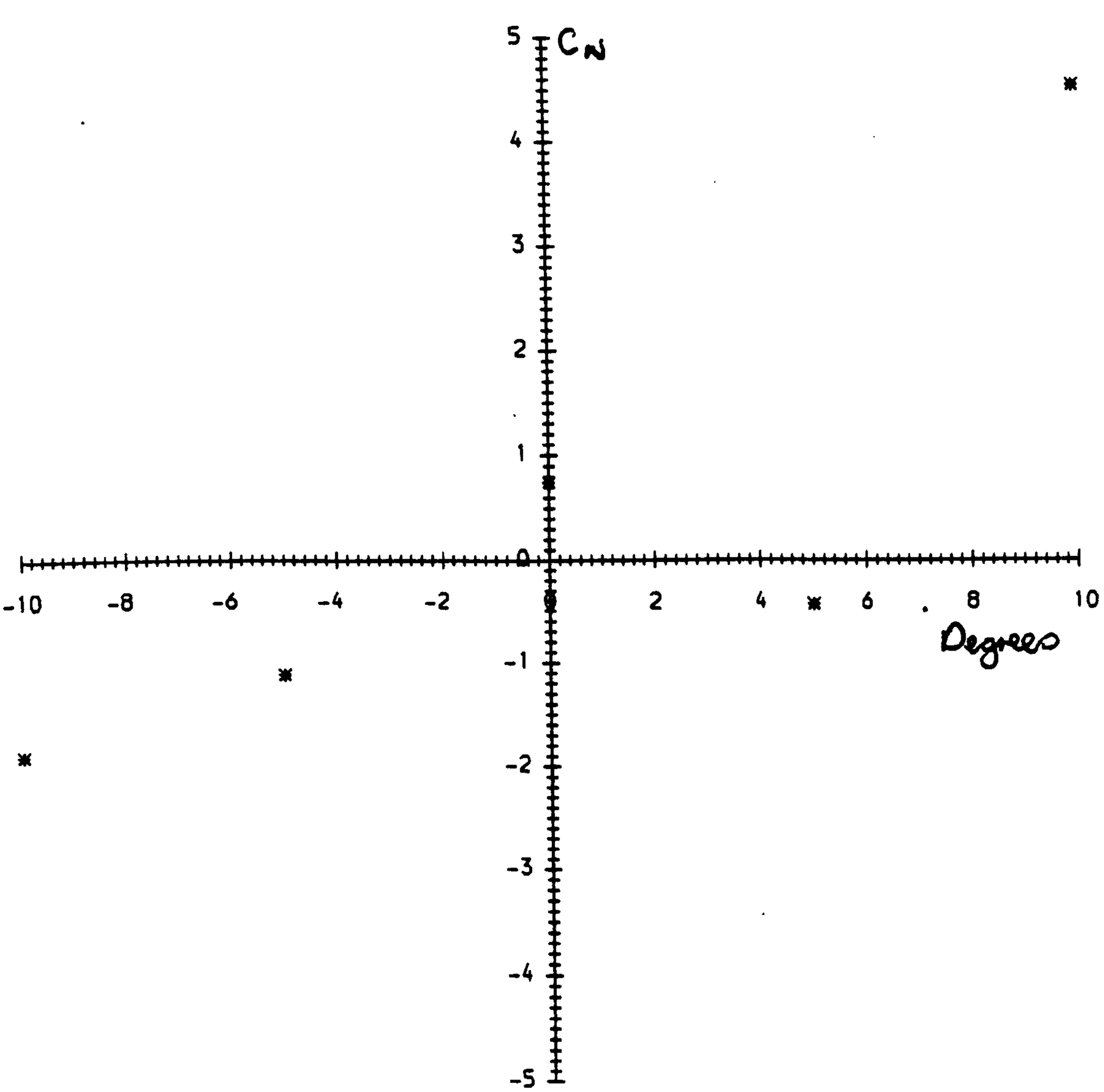

6.5.23. Variation of Normal force Coefficient C_N with Angle of Attack $\alpha°$ for Steady-State Tests.

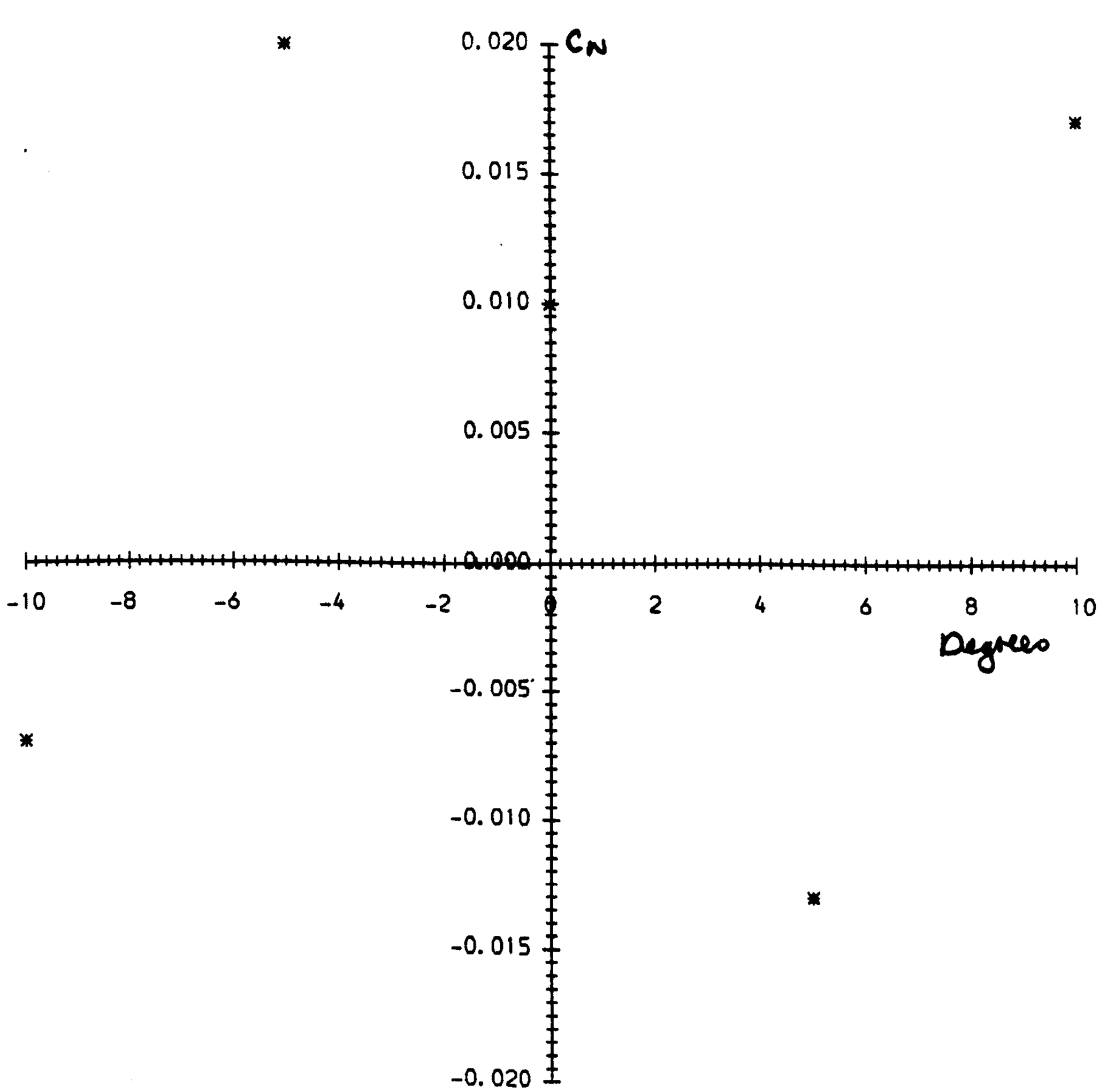

6.5.24. Variation of Normal force Coefficient C_N with Angle of Attack α° for Steady-State Tests.

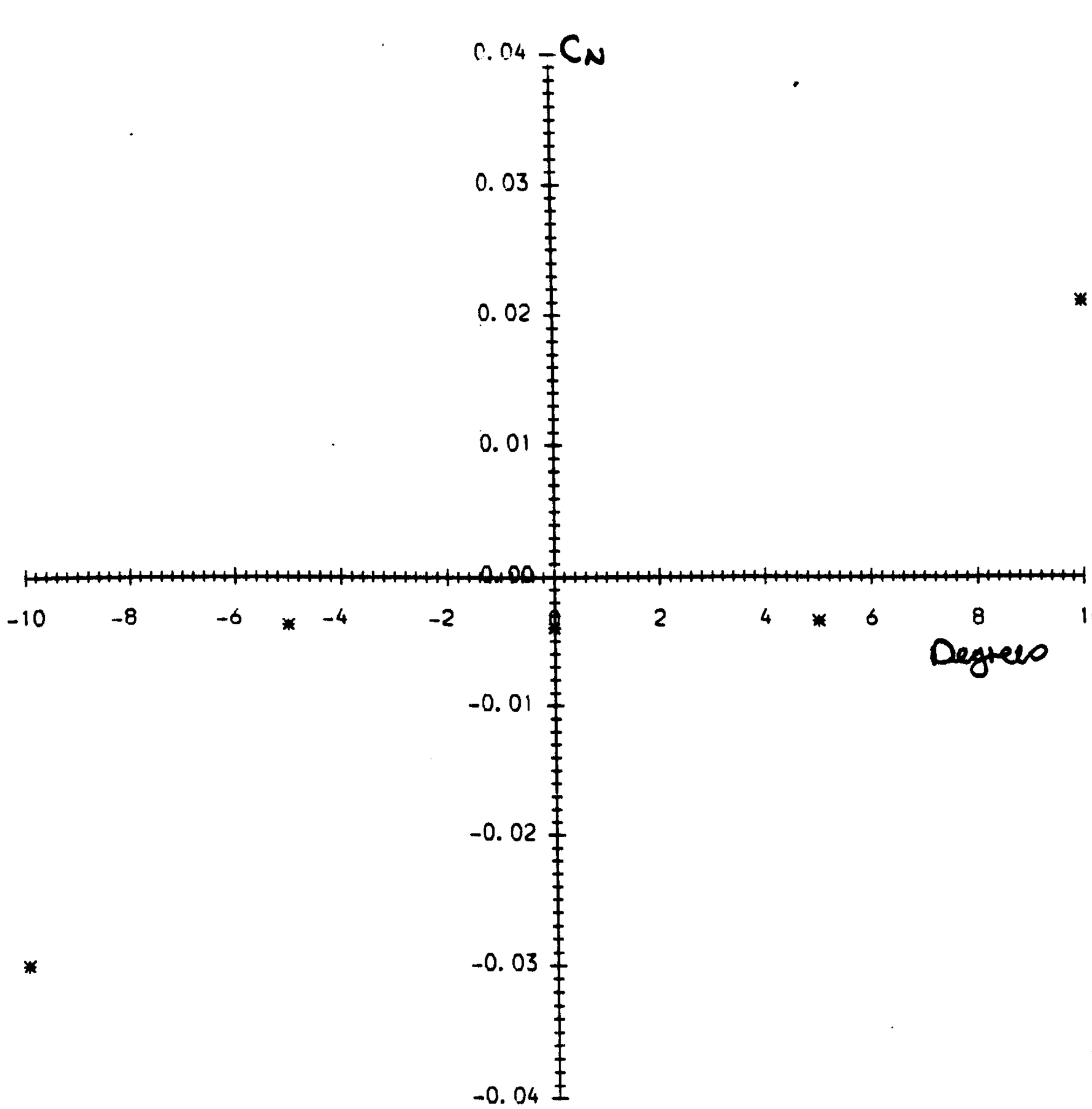

6.5.25. Variation of Normal force Coefficient C_N with Angle of Attack $\alpha°$ for Steady-State Tests.

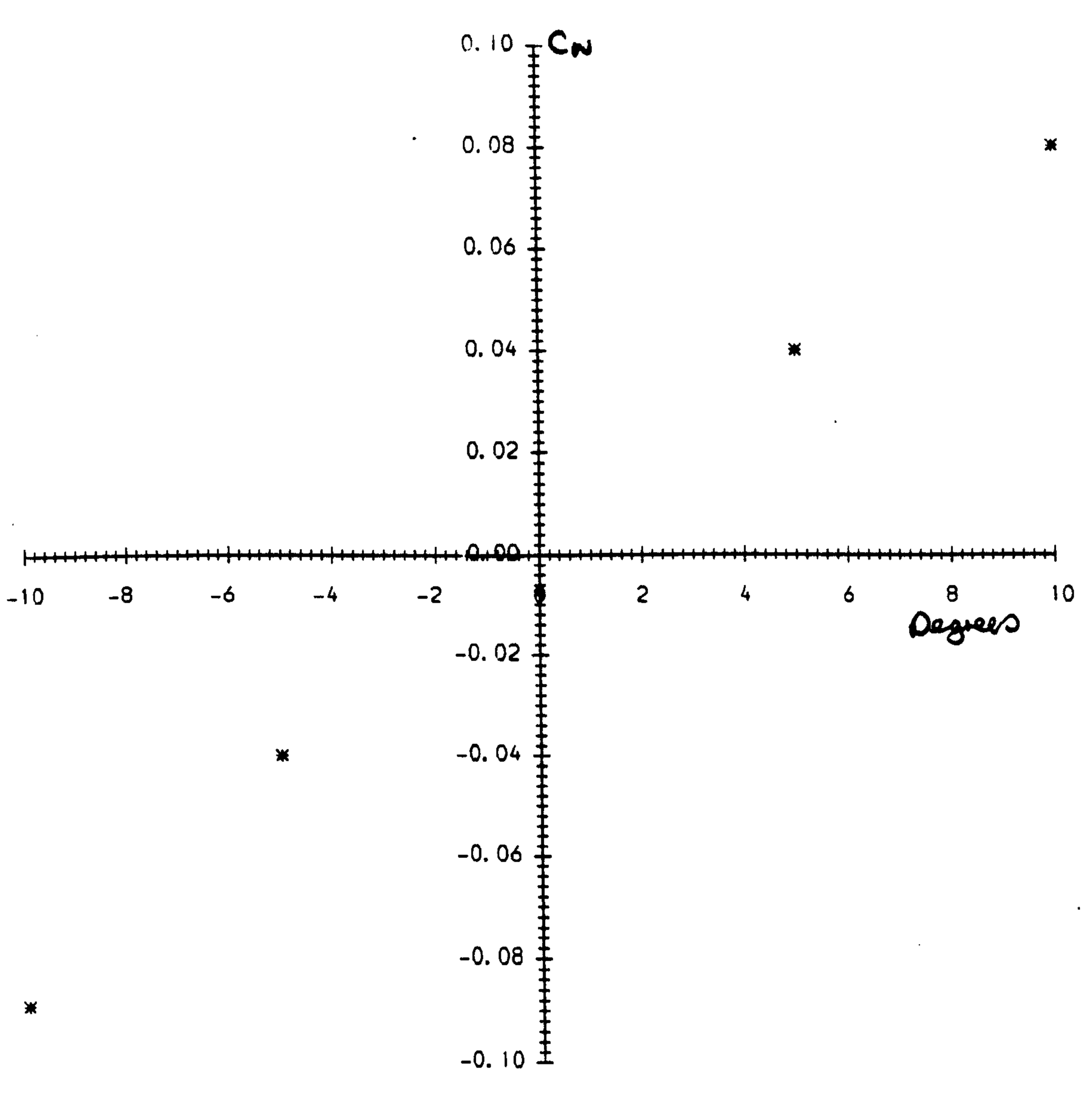

6.5.26. Variation of Normal force Coefficient C_N with Angle of Attack α° for Steady-State Tests.

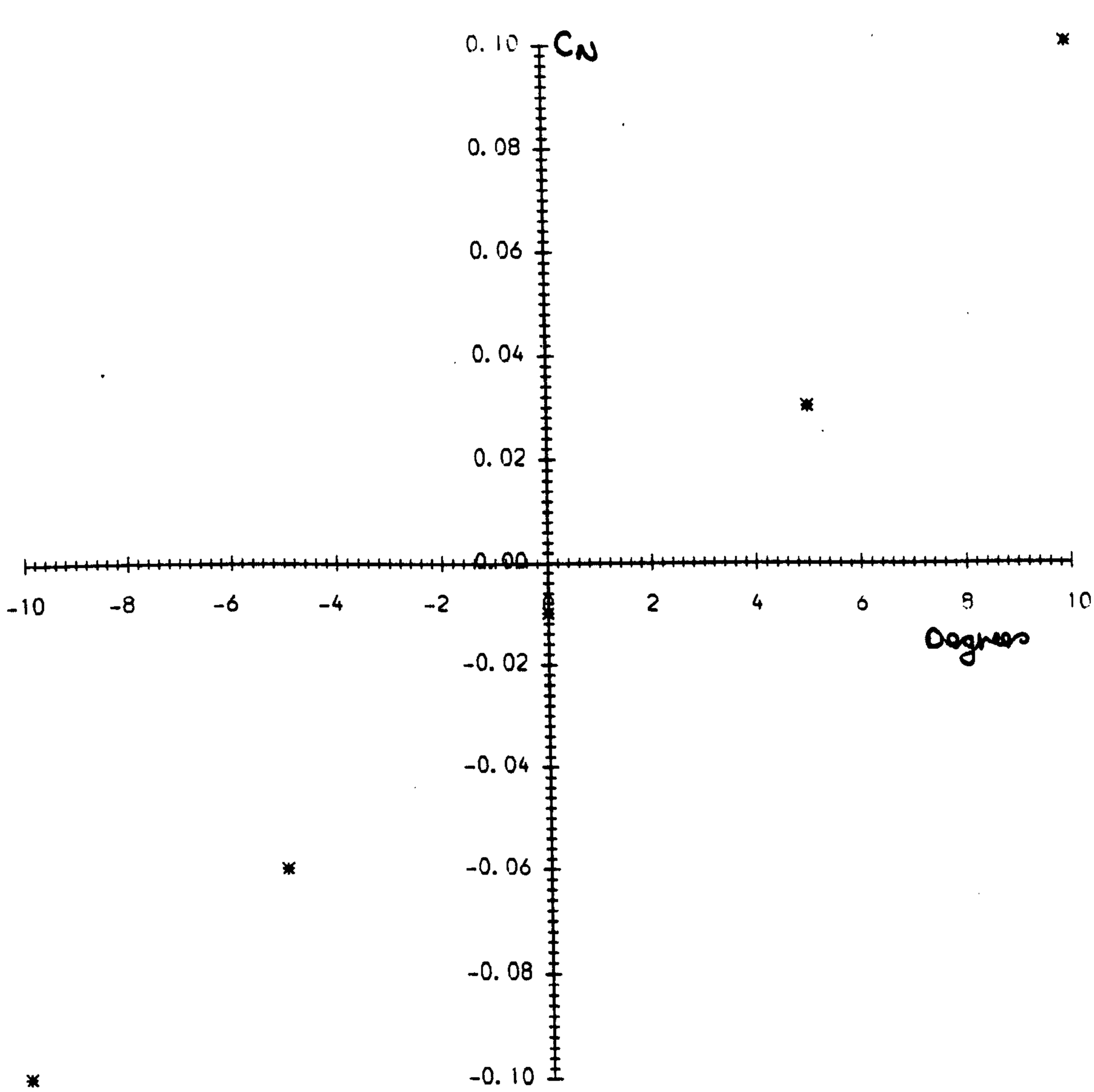

6.5.27. Variation of Normal force Coefficient C_N with Angle of Attack $\alpha°$ for Steady-State Tests.

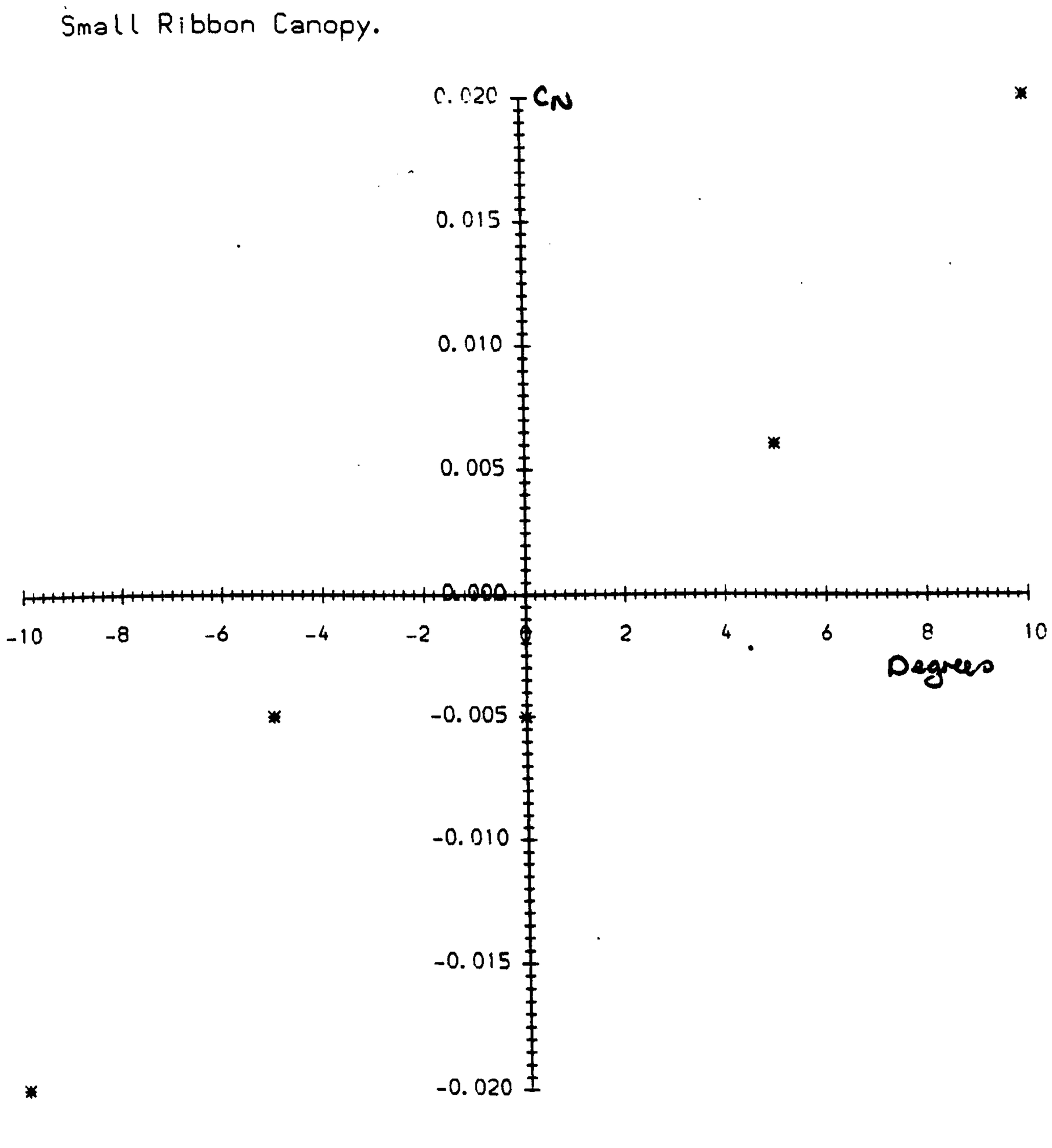

6.5.28. Variation of Normal force Coefficient C_N with Angle of Attack α° for Steady-State Tests.

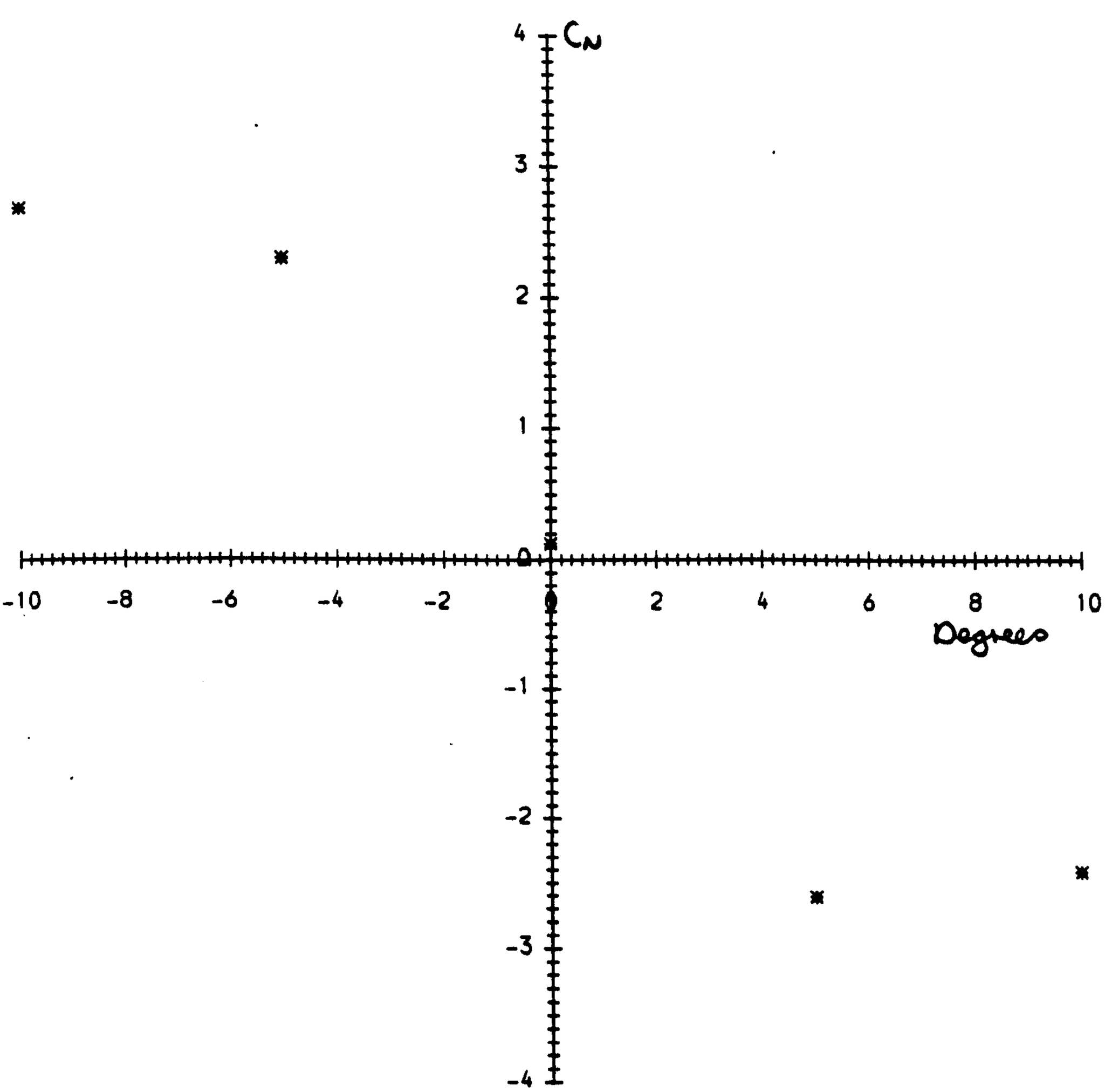

6.5.29. Variation of Normal force Coefficient C_N with Angle of Attack $\alpha°$ for Steady-State Tests.

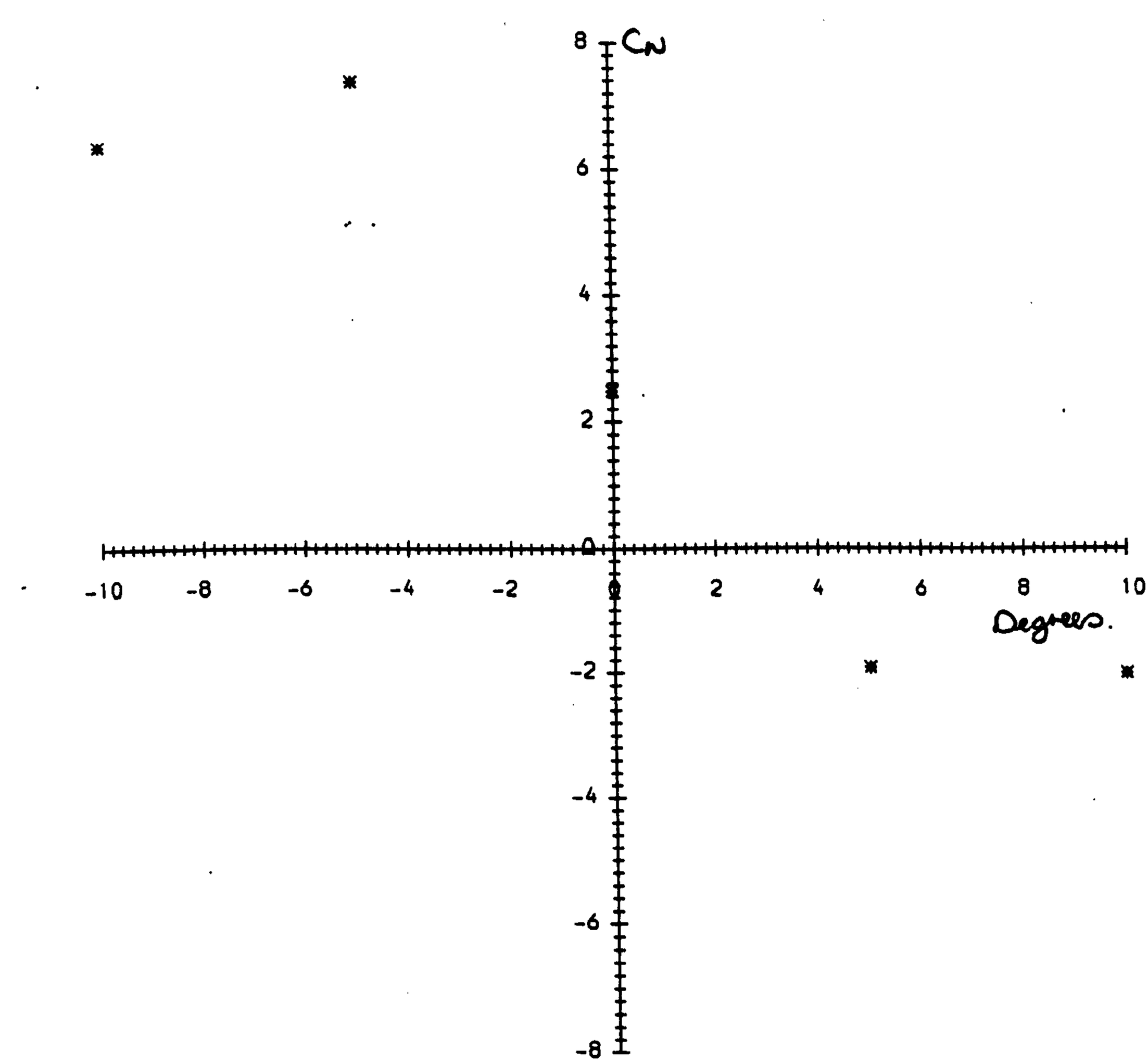

6.6 The 1988 Test Results.

The Tables of results in Section 5.4 for the tests performed in 1988 indicate a dependence of k_{11} on Keulegan-Carpenter number, for all the types of canopy which were tested. This is illustrated by the graphs in section 6.8.

Tests on the smaller canopy models were performed over a greater range of K_C values than the tests conducted with large canopies. Due to the increased vibration from the sting during testing, and the difficulty of maintaining any form of rigidity within the canopy, it was found that data obtained at low K_C numbers on the larger canopies had more scatter when compared with data for the same large canopies tested at higher values in the range of K_C.

For sinusoidal motion the expression for K_C;

$$K_C = \hat{U} \cdot T/D_o \equiv 2\pi R/D_o$$

shows how increasing the size of the canopy, indicated by the nominal diameter D_o, reduces the value of K_C. Thus, the data for the large canopies were obtained for K_C values which were the lowest for the range of K_C tests performed.

The tests conducted at these low K_C numbers were made at a constant period T. Since the oscillatory amplitude 'R' is

small, such low K_C number oscillations have components of oscillatory velocity V_u, that are also small. The component of oscillatory velocity V_u may be expressed as;

$$V_u = \omega \cdot R = (2\pi/T) \cdot R.$$

For such motion where 'R' is low and in this case K_C is low there is a smaller oscillatory component of force present in the overall force measurement. Thus, interference due to mechanical vibration and electrical disturbance constitutes a greater proportion of the unsteady force and acceleration signals obtained from the sting. This results in an increased amount of scatter occuring in the data and hence a higher uncertainty associated with the results. This effect is indicated by the larger uncertainties appearing in Tables 5.4.7 - 5.4.12, data from the 1988 test results for the larger canopy models.

These uncertainties are not systematic, but are random due to scatter. The interference with force and acceleration data may be greater for the large canopies which were tested, than for the small canopies for two reasons:

(i). When the size of the oscillatory velocity is reduced, the unsteady forces are also reduced, and can be swamped by the extraneous effects of mechanical vibration causing scatter in force data.

(ii). The amount of mechanical vibration present for each

of the large canopy tests was observed to be the same. However since scatter is calculated as a percentage of k_{11} it appears greater as a proportion of the smaller k_{11} values which were obtained for these canopies. See Tables 5.4.7 to 5.4.12. Note that decreasing the Keulegan-Carpenter number K_C, results in a reduction of k_{11} (see Tables 5.4.1 to 5.4.7.). The large canopies were tested at the lowest K_C values and produced the smallest values for k_{11}. They also have the highest amount of scatter, in their results.

6.7. The Full-Scale Keulegan-Carpenter Number.

It can be shown that Keulegan-Carpenter K_C numbers for full-scale parachute canopies undergoing steady descent are small, when compared to the K_C numbers for the range of values which was used in this programme of experiments.

This can be demonstrated by using a pendulum model to represent the parachute oscillating in pitch, and thus to describe the oscillatory nature of a parachute undergoing steady descent.

This pendulum model is used to derive formulae for the calculation of K_C numbers in both the axial and lateral directions. The dimensions of two types of full-scale parachute obtained from a paper by Doherr and Saliaris (23) are used to compute its values.

1. Axial Oscillatory Motion.

Assuming the parachute descends steadily with a vertical velocity V_D, but is subject to oscillatory perturbations through an angle θ;

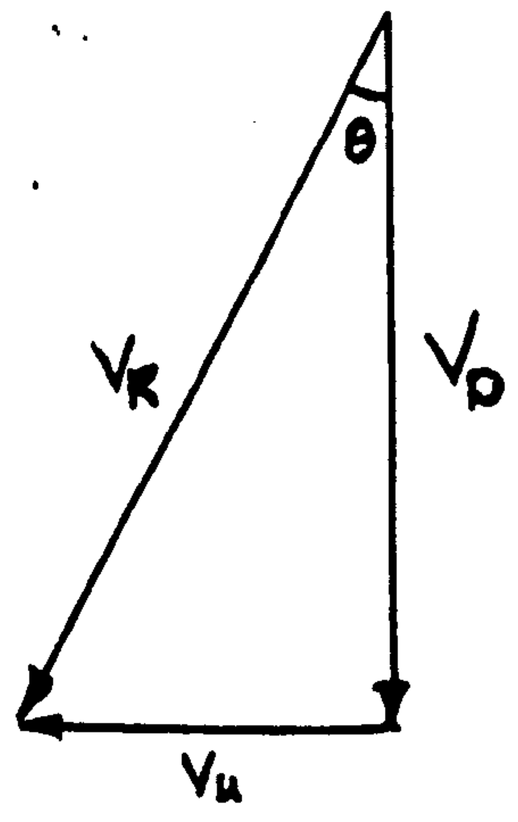

then the unsteady axial velocity, V_{AX} is given by;

$$V_{AX} = V_D \mathrm{Cos}\theta.$$

The total axial velocity due to both steady and unsteady velocity components is given by;

$$V_{AX} = \text{Steady Component} + \text{Unsteady Component}.$$
$$= V_D + V_D \cdot (\mathrm{Cos}\theta - 1).$$

Where for the purposes of obtaining the Keulegan-Carpenter number K_C, the steady component of velocity is disregarded. Thus, the velocity amplitude of the axial velocity V_{AX} is given by;

$$\hat{V} = | V_D \cdot (\mathrm{Cos}\theta - 1) |$$

When the angle of maximum displacement is given by $\theta = 10°$ the value of $\hat{V} \simeq 1/50\ V_D$.

The period T of the oscillations is given by;

$$T = 2 \cdot \pi \cdot \sqrt{(l_B/g)},$$

where l_B is the distance between the store and the origin of the canopy body axes.

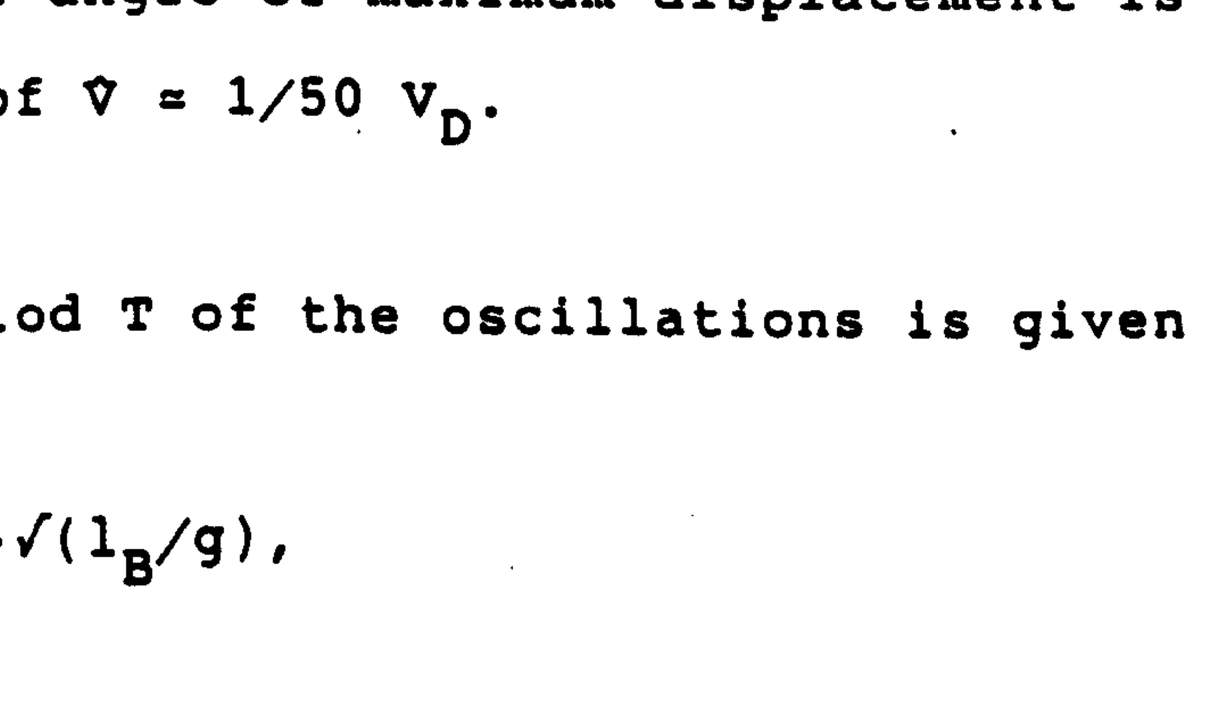

The lateral displacement L is given by;

$$L = l_B \cdot \mathrm{Sin}\theta.$$

Doherr and Saliaris (23), give specifications for two parachute systems which could be used in full-scale conditions: one consists of a large parachute the other of a small parachute. For the large parachute system;

$l_B = 8.1m$, $D_o = 8.6m$, $V_D = 7.27m.s^{-1}$.

For the small parachute system;

$l_B = 0.805m$, $D_o = 0.9m$, $V_D = 12.52m.s^{-1}$.

Using these specifications and the formulae above, the Keulegan-Carpenter numbers K_C in full-scale conditions for the small parachute system are $K_C = 0.5$, and for the large parachute system are $K_C = 0.1$.

2. Transverse Oscillatory Motion.

This calculation of Keulegan-Carpenter numbers uses an energy method in which the maximum kinetic energy of the analogous pendulum system occurs at the point where the potential energy is at its lowest. Therefore assuming energy losses from the oscillatory motion, due to air resistance are negligible, the interchange between kinetic energy and potential energy can be used to obtain a velocity amplitude. Thus;

$$1/2 \cdot m \cdot \hat{v}^2_{LAT} = m \cdot g \cdot \Delta Z.$$

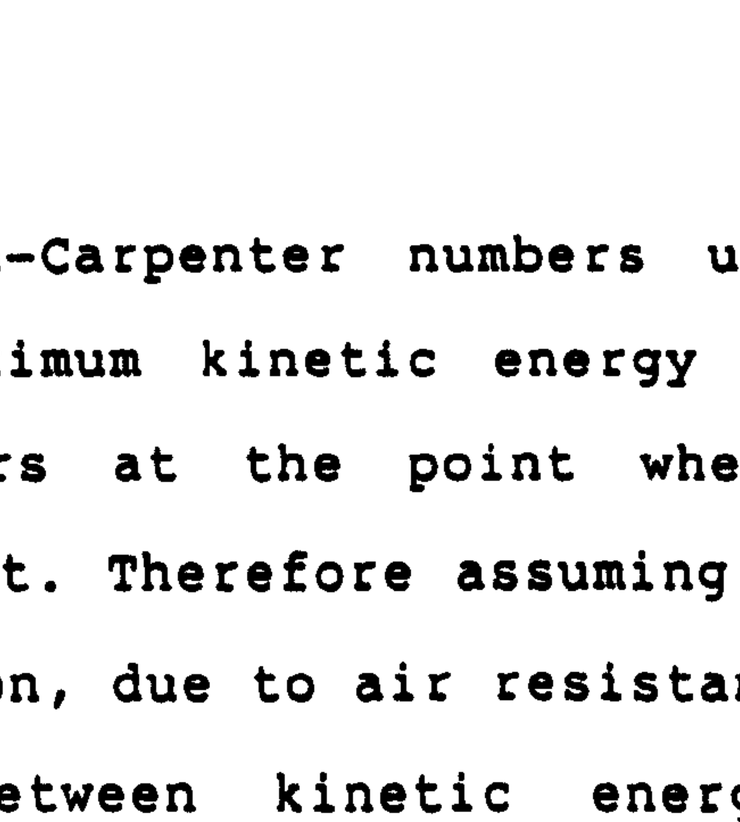

Where;

$$\Delta Z = l_B \cdot [1 - \text{Cos}(10)].$$

Hence;

$$\nabla_{LAT} = \surd[2 \cdot g \cdot l_B \cdot (\ 1 - \text{Cos}\ 10\ )] = 0.55\surd l_B.$$

From the axial case we can use the period of motion T, where;

$$T = 0.84\surd l_B.$$

From these formulae the Keulegan-Carpenter numbers associated with lateral oscillations, for both small and large parachutes in full-scale conditions are given by;

Large Parachute.	Small Parachute.
$K_C = 0.44.$	$K_C = 0.41.$

These Keulegan-Carpenter numbers are illustrative only. The specifications which Doherr and Saliaris (23) used for small and large parachute canopy models do not apply directly to the test models used in the present investigation.

6.8. Comparison With Other Work.

During the progress of this research programme, two other research projects which were of significance to this work were also taking place. These were wind tunnel tests which were undertaken by Shen (35), and analytical work which wasperformed by Frucht (36).

6.8.1. Wind Tunnel Experiments.

The wind tunnel experiments undertaken by Shen (39) and executed under steady conditions indicate similarities between the small set of canopies tested in the two different experimental facilities. A direct comparison of results is made possible by inspection of tables for the velocity dependent force coefficient C_D, obtained from these two research programmes. The following table compares the results obtained from the ship tank tests for the small set of cruciform canopy models used in 1986, with results for the same set of models used in wind tunnel work conducted by Shen.

Table 6.2. A Comparison Between C_D Values for Cruciform Canopies Tested in Both Wind-tunnel and Ship Tank.

Arm Ratio	Porosity $ft^3/ft^2/s$	S_o $/m^2$	C_D Ship-Tank	C_D Wind-Tunnel
4:1	0	0.106	0.79	0.74
3:1	0	0.106	0.74	0.75
3:1	13	0.106	0.71	0.70
3:1	23	0.106	0.61	0.66

This shows results for tests conducted in the wind-tunnel and ship tank differ by approximately 8% in the case of the high porosity 3:1 Arm Ratio canopy, and in the case of the Imporous 3:1 Arm Ratio Canopy by approximately 1%.

6.8.2. An Analytical Model.

In 1987 Frucht (36), introduced an analytical model which sought to predict the aerodynamic forces developed by a parachute canopy. Frucht's model assumes axisymmetric incompressible high Reynolds number flow, in which, in an otherwise potential flow, vorticity is shed from the model into the wake as discrete vortex rings. It can be used in the calculation of aerodynamic characteristics for which the angle of attack, $\alpha = 0°$. For a small imporous hemispherical canopy undergoing axial oscillatory motion the results calculated using this model compare well with experimental data.

The following graphs in Figs 6.8.1 and 6.8.2 which were derived from data for the Hemispherical parachutes, show how the force predicted by the model compares with experimental

data as obtained from the Southampton tests. The small model used in 1986, provided the data on Graph 6.8.1. The large model used in 1987, provided the data on Graph 6.8.2. Results for both these canopies are given in Chapter 5, Table 5.2.3.

Fig. 6.8.1. Axial Force Coefficients Developed on The Small Hemispherical Canopy (1986 Tests) in Axial Oscillatory Motion (experimental and Frucht's theoretical results).

Ref: Frucht (36).

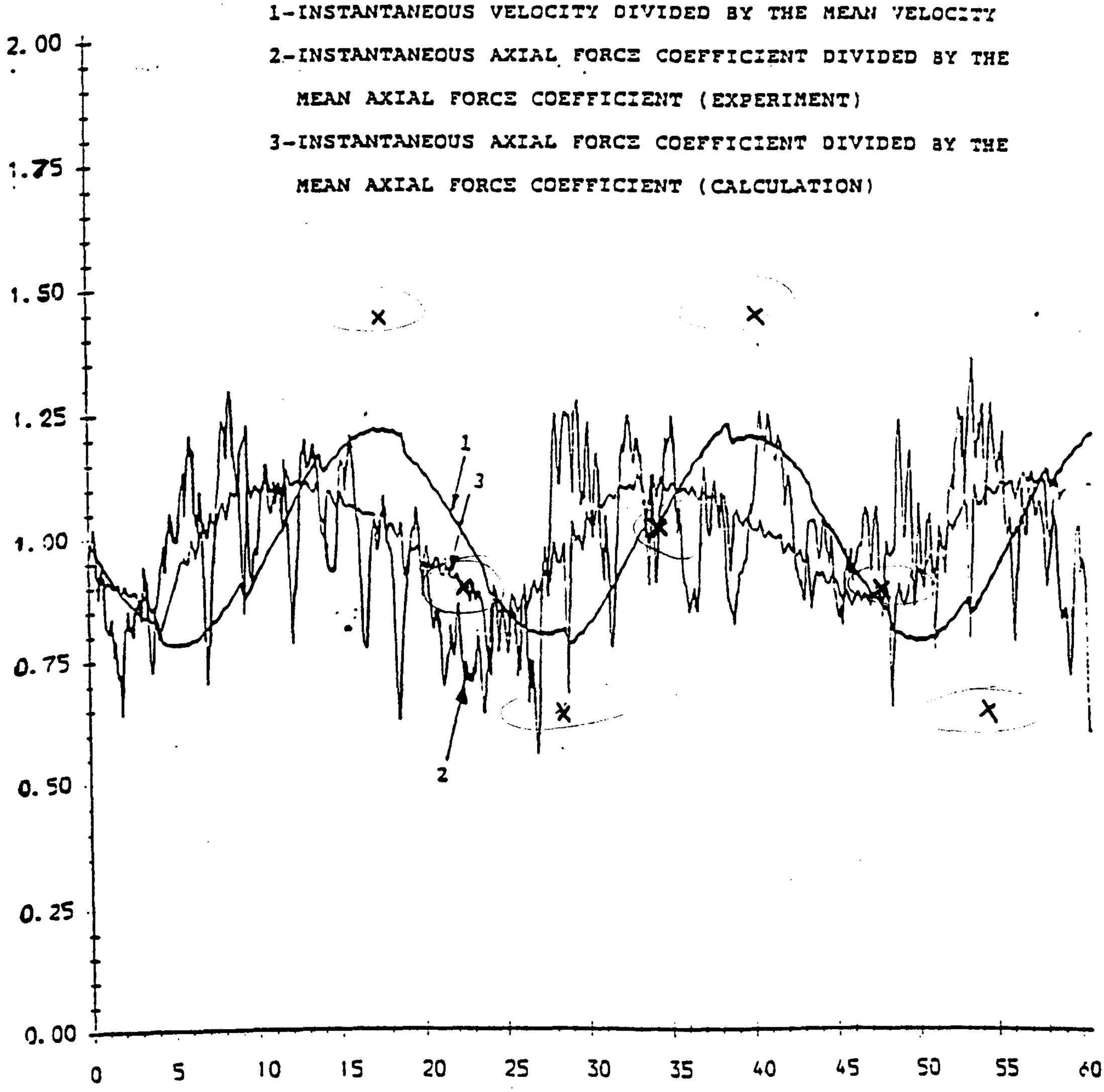

Fig. 6.8.2. Axial Force Coefficients Developed on The Large Hemispherical Canopy (1987 tests) in Axial Oscillatory Motion (experimental and Frucht's theoretical results).

Ref: Frucht (36).

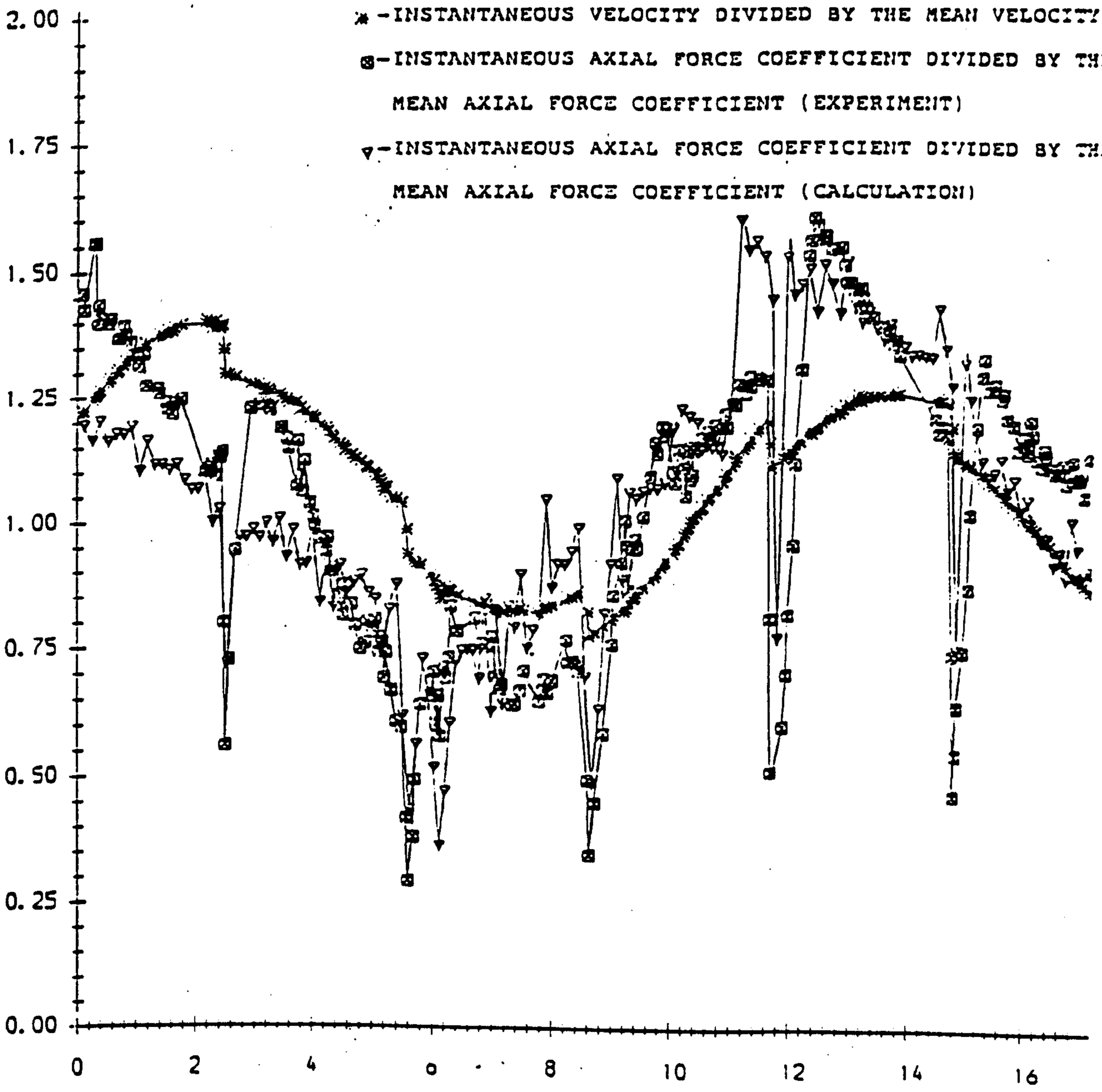

In Fig.6.8.1, the horizontal axis uses a dimensionless time as the independent variable, the vertical axis represents the ratio of the instantaneous axial force coefficient C_T to the mean force coefficient C_D.

Graph 2, which was obtained by Frucht (36), expresses this ratio using experimental data gained from the 1986 Southampton tests. The inertial term containing the added mass coefficient k_{11} has not been expressed as a separate component. Instead it is implicit within the instantaneous axial force coefficient. Thus Graph 2 expresses a ratio of velocity dependent coefficients.

6.8.2.1. Reproducing Experimental Results.

The crosses marked in Fig. 6.8.1, are an attempt to reproduce, using the derived mean force coefficients C_D and k_{11}, a ratio of the total instantaneous axial force coefficient C_T, to the sum of the mean axial force coefficient C_D and an inertial term containing k_{11}. The intention being to produce a series of points corresponding to Graph 2, thus providing a comparison with the original experimental data from which the coefficients C_D and k_{11} were derived.

This tests the ability of Morison's equation to model the original data, using the mean values of C_D and k_{11}.

6.8.2.2. Explanation of the Graph Points.

The crosses marked on Fig 6.8.1 were obtained by use of the governing equation of motion;

$$F = (1/2)\cdot\rho\cdot S_o\cdot C_D\cdot V^2 + \rho\cdot V_o\cdot k_{11}\cdot(dV/dt) \qquad [6.1],$$

in which C_D and k_{11} are derived mean coefficients from experimental results. The nominal volume of the parachute canopy is represented by V_o. The total velocity V is the sum of the steady velocity V_s due to the towing carriage, and the oscillational component V_u. Therefore;

$$V = V_s + V_u,$$

and;

$$dV/dt = dV_u/dt,$$

$$\therefore |dV/dt| = \omega^2\cdot R.$$

The total axial force may also be expressed in terms of the average velocity V_s and an overall coefficient C_T which encompasses the inertial effect and hence the added mass term. Thus;

$$F = (1/2)\cdot\rho\cdot S_o\cdot C_T\cdot V_s^2 \qquad [6.2].$$

Substituting for the total force F in equations 6.1 and 6.2 gives;

$$C_T = C_D\cdot(V^2/V_s^2) + [V_o\cdot k_{11}\cdot(dV/dt)]/[(1/2)\cdot S_o\cdot V_s^2] \qquad [6.3].$$

Insertion of points onto Fig. 6.8.1, which accord to

equation 6.3 above, accounts for the added mass effect arising from k_{11}. The following data as used in the ship tank test have been used for the points, indicated by crosses, which compare with Graph 2 of this figure.

$C_D = 0.64$

$k_{11} = 1.1$

$V_s = 1.27\ m.s^{-1}$

$|V_u| = (2\pi \cdot R)/T$

$R = 0.173m$ (oscillatory amplitude)

$T = 4.3$ sec (period of oscillation)

$D_o = 0.305m$

$V_o = 7.43 \times 10^{-3}\ m^3$

$S_o = 7.26 \times 10^{-2}\ m^2$

$|dV/dt| = \omega^2 \cdot R = 0.37\ m.s^{-2}$.

$K_C = 2\pi \cdot R/D_o = 3.56$.

These above data provided points which were inserted at the following positions of maximum and minimum velocity and acceleration, on Fig. 6.8.1.

(i) V = Maximum, dV/dt = 0:

$C_T = 0.92$, giving $C_T/C_D = 1.43$.

(ii) V = Minimum, dV/dt = 0:

$C_T = 0.41$, giving $C_T/C_D = 0.64$.

(iii) $V = 1.27\ m.s^{-1}$, $dV/dt = +0.37\ m.s^{-2}$:

$C_T = 0.69$, giving $C_T/C_D = 1.08$.

(iv) $V = 1.27\ m.s^{-1}$, $dV/dt = -0.37\ m.s^{-2}$:

$C_T = 0.59$, giving $C_T/C_D = 0.92$.

To summarise, this method produces a crude approximation to the graph which describes the ratio of instantaneous axial force coefficient to mean axial force coefficient, these coefficients referring to the oscillatory component of force and that resulting from the steady towing carriage velocity, respectively. Thus giving an indication of the limited extent to which the average values of C_D and k_{11} can be applied. However there are two redeeming factors which are relavent to this comparison.

This particular test has been performed by using the derived coefficients to remodel the data at high Keulegan-Carpenter numbers; conditions unrepresentative of normal full scale parachute motion, as discussed in Section 6.7.

The use of average values of C_D and k_{11} in a model, is more readily applicable than a time varying function.

Thus average values of coefficients obtained at lower, more representative values of the Keulegan-Carpenter number as applied to full-scale motion, could still provide a useful model.

6.8.2.3. Discontinuities.

In Fig. 6.8.2, the discontinuities in the graph displaying experimental data, represented by the square data points,

were caused by the wheel interupt signals interfering electrically with the other data channels during a test run. This caused a false signal of approximately -70 Newtons to appear momentarily on the axial force channel. Once the cause of this fault had been identified the corresponding data was removed from the data file. In the theoretical model developed by Frucht (36), the results of which are represented by the graph consisting of triangular data points in Fig 6.8.2, this effect is also seen. Since the removal of momentary experimental force data required removal of the corresponding time velocity and acceleration data, Frucht rendered his data void at these points, in order to remain synchronised with the periodic trace. Hence the discontinuities in the graphs of both experiment and theory. This is not a parachute phenomenon.

6.9. Discussion of Objectives.

The objectives of this project as stated in the Research Proposals, Chapter 2, Section 2.7, will now be discussed to determine the extent to which they have been satisfied by this work. Each objective, as set out in Section 2.7, has a numbered paragraph heading. These will be discussed in the same order.

1.

A range of canopy models has been tested. The inertial and velocity dependent characteristics of these canopy models have been investigated in the ship tank. As required by the objective, various porosities of canopy fabric were used and tested. These canopy models covered a range of porosities for the 3:1 Arm Ratio Cruciform Canopies. The effects of geometric porosity variation may be considered by inspection of results for the Hemispherical and Ribbon Canopies.

2.

An experimental programme for the ship tank has been devised and implemented in three stages. Each stage has consisted of at least one week spent collecting data from tests conducted in the Ship Tank of the Southampton Institute of Higher Education. In total, three hundred and fifty experimental test runs along the ship tank were achieved and these provided the data for the range of canopies tested.

(a). Minimisation of Interference Effects.

For the support structure, a minimisation of interference effects was accomplished by enclosing the instrumented sting in an aluminium shroud. This reduced the effects of fluid flow around the instrumented component of the sting, which would otherwise interfere with the forces produced on the canopy model under test. The use of two different sizes of canopy models has highlighted the problems of interference encountered when using the larger canopy models. Mechanical vibration in the sting and its supporting structure was reduced when the smaller canopy models were tested.

(b). The Effect of Variation of Canopy Porosity.

This aspect is best illustrated by referring to results for the 3:1 Arm Ratio Cruciform Canopies, which provide a comparison of different fabric porosities. The results for the Hemispherical and Ribbon Canopies show the differences that arise between an imporous canopy and a canopy with a high geometric porosity. Referring to Tables 5.2.2, and 5.2.4 for lateral motion in both steady and unsteady conditions, it can be seen that the stability parameter $\partial C_N/\partial\alpha$ is negative in the case of the Hemispherical canopies, with the exception of the small canopy in unsteady motion, which has a small value approaching zero.

This indicates a parachute which is certainly unstable statically and which is probably unstable dynamically also, as Doherr and Saliaris's stability model (23) described in

Chapter 3 makes clear. The corresponding value of $\partial C_N/\partial \alpha$ for the Ribbon Canopy is strongly positive, indicating a system which is both statically and dynamically stable.

(c). Blockage and Canopy Forebody Effects.

Blockage effects have been discussed in Chapter 4, Section 4.2.2.(i), and some corrected coefficients C_D^*, are given in Tables 5.2.1. and 5.2.3.. It is assumed these effects are most apparent for the velocity dependent force coefficient C_D obtained from tests conducted on the large size canopies as used in 1987 and 1988. The application of Maskell's blockage correction, equations [4.2] and [4.3] to results obtained for the added mass coefficients k_{11} was considered unnecessary since for the large canopies, the values for these coefficents were generally small and would have been reduced by approximately 10%, which is within the bounds of experimental uncertainty for these canopies. Thus the value -0.26 for k_{11} in Table 5.4.10, would become -0.23. Other values from this table are generally smaller than this.

The relatively small value which the k_{11} coefficients assume for the large canopies has been obtained at low Keulegan-Carpenter K_C numbers. This effect is consistent with the results obtained for the smaller canopy models, which showed a tendency for a reduced added mass coefficient at low values of K_C.

The effect of the canopy forebody which consists of a load or store and rigging lines, the length of which would have

been variable, has not been investigated during this programme of research. Sufficient material for investigation existed in relation to the added mass and velocity dependent force coefficient effects for the actual canopy. To investigate the canopy forebody effect would have required a similar programme of research in which the store and rigging lines were varied. There is no doubt that the presence of a forebody does influence canopy characteristics, see Knacké et al reference 27, and such an investigation would be a necessary part of a programme of further work.

(d). Parameter Identification Technique.

A parameter indentification technique has been developed which employs a computer program for processing the canopy test data. This yields the force coefficients associated with unsteady motion and two simultaneously occuring force parameters which are contained in one equation have been evaluated. The technique adopted, also allows the amount of scatter present in the data, due to interference, to be determined. The analysis of steady motion has been conducted using a computer program which identifies one parameter, the velocity dependent force coefficient. Both of the above programs have been developed over the life time of this research project.

(e). Flow Visualisation.

Two methods of flow visualisation, for use in the ship

tank were attempted during the course of this experimental programme. Both involved photography from above the surface. In the first attempt air bubbles were released in front of the canopy as it travelled along the tank. This was unsuccessful since the air bubbles were not neutrally buoyant, and thus rose to the surface, resulting in a different trajectory from that of the water in the flow-field around the canopy. Therefore, these air bubbles do not indicate the pathlines in the fluid.

A second attempt was made in which strands of dark cotton thread were attached to different points on the canopy. This gave an indication of the nature of pathlines around the inflated canopy.

There are disadvantages in hand-held still-photography from above the surface of the ship tank for the obsevation of submerged unsteady motion. The facility which would be best suited to this task is that of underwater video. This could be used to record the nature of fluid flow around the canopy using dye streams, and is well suited for both steady and unsteady motion.*

For both of the objectives 1. and 2. above, and as listed in Chapter 2, in addition to work that was to be conducted in the ship tank, the programme of research required work to be performed in a wind tunnel. The advantages of using the ship tank have been discussed in Chapter 4, however, some of the disadvantages of using a wind tunnel for these tests will now be discussed. The version of Morison's equation for axial

*see recommendations p.203(a)

motion, will be used.

$$F(t) = 1/2 \cdot \rho \cdot C_D \cdot V^2 \cdot S_o + \rho \cdot V_o \cdot k_{11} \cdot [\ dV/dt\ ].$$

Where the total velocity $V = V_s + V_u$. The nominal surface area and volume are denoted by S_o and V_o respectively.

The form which this equation takes indicates that the relative size of the two components of the total force is independent of the type of medium in which the equation is applied. Thus for the purposes of verifying the results of this research programme, and applying the results to full-scale parachutes descending in air, the use of a wind tunnel would appear desirable.

The wind tunnel at Leicester University can give a maximum flow velocity of approximately 10 $m.s^{-1}$ in its large working section, for which the blockage constraint when using the present set of canopy models is equivalent to that of the ship tank. The velocities used in the ship tank were typically 1.5 $m.s^{-1}$. The 'V^2' term in the velocity component of the equation above would therefore be around 40 times larger for experiments conducted in the wind tunnel.

However, the density of water used in the ship tank is one thousand times larger than that of the air in the wind tunnel. Therefore, forces as measured in the ship tank are very much greater than they are for the same models flown in the wind tunnel.

Oscillatory motion tests would have been more difficult to conduct in the environs of the wind tunnel. This is because the required oscillatory velocity would have to be very much higher. Otherwise, due to the higher steady velocity that would have been used in air, around $10m.s^{-1}$, the steady velocity component V_s of the total velocity component V would have swamped the oscillatory component V_u. The use of a rig to impose the unsteady velocity would have meant increased blockage for the wind tunnel working section, and the construction of an additional rig, to that which was used in the ship tank, to provide the necessary unsteady velocities.

Work currently being conducted in the wind-tunnel at Leicester University faces an additional problem of flow non-uniformity. This is caused by the presence of the fan driving the air which induces periodicity into the flow and this is amplified by the changing shape of the tunnel as it widens from the fan to the large working section, and the bends in the tunnel circuit around which the air is forced to move. The ship tank did not present these problems, since the canopy models were towed through otherwise undisturbed water. Any extraneous movement existent in the water after each test run was removed by baffles which were attached to the ship tank walls.

Wind tunnel work could have been attempted at other facilities, for example in the 24 ft diameter wind tunnel at The Royal Aerospace Establishment, Farnborough, though this offered few direct advantages compared with that of the

previous experience which had been gained in using the Southampton ship tank on a number of different occasions since April 1986.

3. Application of Results.

Interpretation of the results of these experiments has lead to conclusions being drawn about the behaviour of the various force coefficients over a range of Keulegan-Carpenter numbers.

The paper by Doherr and Saliaris (23) displays graphically results which can be obtained according to the values of coefficients which are used in their mathematical model. It is recommended that when applying average values of the coefficients to the Doherr and Saliaris model the following procedure is adopted:

Assume that both k_{11} and k_{33} are negligible in magnitude and the velocity dependent drag coefficient C_D for all canopy models conforms to a mean value of that presented in Chapter 5, Tables; 5.4.1 to 5.4.6.

These results can be incorporated into the input files for the Leicester University Parachute Performance Prediction Model described by Cockrell (38), and their effect can also be examined by reference to the Doherr and Saliaris stability model (23). Doherr and Saliaris's model is essentially a linearisation of the equations of motion used in the Leicester performance prediction program. The two models are

linear and non-linear versions respectively of the same system of equations.

CHAPTER 7

7. RECOMMENDATIONS AND CONCLUSIONS

7.1. Recommendations for Future Investigations.

Introduction

The programme of tests conducted so far, have indicated the substantial dependence of the axial added mass coefficient k_{11} on the Keulegan-Carpenter number K_C. The behaviour of the velocity dependent force coefficient C_D has also been shown under conditions of both steady and unsteady flow. The behaviour of the lateral added mass coefficient k_{33} with varying K_C has not been tested as substantially as has k_{11} in this respect. The test programmes of 1986 and 1987 in which the majority of the lateral unsteady tests were conducted provide two data points per canopy type for the lateral force coefficients k_{33} and $\partial C_N/\partial\alpha$ at different Keulegan-Carpenter numbers. This is shown in the Tables 7.1. and 7.2. below.

Table 7.1. Lateral Motion Keulegan-Carpenter Numbers.

1986 Tests.

Canopy	K_C	k_{33}	$\partial C_N/\partial\alpha$
Hemispherical Imporous	3.56	0.17	0.05
Cruciform Arm Ratio 3:1			
Imporous	2.9	0.26	0.13
Porosity = 13 $ft^3/ft^2/s$	2.9	0.21	0.25
Porosity = 23 " "	2.9	0.08	0.41
Cruciform Arm Ratio 4:1			
Imporous	2.9	0.43	0.43
Ribbon	3.04	0.17	0.17

Table 7.2. Lateral Motion Keulegan-Carpenter Numbers.

1987 Tests.

Canopy	K_C	k_{33}	$\partial C_N/\partial\alpha$
Hemispherical Imporous	1.78	0.02	-0.23
Cruciform Arm Ratio 3:1			
Imporous	1.48	0.20	0.1
Porosity = 12 $ft^3/ft^2/s$	1.48	0.11	0.1
Porosity = 25 " "	1.48	0.06	0.14
Cruciform Arm Ratio 4:1			
Imporous	1.48	0.11	0.27
Ribbon	1.52	0.07	0.16

For the rotationally symmetric canopy models which would appear to supply the most reliable data, these test results indicate that a reduction in Keulegan-Carpenter number for lateral oscillations results in a reduction in the lateral added mass coefficient k_{33}. Thus, it would be useful to determine the behaviour of k_{33} over a range of K_C values similar to those over which k_{11} was investigated. This would give a better indication of the behaviour of k_{33} compared to the current data, which provides values at only two points in the range. Such tests are best conducted with rotationally symmetric canopy models. It should be noted that choice of the desired range over which the angle of attack varies can ultimately place contraints on the range of K_C numbers investigated. This is because the oscillatory amplitude required to provide the correct range of angles of attack does not coincide at all points with the amplitude required for a given Keulegan-Carpenter number.

As shown in Section 6.7 the K_C number for a full-scale parachute undergoing steady descent is small compared to the range of values used in these tests. Thus an investigation into the variation of both the axial added mass coefficient k_{11}, and the lateral added mass coefficient k_{33} with K_C in the region of small K_C is recommended. This would accomplish two things:

(a) it would determine whether or not extrapolation to the region of low K_C of the results gained in the present test programme is valid or not.

(b) It would determine what dependency exists, for the added mass coefficients k_{11} and k_{33} with K_C in the region of low K_C.

Inspection of the graphs in section 6.5 demonstrates how the k_{11} values depend on K_C, although in the low region of the K_C range, the behaviour of k_{11} is more difficult to determine.

The use of one set of small canopies and one set of large canopies may help verify the effects of scaling up, with a view to applying these test results to full-scale canopies. However, any future investigations which involve the use of parachute models in the Southampton ship tank would be best conducted with models of the same dimensions as the smaller model canopies used in 1986 and 1988. Compared to the large canopies they offer reduced blockage and smaller sting

vibrational effects. On these smaller models smaller forces are developed permitting testing over a greater range of velocities and oscillational parameters.

Therefore, the use of large canopy models is not recommended in conjunction with the present facilities. In addition to the possible effects of blockage, the range of K_C values is reduced using the present test rig when the dimensions of the canopy test models are increased.*

7.1.1. Ram - Air Canopies.

The present facilities could also be used to support a test programme investigating the behaviour of less conventional parachute types such as Ram-Air, or gliding parachutes.

The Ram-Air design has important sporting and military applications. The models used in the present experiments consisted of the aerofoil or canopy part only. For the purpose of these experiments the rigging lines assembly was replaced with a rigid framework.

Given that the nominal surface area of a Ram-Air parachute is S_o, a typical linear dimension for this model is given by D_o where;

$$D_o = \sqrt{(4S_o/\pi)} = 357mm.$$

*see p.201(a)

Having completed the tests, it is recommended that a critical look at the sting design is conducted, with attention paid to the following aspects:

(i) Vibration.
(ii) Mass of moving parts (dynamic mass).
(iii) Streamlining.

(i) Vibration is a problem with the current design which is accentuated with large canopy models. This is because the forward sting-rod is long and therefore difficult to damp. Flow interaction induces vibration on exposed parts of the sting, in particular the horizontal forward member.

(ii) For the present design, use of lighter materials would alleviate the swamping effect of sting inertia over canopy inertia.

(iii) Streamlining the current design would reduce vortex interactions and thus lessen vibration.

The above aspects all had adverse effects on the measurement of the weakest added mass coefficient k_{33}.

One solution encompassing the above aspects uses a radically different design in which only the horizontal sting member is oscillated. The oscillation mechanism would be housed in a submerged "keel" structure underneath the towing trolley. This reduces the sting's dynamic mass by removing the previously oscillated vertical member.

This solution would substantially reduce the dynamic mass of the sting, and hence the swamping effect experienced in the determination of k_{33}.

Table 7.3. Ram-Air Canopy Specifications.

Aspect Ratio	Span/mm	Chord/mm	S_o/m^2	D_o/mm
1.8 : 1	430	240	0.1	357
2.8 : 1	533	190	0.1	357

During the first stage of this test programme preliminary tests were conducted in unsteady conditions with two such parachute models to test possible experimental procedures when using the canopy design in the ship-tank. Although aerodynamic results proved inconclusive some areas in which problems arise were identified.

Difficulties encountered in the testing of these models were associated with the supporting framework, and the method of attaching the canopy to this framework. The framework was of steel construction which added a disproportionate mass to the system which was unrepresentative of the rigging lines it replaced.

Models were held to this framework by a series of wire "stitches", which were secured by Araldite glue. This attachment method can cause interference with the fluid flow around the model.

However, a framework is required when testing such models so that aerodynamic forces are conveyed to the sting. The framework also provides rigidity and ensures the canopy flies at an appropiate angle of attack conducive to inflation.

To conduct a test programme investigating the velocity dependent and inertial characteristics of Ram-Air parachute canopies it is important to test the canopies at a zero angle

of attack. The models used above were designed to fly at equilibrium at a preset angle of attack or glide angle. The presence of a glide angle introduces added mass coupling moments, Lingard (2), which present too many variables for the solution of the governing equation of motion by the present method. Setting the preset angle of attack to zero would eliminate the effect of these coupling moments, and allowing the determination of velocity dependent drag and lift coefficients and also the added mass coefficients associated with these directions. However additional inflation problems would be presented.

Flow History Effects

Flow history is a function of the mode of motion. The mode of motion may be expressed as a function of the Keulegan-Carpenter number K_C. Thus flow history may be expressed as a function of K_C.

Future investigations into the nature of flow histories for parachutes should consider this relationship. K_C may provide a more verstile representation of flow history than a single-dimensioned phase-lag parameter such as τ in Polpitiye's (26) work.

Flow Visualisation

If future investigations into unsteady parachute motion involving the ship tank require a flow visualisation capability it is strongly recommended that real-time filming e.g. video should be used. This could be either under the water or over its surface, above the submerged object. The method would require dye stream indication. The advantage is that unsteady motion and flow history development can be continuously observed, compared to still photography with which it is more difficult to observe development of flow interactions.

7.2. Conclusions.

1. Variation of k_{11} with K_C.

For a steady flow onto which oscillations are imposed, in the range of K_C from 0.48 to 4.10, for which these measurements have been taken, there is a dependency for the average value per cycle of the added mass coefficient k_{11} on the Keulegan-Carpenter number K_C which is defined as $\hat{U} \cdot T/D_o$, where $\hat{U}$ is the maximum value of the oscillatory component of velocity.*

2. Variation of C_D with K_C.

For the small canopies tested there is an alteration in the value of the tangential velocity dependent force coefficient C_D at $\alpha = 0°$, as the value of the Keulegan-Carpenter number K_C is increased. This variation in C_D is not as substantial as that of the added mass coefficient k_{11}, but is consistent over the range of K_C for the canopies tested. Thus the value of C_D is greater at higher K_C numbers. This is shown by the results for unsteady motion over a range of K_C numbers for which there are no steady state results see Chapter 5 Tables 5.4.2 - 5.4.12. Table 6.1 shows that values of C_D obtained for unsteady motion were greater generally when compared to those obtained for steady motion.

*This is the first time for parachutes that added mass coefficients have been quantified as varying with Keulegan-Carpenter number.

3. Variation of k_{33} with K_C.

Referring to Tables 7.1 and 7.2, for the tests conducted in 1986 and 1987, in which two sizes of canopy were used at two different Keulegan-Carpenter numbers, there is a tendency for the lateral added mass coefficient k_{33} to reduce with decreasing K_C. This is most apparent with the results for the rotationally symmetric canopy models; the Hemispherical and the Ribbon Canopies. The results for the Cruciform Canopies do not show the same variation, the differences between k_{33} for the two values of K_C being less pronounced.

Cruciform canopies have a tendency to rotate randomly during experiments, the arms and gaps between arms move through the plane of rotation. Thus, the value of k_{33} for the cruciform canopies will be a mean value associated with this effect. The rotationally symmetric canopies such as the Hemispherical Canopy and the Conical Ribbon Canopy provide data which is less prone to the effects of rotation.

4. Variation of $\partial C_N/\partial\alpha$ with K_C.

Refering to Tables 7.1 and 7.2; the results for the variation of the stability parameter $\partial C_N/\partial\alpha$ with the Keulegan-Carpenter number K_C show that for the Hemispherical Canopy which is rotationally symmetric and thus less susceptible to the random effects of rotation, a reduction in K_C number results in a value for $\partial C_N/\partial\alpha$ which increases in magnitude and becomes negative; an unstable condition. For

the small Hemispherical Canopy which was tested at a higher Keulegan-Carpenter number, $\partial C_N/\partial\alpha$ assumes a small but positive value. This indicates a weak stability close to the point of neutral stability; where $\partial C_N/\partial\alpha = 0$ rad^{-1}.

When subjected to different values of K_C the Conical Ribbon canopy, which is rotationally symmetric, shows low variation in the value of its stability parameter $\partial C_N/\partial\alpha$, which is positive and equal to 0.17 and 0.16 for the small and large canopies respectively. This shows the canopy to be highly statically stable and thus, most probably dynamically stable as well.

The Cruciform Canopies which were prone to axial rotation and thus rotation through the plane of lateral oscillation, give values of $\partial C_N/\partial\alpha$ which show low variation for the different K_C numbers. This is a mean effect associated with the random effects of rotation during a run, and does not provide any conclusive proof about cruciform stability. These tests have made it quite clear that the stability of cruciform canopies in pitch is a function of canopy orientation, i.e. whether or not the arms or gaps of the canopy are present in the plane of pitching.

5. Appropiate input data for various canopy models.

Given the Keulegan-Carpenter numbers for the oscillations of the full-scale Canopies in descent, the added mass coefficients k_{11} and k_{33} are negligible. This is supported by

the following:

(i) extrapolation of results from the graphs of Section 6.5 would indicate that k_{11} tends to a zero value as K_C tends to zero,

(ii) the results for k_{11} obtained at the lowest K_C values for which these canopies were tested, see Tables 5.4.7 to 5.4.12, in which the added mass coefficient k_{11} is of the order of 10^{-2},

(iii) the results for the rotationally symmetric models, i.e. the Hemispherical and Ribbon Canopies, also indicate a reduction in the value of the lateral added mass coefficient k_{33} with decreasing Keulegan-Carpenter number.

Thus for full-scale parachute motion in steady descent the added mass coefficients k_{11} and k_{33} can be treated as negligible and set to zero in the aerodynamic stability models which are applicable to parachutes.

6. The Appropiate Stability Model.

The above conclusions concerning the nature of k_{11} and k_{33} at low K_C numbers suggests that values of velocity dependent and added mass coefficients can now be chosen which will render Doherr and Saliaris's model a valid representation of the full-scale case.

1.

For large parachutes Fig 7.1 indicates that when

$\alpha_{11}/m_a = \alpha_{33}/m_a \simeq 0$, where m_a is one-quarter of the mass of air contained within a Hemispherical Canopy whose radius is equal to the projected radius of the canopy, i.e.

$$m_a = (1/4)\cdot(4/3)\cdot(D_p^{\,3}/8),$$

by adopting condition A in Fig 7.1 it is seen that at $\alpha = 0°$ dynamic stability prevails except when $\partial C_N/\partial\alpha$ is small and positive. The latter condition applies to a cross-shaped canopy having an arm ratio of 3:1 and of medium porosity, or to one which is imporous and has an arm ratio of 4:1. For such canopies the static stability criterion is marginal and the canopy exhibits dynamic stability only if $\partial C_N/\partial\alpha$ exceeds a value of $\simeq 0.09C_D$. Since C_D is equal approximately to 85% of its equivalent value in steady state ($C_{D(s)}$) the canopy is stable if $\partial C_N/\partial\alpha$ is positive and exceeds a value of approximately $0.08C_{D(s)}$.

Characteristic values of $C_{D(s)}$ under these conditions are 0.77 for an imporous canopy of arm ratio 4:1 and 0.68 for a medium porosity canopy of arm ratio 3:1. Thus the dynamic stability criteria are that $\partial C_N/\partial\alpha$ is positive and exceeds $0.06.\text{rad}^{-1}$ and $0.05.\text{rad}^{-1}$ respectively. Since in the first case $\partial C_N/\partial\alpha \simeq +0.1.\text{rad}^{-1}$ both of these large parachutes exhibit dynamic stability.

2.

For small parachutes condition A on Fig 7.2 indicates that provided $\partial C_N/\partial\alpha$ is positive then at $\alpha = 0°$ the parachute will

be stable. The smaller the parachute the more dynamically stable it will be.

3.

Hemispherical Canopies are statically unstable at $\alpha = 0°$; at this angle they also exhibit dynamic instability.

4.

Since Ribbon Canopies are extremely porous they exhibit strong static and dynamic stability at $\alpha = 0°$.

7.1. A Parametric Representation of the Stability of a Large Parachute System.

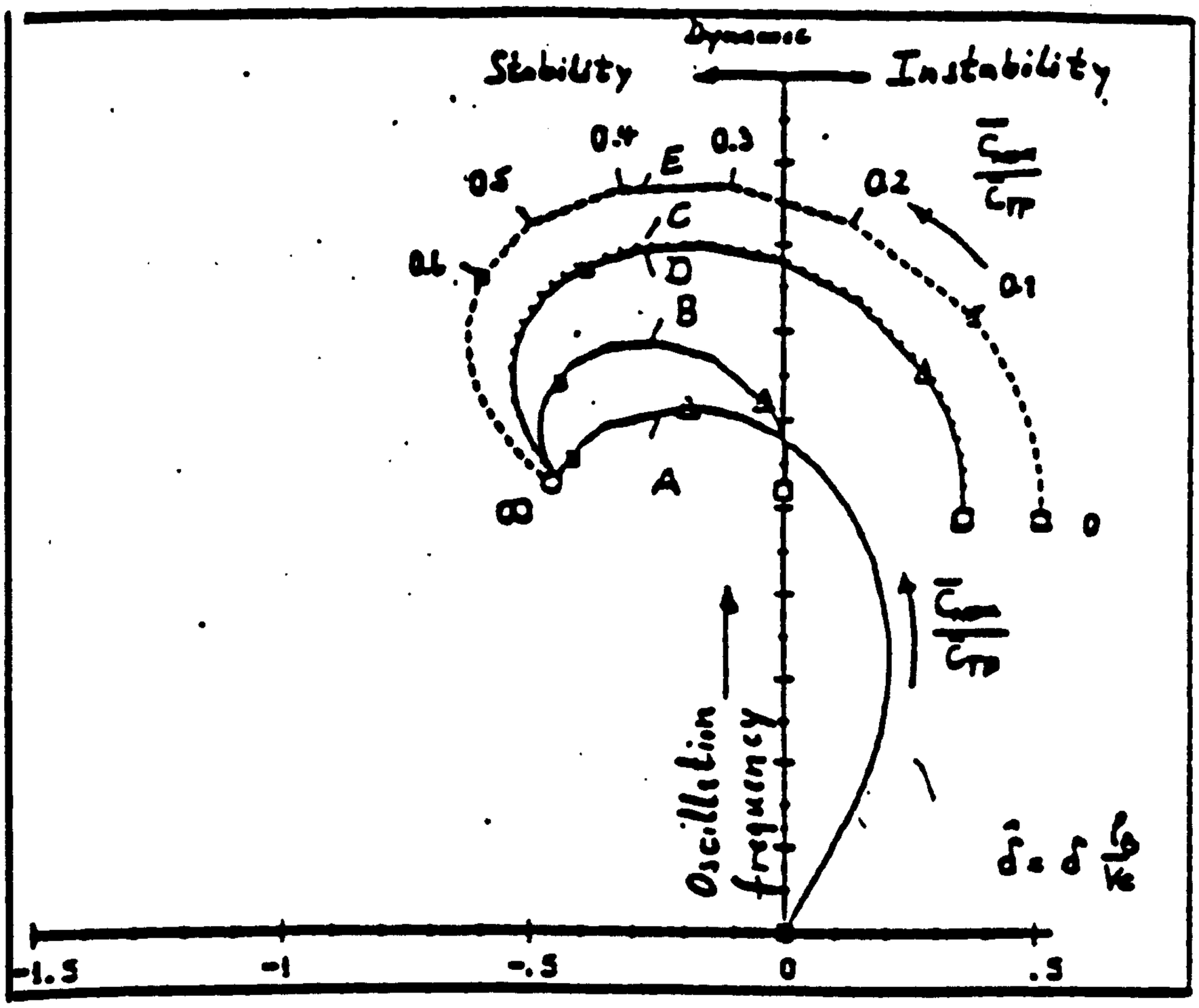

7.2. A Parametric Representation of the Stability of a Small Parachute System.

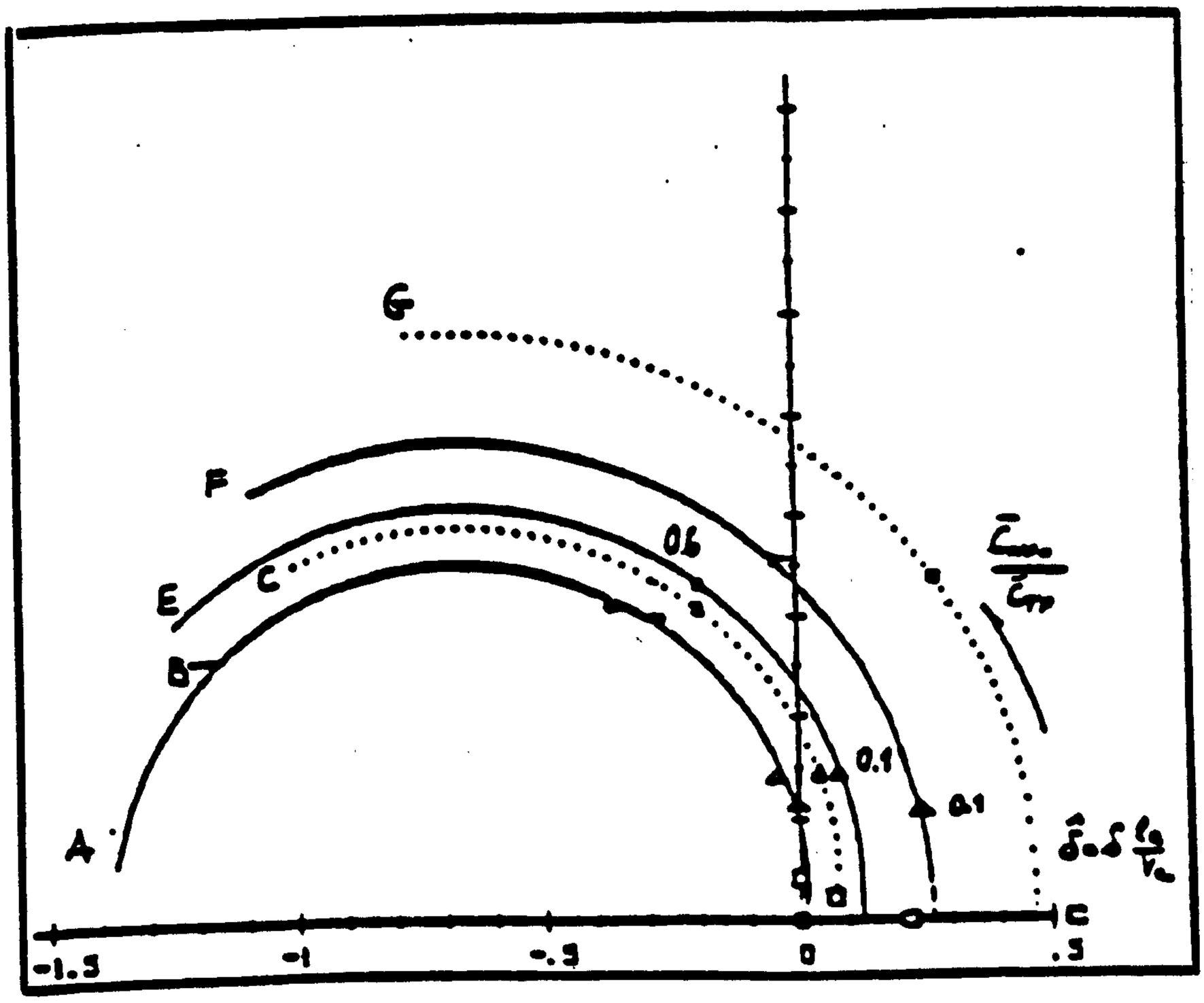

REFERENCES

REFERENCES

1 Lester. W.G.S. — A Note on the theory of parachute stability. Ministry Of Aviation, Aeronautical Research Council - Reports and Memoranda No.3352. H.M.S.O. 1964.

2 Lingard. J.S. — The Performance and Design of Ram-Air Gliding Parachutes. R.A.E. Technical Report 81103 1981.

3 Cockrell D.J. Shen. C.Q. Harwood R.J. Baxter A.C. — Aerodynamic Forces Acting On Parachutes in Unsteady Motion and the Consequential Dynamic Stability Characteristics. AIAA 86-2470-CP the 9th Aerodynamic Decelerator And Balloon Technology Conference. Albuquerque 1986.

4 Doherr. K.F. Saliaris C. — On The Influence Of Stochastic and Acceleration Dependent Aerodynamic Forces on the Dynamic Stability of Parachutes. AIAA 81-1941.The 7th Aerodynamic Decelerator and Balloon Technology Conference 1981.

5 Sarpkaya. T. Isaacson. M. — Mechanics of Wave Forces On Offshore Structures. Van Nostrand Rienhold 1981.

6 Milne-Thomson. L.M. — Theoretical Hydrodynamics. 5th edition. Macmillan & Co. Ltd. 1968.

7 Etkin. B. — Dynamics of Flight Stability and Control. 2nd Edition. John Wiley & Sons. Inc. 1982.

8 Duncan. W.J. — Control & Stability of Aircraft. Cambridge University Press. 1959.

9 Robertson. J.M. — Hydrodynamics in Theory and Application, Prentice Hall International Inc. 1965.

10 Cockrell. D.J. Doherr K.F. — Preliminary Consideration of Parameter Identification Analysis from Parachute Aerodynamic Test Data. AIAA 81-1940, 7th Aerodynamic Decelerator and Balloon Technology Conference 1981.

11 Yavuz. T. — Aerodynamics of Parachutes and Like Bodies in Unsteady Motion. Ph.D Thesis. University of Leicester 1982.

12 Ibrahim. S.K. — Apparent Added Mass and Moment of Inertia of Cup-shaped Bodies in Unsteady Incompressible Flow Ph.D. Thesis, University of Minnesota 1965.

13 Milne-Thomson. L.M. — Theoretical Aerodynamics 2nd Edition. Macmillan & Co. 1952.

14 Henn. H. — Die Absinkeigenschaften von Fallschirmen (Descent characteristics of Parachutes). Deutsche Luftfahrtforschung. ZWB-U & M6202 1944 .U.K. R.A.E. Translation 233, 1948.

15 (i) Shen. C.Q. Cockrell D.J. — Aerodynamic Characteristics and Flow Aroun Cross Parachutes in Steady Motion. AIAA 86 9th Aerodynamic Decelerator and Balloon Technology Conference, Albuquerque, 1986.

16 (ii) Shen. C.Q. Cockrell D.J. — Some Steady Aerodynamic Characteristics of Cross Parachute Canopies. Report 86-1 University of Leicester Engineering Dept 1986.

17 Kirby-Smith. T. — Cruciform Parachute Stability Investigations - Phases 1 & 2. R.A.E. Technical Report 83041, May 1983.

18 Morison. J.R. O'Brien M.P. Johnson J.W. Schaff. S.A. — The Force Exerted By Surface Waves On Piles. Transactions of The American Institution Of Mining and Metallurgical Engineers, Petroleum Branch. 1950, Vol 189 pp (149-154).

19 Morison. J.R. Johnson. J.W. O'Brien M.P. — Experimental Studies Of Forces On Piles. Coastal Engineering, Proceedings Of The 4tl Conference. 1953.

20 Yee Tak Yu. — Virtual Masses and Moments of Inertia of Disks, and Cylinders in Various Fluids. Jou. App. Phys. Vol 13 pp 66-69. 1942.

21 Cockrell. D.J. Doherr K.F. Polpitiye S. — Further Experimental Determination of Parachute Virtual Mass Coefficients. AIAA, 8th Aerodynamic Decelerator and Balloon Technology Conference. Hyannis, Massachusetts. 1984.

22 Darwin. C. — A Note On Hydrodynamics. Proc. Camb. Phil. Vol 49, pp 241-273. 1953.

23 Doherr. K.F. Saliaris C. — Dynamic Stability Analysis of Parachutes. Parachute Systems Technology, Fundamentals Concepts and Applications. CCG-University of Minnesota course; F12.01. 1987 Oberpfaffenhofen.

24 Ibrahim. S.K. — Experimental Determination of The Apparent Moment of Inertia of Parachutes. Technical Documentary Report No. FDL-TDR-64-153. Air Force Flight Dynamics Laboratory Research and Technology Division. Air Force Systems Command , Wright Patterson AFB, Ohio. 1965

25 Maull. D.J. Milliner. M.G. — Sinusoidal Flow Past A Circular Cylinder. Coastal Engineering 2. pp 149-168. 1978.

26 Polpitiye. S.J. Unsteady flow Around Certain Bluff Bodies. Ph.D. Thesis, University of Leicester, 1986.

27 Ewing. E.G.
Bixby. H.W.
Knacké. T.W. Recovery Systems Design Guide. AFDL-TR-78-151. December 1978.

28 Maskell. E.C. A Theory of the Blockage Effects on Bluff Bodies and Stalled Wings in a Closed Wind Tunnel. R.A.E. Reports & Memoranda No 3400 1963.

29 Srokosz. M.A. The Submerged Sphere as an Absorber of Wav Power. J. Fluid Mech. (1979), Vol.95, prt 4, pp. 717-741.

30 Lamb. H. Hydrodynamics, 6th Edition. Cambridge University Press. 1932.

31 Bearman P.W.
Chaplin J.R.
Graham J.M.R.
Kostense J.K.
Hall P.F.
Klopman G. The loading on a Cylinder In Post Critical Flow Beneath Periodic And Random Waves. Behaviour of Offshore Structures. Elsevier Science Publishers B.V. Amsterdam 1985.

32 Keulegan G.H.
Carpenter L.H. Forces on Cylinders and Plates in an Oscillating Fluid. Journal of Research of the National Bureau of Standards. Vol 60, No 5. May 1958. Research Paper 2857.

33 Babister A.W. Aircraft Stability And Control. Pergamon Press 1961.

34 Bessel F.W. On the Incorrectness of the Reduction to a Vacuum Formerly Used in Pendulum Experiments. Berlin Academy, 1826.

35 Shen C.Q. Flow Field Characteristics Around Bluff Parachute Canopies, Ph.D. Thesis, University of Leicester, 1987.

36 Frucht Y.I. High Reynolds Number Incompressible Flow Simulation About Parachute Canopies and Similar Bluff Bodies. Ph.D. Thesis, University of Leicester 1987.

37 Jorgensen, D.S. Cruciform Parachute Aerodynamics. Ph.D. Thesis, University of Leicester, 1982.

38 Cockrell, D.J. A Valid Performance Prediction for Fully-Deployed Parachute Canopies. University of Leicester, Department of Engineering, Internal Report 87-8. August 1987.

39 Shen. C.Q.
Cockrell. D.J. Aerodynamic Characteristics and Flow Round Cross Parachutes in Steady Motion. AIAA Journal of Aircraft, April 1988.

40 Fox & MacDonald. Introduction to Fluid Mechanics. John Wiley & Sons. 1973.

41 Cockrell. D.J. The Aerodynamics of Parachutes. AGARD-AG-295. July 1987.

42 Cockrell. D.J.
Harwood. R.J.
Shen. C.Q. Measurements of Aerodynamic Forces on Unsteadily Moving Bluff Parachute Canopies AGARD-CP-413. October 1986.

43 Doherr. K.F. Private Communication.

APPENDICES

APPENDIX I

Appendix I

The Least Squares Method of Analysis.

Introduction

The data collected from the Southampton test programme has been analysed using a least squares method which is implemented on a two parameter form of the governing equation of motion, the original of which is shown below;

$$F(t) = a \cdot V^2(t) + b \cdot \dot{V}(t) \qquad [1].$$

This equation becomes;

$$F(t)/\dot{V}(t) = a \cdot V^2(t)/\dot{V}(t) + b \qquad [2].$$

The two sets of data representing a vertical and a horizontal axis are $F(t)/\dot{V}(t)$ and $V^2(t)/\dot{V}(t)$ respectively. The equation [2], is essentially of the form;

$$Y_i = m \cdot X_i + c. \qquad [3].$$

The 'i' subscript refers to individual sets of data obtained during the run, for example the force and acceleration data, and the derived velocity data which go to make up the variables shown in equation [2].

The Least Squares Fit.

Given a set data (X_i, Y_i), for which it is assumed that Y_i is a linear function of X_i, i.e;

$$Y_i = m \cdot X_i + c.$$

First determine the four functions;

$$1.\ \sum_{1}^{n}(X_i), \quad 2.\ \sum_{1}^{n}(Y_i), \quad 3.\ \sum_{1}^{n}(X_i^{\,2}), \quad 4.\ \sum_{1}^{n}(X_i \cdot Y_i).$$

From the above the functions;

$$\left[\sum_{1}^{n}(X_i)\right] \cdot \left[\sum_{1}^{n}(Y_i)\right]/n, \quad \& \quad \left[\sum_{1}^{n}(X_i)\right]^2/n$$

are obtained.

Then in the expression $Y_i = mX_i + c$, the slope 'm' is given by;

$$m = \left[\sum_{1}^{n}(X_i \cdot Y_i) - \{[\sum_{1}^{n}X_i] \cdot [\sum_{1}^{n}Y_i]\}/n\right] \Big/ \left[\sum_{1}^{n}(X_i^{\,2}) - \{[\sum_{1}^{n}(X_i)]^2\}/n\right] \qquad [4].$$

The intercept 'c' is obtained from;

$$c = \left[\sum_{1}^{n}(Y_i) - [m \cdot \sum_{1}^{n}X_i]\right] / n \qquad [5].$$

To find the values of uncertainties due to the scatter of the data, the deviation of individual data items from the slope and intercept given in equations [4] & [5] can be determined. These are obtained from the standard deviation in the vertical scatter from the straight line which is specified by m and c.

For example, a value Y_i from the data collected, will not necessarily lie on the curve specified by m and c. There may

exist a value 'n_a', such that;

$$n_a = (m \cdot X_i + c) - Y_i, \qquad \text{where } n_a \text{ is non-zero.}$$

Since 'n_a' may be either positive or negative, it is squared, then summed for all the Y_i values, and the square root taken of the resulting sum. This provides the root - mean - square measure of the uncertainty, or the standard deviation. It represents a deviation from the 'mean', as defined by the slope and intercept. This deviation is directly proportional to the amount of scatter of all the individual data points.

$$\text{R.m.s. deviation; } \delta = (1/n) \cdot \surd \{ \sum_{1}^{n} [(m \cdot X_i + c) - Y_i]^2 \} \quad [6].$$

For the range of X_i, the domain of Y_i is given. So the maximum and minimum values of the two variables can be found. The uncertainty in the value of the intercept 'c' is given by the root mean square deviation, [6].

By using the root mean square deviation σ, the maximum and minimum values for the slope can be determined. Thus the uncertainty in the value of the slope 'm' can be determined.

The uncertainty in the value of the slope is obtained by calculating the possible values of the maximum slope and the minimum slope.

$$\text{Slope}_{max} = [(y_{max} + 3\delta) - (y_{min} - 3\delta)]/[x_{max} - x_{min}].$$

$$\text{Slope}_{max} = [(y_{max} - 3\delta) - (y_{min} - 3\delta)]/[x_{max} - x_{min}].$$

These are then used to give an uncertainty expressed as a percentage of the mean slope.

APPENDIX II

Appendix II

Computer Program for the Data Analysis of Unsteady Motion.

1. Program Documentation: "CANOPY2.BAS".

Description

This computer program has been written using a microprocessor, running microsoft BASIC[1] in a CP/M environment. For the particular hardware employed during this research programme, a "Research Machines 380z", the software requirement is recommended as 56k CP/M for which the file "SBASG2.COM" provides the BASIC interpreter. Revised versions of the program "CANOPY2.BAS" have been written to account for changes in the strain gauge calibration parameters, however apart from this the program remains unchanged.

Having loaded and issued the run command the user selects the test to be inspected. Calibrations are dealt with under the "run " command . Actual analysis begins with the subprogram ANALYSE(MODE$).

This sets up variables to determine whether the oscillation is decreasing or not; by monitoring the recorded accelerometer output, as follows;

PROC Skipwheels (n)

---

[1]Beginners All Symbolic Instruction Code and CP/M: Control Program for Microprocessors.

Gets into the data file by counting 'n' wheel interupts on channel r(o). This requires prior editing of lines 1360 & 3180.

PROC dotwentyone (DO21)

Samples 21 bits of data from the accelerometer signal, and checks whether these are positive or negative. If positive, the number of increments (noincs), is increased by 1. If negative, (i.e. a deceleration), the number of decrements (nodecs), is increased by 1. This procedure also obtains a velocity from the accelerometer signal by integrating it. "Analyse (mode$)", then tests the condition of a variable called "decreasing"; lines 3232-3240. The value of decreasing (determined from DO21),indicates whether the acceleration signal is rising or falling.

PROC peakspassed (Line 3626)

With the value of "decreasing " set either true or false, the "noincs" are compared against the "nodecs", so that a peak , either a maximum or minimum can be detected . This peak refers to a peak in the velocity signal. The resulting maxima & minima are stored as array variables; i.e. maxvel (k), & minvel (k), where $0 \leq k \leq 10$. The initial settings; minvel = 1E + 10 & maxvel = -1E + 10, reset the possible values of the maxima and minima out of bounds of any likely value so that previous values of maxima and minima are not accidently re-recorded having already passed through the procedure once or more. Proc's "DO21, & "Peakspassed", operate within a loop after the state of "decreasing" has

been determined. This loop is repeated "noblocks" (the number of blocks of data to be analysed) times, resulting in further values for peaks (crests & troughs, or maxvels & minvels respectively) being stored in their respective arrays.

PROC Gettrend (Line 6500)

There exists a trend; visible on a plot of the velocity trace, where there is a gradual negative or downwards slope of the velocity signal.

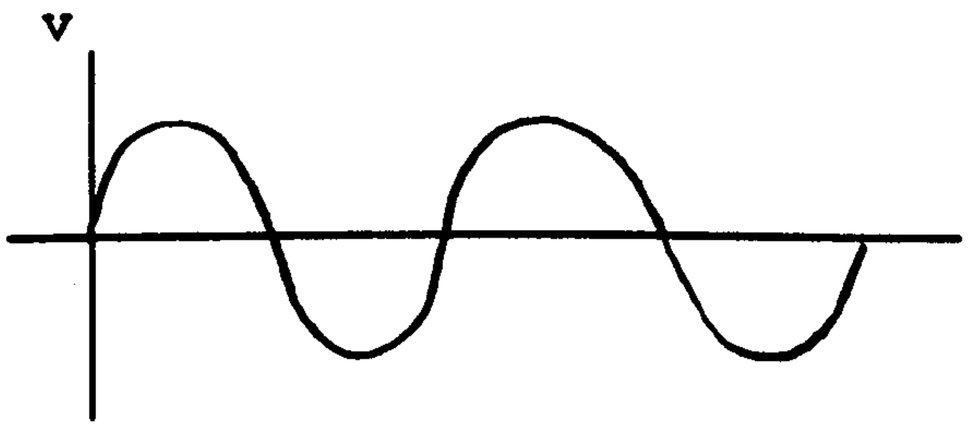

Fig (i) Desired Data.

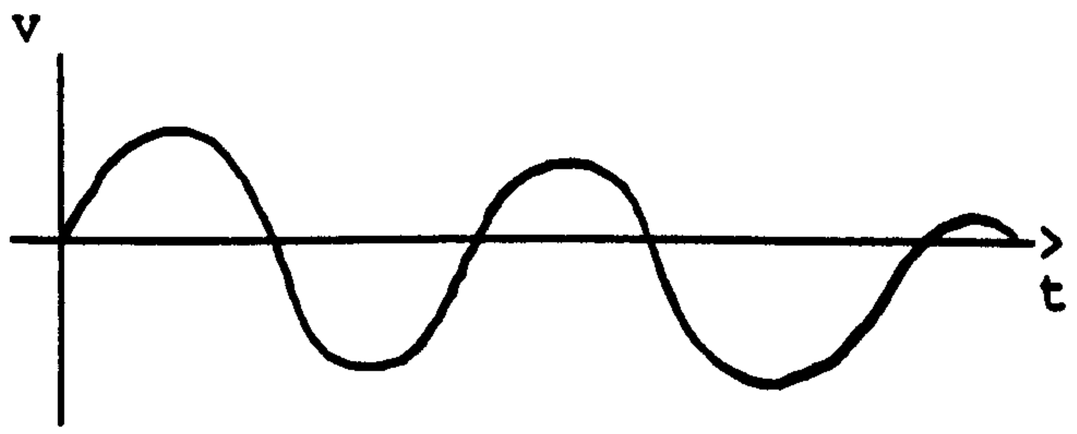

Fig (ii) Actual Data.

The trend can be determined as the size of the slope describing the locus of 4 peaks. It is assumed this trend arises due to a bias in the accelerometer. If this is the case the bias is equivalent to an error of less than 1% in the accelerometer output. Once the size of the trend is determined, any further use of the accelerometer output can be corrected by subtraction of this trend. Lines 6520- 6540, of the data reduction program correct the values of the max(n), & min(n) velocity values. At this stage in the program a printed value is displayed and this can be compared with the previous (uncorrected value). Any corrected accelerometer output should only be used in the vicinity of the determined trend, say no more than 2 or 3 wavelengths

away.

This completes the first pass through the data (line 1340: CLOSE#10). The oscillatory velocity, and its zero crossings are now known. The zero crossings are shown in Figs (i) and (ii).

The second pass through the data starts at 1350 (Openandheader1 (f$)). This is followed by skipwheels(n) to get to the point in the data reached in the first pass where the sampling started before. The program now searches the velocity for the first zero crossing again, since this can now be compared with the calculated value. Having reached the zero crossing we now know the exact point during the cycle at which the program is, for example the beginning of a wave form, at its zero crossing, as well as the correct values for velocity at this point, in the case of either lateral or longitudinal motion. Here (line 1380), the procedure (PROC) "Storedata" is called.

PROC Storedata

This procedure fills up two array variables, x(j), & y(j), with 250 bits of data each. The data has been obtained by dividing any force signal by its corresponding acceleration signal, and also dividing any "velocity^2 ", signal by its corresponding acceleration data. This process renders the governing equation into a two component form, which can subsequently be treated using a least squares method. Storedata also rejects values of acceleration which are less than 0.1 ms^{-2}, and any negative values of drag. This rids the

data arrays of unwanted information.

PROC Lstsqsfit

Calls up the variables x(j), & y(j) from the stored arrays, and treats them as data for a least squares fit. It determines values of slope which yield drag coefficient, and intercept which gives the added mass. It also provides information about the scatter these variables exhibit refered to their mean value. This provides, in addition to the desired parameters, a measure of the error in their values.

Since the arrays only store a maximum of 250 bits of data, the whole of each set of test data are treated, by moving through at intervals of every four wheel interupts. Finally, the average is then taken of the drag and added mass coefficient values for a whole run, which is equivalent to approximately thirty wheel interupts.

2. Program Listing: "CANOPY2.BAS".

```
1000 REM:CANOPY2 R.J.H. 22:5:87.Prints   out M.O.J.S as fn of
     2 variables.(divided by ACCELn).
1005 REM:IMPORTANT! EDIT LINES 1360,3180,& 6755 FOR ACCURATE
     ANALYSIS. 1010 CLEAR 5000
1020 CALL" RESOLUTION",0,1
1030 TEXT
1040 PRINT CHR$(31)
1045 DIM x(250),y(250)
1050 DIM r(9)
1055 DIM min(10),minpktime(10),max(10),maxpktime(10)
1060 GLOBAL r(),a1,a2,d1,d2,s1,s2,c1,c2,f$,sinangle,drag,
     side,moment,interval,expansion,x,skips,ints.per.rev
1062 GLOBAL a1b,a2b,d1b,d2b,s1b,s2b,c1b,c2b,aa1,aa2
1063 GLOBAL min(),minpktime(),max(),maxpktime(),x(),y()
1064 GLOBAL accel,dragb,sideb,momentb,tspeed,period,trend,
     zerovel,start.time
1066 GLOBAL maxvel,maxtime,minvel,mintime,decreasing,
           minpeakcount,maxpeakcount
1068 GLOBAL title$,date$,time$,body$,setting$,mode$,
           temperature,length
1070 PRINT"PROGRAMME TO ANALYSE DATA FILE CREATED BY 'READIT'
          DAT LOGGING PROGRAM"
1080 REM FILE DUMPED IN S-BASIC COMPILER INTERNAL FORMAT FOR
     SPEED
1090 title$="":date$="":time$="":body$="":setting$=""
1100 tspeed=0:temperature=0:interval=0
1110 INPUT "WHAT FILE IS TO BE VIEWED? E.G. B:TEST001.DAT
     ",f$
1120 OPEN #10 , f$
1130 ON EOF GOTO 1340
1140 REM This forces exit at end of each file reading case
1150 rdstring (title$)
1160 rdstring (date$)
1170 rdstring (time$)
1180 rdstring (body$)
1190 rdfixed (tspeed)
1200 rdstring (setting$)
1210 rdfixed (temperature)
1220 rdint (interval)
1225 rdint(ints.per.rev)
1230 PRINT title$,date$,time$
1240 PRINT body$
1250 PRINT " TROLLEY SPEED = " tspeed" M/S"
1290 PRINT setting$" OSCILLATIONS"
1300 PRINT "WATER TEMPERATURE = " temperature " DEG.C"
1310 PRINT "DATA LOGGED AT " interval " mSEC INTERVALS"
1315 PRINT ints.per.rev " Interrupts per trolley wheel
          revolution"
1320 get.calib
1321 REPEAT
1322   INPUT"Lateral or Longitudinal?  (LAT/LONG)";mode$
1323 UNTIL mode$="LAT" OR mode$="LONG"
1330 analyse(mode$)
1340 CLOSE#10
1350 openandheader1(f$)
```

```
1360 skipwheels(10)
1370 getzero
1380 storedata
1400 lstsqsfit
1440 STOP
1500 endit: CLOSE#10:TEXT:STOP
1980 REM
1990
REM*****************************************************
2000 REM
2010 PROC rdstring (name$)
2020   length=GET(#10)
2030   FOR i = 1 TO length : name$=name$+GET$(#10) : NEXT i
2040 ENDPROC
2045 REM:-----------------------------------
2050 PROC rdfixed (fixtvar)
2060   string$=""
2070   FOR i = 1 TO 6
2080     temp = GET(#10)
2090     dig1= INT( temp/16):dig2= temp-dig1*16
2100     string$=CHR$(48+dig1)+CHR$(48+dig2)+string$
2110   NEXT i
2120   fixtvar=VAL( string$)/1000
2130 ENDPROC
2140 REM:-----------------------------------
2150 PROC rdint(integer)
2160   integer=GET(#10)+GET(#10)*256
2170   IF integer > 32768 THEN integer = integer - 65536
2180 ENDPROC
2190
REM*****************************************************
3130 PROC analyse(mode$)
3135   interval=interval*.001
3136   REM CONVERT TO SI (SECS)
3160   noblocks=50
3170   REM:Of 30 readings
3180   skipwheels(10)
3185   time=0
3190   maxtime=0
3191   mintime=0
3193   CASE mode$ OF
3194     WHEN "LONG"
3195       velocity=tspeed
3196       EXIT
3197     WHEN "LAT"
3198       velocity=0
3199   ENDCASE
3205   noincs=0
3206   nodecs=0
3208   maxvel=-1e+10
3210   minvel=+1e+10
3215   minpeakcount=0
3220   maxpeakcount=0
3225   period=0
3230   dotwentyone(velocity,time,noincs,nodecs)
3232   IF nodecs>noincs THEN
3234       decreasing=TRUE
3236     ELSE
3238       decreasing=FALSE
```

```
3240    ENDIF
3244    PRINT"Decreasing= "decreasing
3255    FOR i=1 TO noblocks
3257      dotwentyone(velocity,time,noincs,nodecs)
3300      peakspassed(noincs,nodecs)
3380    NEXT i
3382    gettrend
3390  ENDPROC
3400  REM ********************************
3410  PROC dotwentyone(velocity,time,noincs,nodecs)
3420    noincs=0
3430    nodecs=0
3440    FOR j=1 TO 21
3450      getreading
3460      time=time+interval
3480      velocity=velocity+accel*interval
3500      IF accel>=0 THEN
3502          noincs=noincs+1
3504        ELSE
3511          nodecs=nodecs+1
3513      ENDIF
3520      IF velocity>maxvel THEN BEGIN
3530        maxvel=velocity
3540        maxtime=time
3542      END
3560      IF velocity<minvel THEN BEGIN
3570        minvel=velocity
3580        mintime=time
3582      END
3600    NEXT j
3624  ENDPROC
3625  REM*********************************
3628  PROC peakspassed(noincs,nodecs)
3630    peaked=FALSE
3640    IF noincs>nodecs AND decreasing THEN BEGIN
3645      min(minpeakcount)=minvel
3650      minpktime(minpeakcount)=mintime
3660      minpeakcount=minpeakcount+1
3662      maxvel=-1e+10
3665      REM:Found a minimum
3670    END
3680    IF noincs<nodecs AND NOT decreasing THEN BEGIN
3685      max(maxpeakcount)=maxvel
3690      maxpktime(maxpeakcount)=maxtime
3700      REM:Found a maximum
3702      minvel=+1e+10
3705      maxpeakcount=maxpeakcount+1
3710    END
3720    IF noincs<nodecs THEN decreasing=TRUE ELSE
        decreasing=FALSE
3730  ENDPROC
3740  REM*********************************
3750  PROC skipwheels(n)
3760    FOR i=1 TO n
3770      REPEAT
3780        r(0)=GET(#10):r(1)=GET(#10):r(2)=GET(#10):
            r(3)=GET(#10):r(4)=GET(#10)
3790        r(5)=GET(#10):r(6)=GET(#10):r(7)=GET(#10):
            r(8)=GET(#10)
```

```
3800      UNTIL r(0)
3810    NEXT i
3820  ENDPROC
3830  REM*********************************
3900  PROC getreading
4000    REPEAT
4010      r(0)=GET(#10):r(1)=GET(#10):r(2)=GET(#10):
          r(3)=GET(#10):r(4)=GET(#10)
4020      r(5)=GET(#10):r(6)=GET(#10):r(7)=GET(#10):
          r(8)=GET(#10)
4030    UNTIL NOT r(0)
4040    REM:IGNORE WHEEL INTERRUPTS AND COLLECT ACCELn DATA
4050    sinangle=((a1+a2*r(1))*1000+.5)*.001:REM SIN OF CRANK
        ANGLE FROM A/D
4060    drag=(d1+d2*r(2)+.5):REM N
4070    dragb=(d1b+d2b*r(5)):REM Backup drag N
4080    side=s1+s2*r(3)
4090    sideb=s1b+s2b*r(6):REM Backup normal force N
5000    moment=c1+c2*r(4):REM Nm
5010    momentb=c1b+c2b*r(7):REM backup moment in Nm
5020    accel=aa1+aa2*r(8):REM Acceleration in m/s/s on
        channel 8
5030  ENDPROC
5035  REM:*********************************
5040  PROC get.calib
5045    RESTORE calib.data
5050    READ ch$(1),a1,a2,ch$(2),d1,d2
5055    READ ch$(3),s1,s2,ch$(4),c1,c2
5060    READ ch$(5),a1b,a2b,ch$(6),d1b,d2b,ch$(7),s1b,s2b,
        ch$(8),aa1,aa2
5065    calib.data:
5070    DATA "Potentiometer",-1.175,9.1e-3:REM 1983 data?
5075    DATA "Tangential 1",-85.44,0.669
5080    DATA "Normal 1",-95.415,0.75
 1",-95.415,0.75
5085    DATA "Torsion 1",-44.357,0.345
5090    DATA "Tangential 2",-87.02,0.681
5095    DATA "Normal 2",-90.56,0.713
6000    DATA "Torsion 2",-51.069,0.401
6005    DATA "Accelerometer",-1.25,0.00977:REM FROM RUN 013
6010    REM:Calibration factors c & m in Eqn:Quantity=c+m*(A/D
        Reading Recorded)
6020    REM:Order;Pot,Tan1,Norm1,Tors1,Tan2,Norm2,Tors2,Accel
6030  ENDPROC
6035  REM:*********************************
6360  PROC openandheader1(f$)
6365    OPEN #10,f$
6370    ON EOF GOTO endit
6375    rdstring (title$)
6380    rdstring (date$)
6385    rdstring (time$)
6390    rdstring (body$)
6395    rdfixed (tspeed)
6400    rdstring (setting$)
6405    rdfixed (temperature)
6410    rdint (interval)
6415    rdint (ints.per.rev)
6420  ENDPROC
6425
```

```
REM:**********************************************************
6500 PROC gettrend
6505   mintrend=(min(1)-min(0))/(minpktime(1)-minpktime(0))
6510   maxtrend=(max(1)-max(0))/(maxpktime(1)-maxpktime(0))
6515   trend=(mintrend+maxtrend)/2
6517   PRINT "Trend= "trend
6520   FOR n=0 TO 4
6525     max(n)=max(n)-trend*maxpktime(n)
6530     min(n)=min(n)-trend*minpktime(n)
6535     PRINT max(n),min(n)
6540   NEXT n
6545   PRINT max(0),max(1),min(0),min(1)
6547   PRINT maxpktime(0),maxpktime(1),minpktime(0),
             minpktime(1)
6550 ENDPROC
REM:**********************************************************
6570 PROC getzero
6580   interval=interval*.001
6590   REM:CONVERT TO S.I.(SECS)
6600   time=0
6605   zerovel=0
6607   CASE mode$ OF
6608     WHEN "LONG"
6609       velocity=tspeed
6610       EXIT
6611     WHEN "LAT"
6612       velocity=0
6613   ENDCASE
6620   REM:ARBITRARY SETTING
6630   zerovel=(max(0)+max(1)+min(0)+min(1))/4
6635   PRINT "Zerovel= "zerovel
6637   IF velocity<zerovel THEN 6640 ELSE 6705
6640   WHILE velocity<zerovel DO
6650     getreading
6660     velocity=velocity+(accel-trend)*interval
6670     time=time+interval
6680   ENDWHILE
6685   PRINT "Hit first zero"
6687   CASE mode$ OF
6688     WHEN "LONG"
6690       zerovel=velocity-zerovel+tspeed
6691       EXIT
6692     WHEN "LAT"
6693       zerovel=velocity-zerovel
6694   ENDCASE
6695   start.time=time
6700   PRINT "Zerovel= "zerovel,start.time
6702   EXIT
6705   WHILE velocity>zerovel DO
6710     getreading
6715     velocity=velocity+(accel-trend)*interval
6720     time=time+interval
6730   ENDWHILE
6735   PRINT "Hit first zero"
6737   CASE mode$ OF
6738     WHEN "LONG"
6740       zerovel=velocity-zerovel+tspeed
6741       EXIT
6742     WHEN "LAT"
```

```
6743        zerovel=velocity-zerovel
6744      ENDCASE
6745      start.time=time
6747      PRINT "Zerovel= "zerovel,start.time
6748  ENDPROC
6749
REM:**********************************************************
6750  PROC storedata
6755      tspeed=1.284
6765      time=0
6766      cone=0
6768      ctwo=0
6770      CASE mode$ OF
6775        WHEN "LAT"
6780          velocity=0
6785        WHEN "LONG"
6795          velocity=tspeed
6800      ENDCASE
6810      FOR j=1 TO 250
6815        getreading
6820        LET veve=ABS(accel-trend)
6825        time=time+interval
6830        velocity=velocity+(accel-trend)*interval:truevel=
            =SQR(velocity^2+tspeed^2)
6833        IF veve<.1 OR drag<0 THEN 6815 ELSE 6835
6835        CASE mode$ OF
6837          WHEN "LONG"
6840            y(j)=drag/(accel-trend)
6841            x(j)=(velocity^2)/(accel-trend)
6842            REM:*PRINT time,x(j),y(j),drag,velocity,
                          (accel-trend)
6843          WHEN "LAT"
6844            y(j)=side/(accel-trend)
6846            x(j)=(velocity*(truevel^2))/(accel-trend)
6850            REM:*PRINT time,x(j),y(j),side,velocity,
                          (accel-trend)
6855        ENDCASE
6870      NEXT j
6872  ENDPROC
6871  REM**********************************************************
6874  PROC lstsqsfit
6875      p=1
6877      q=250
6878      minslope=0
6879      xmin=10e+4
6880      x=0
6881      xmax=0
6882      y=0
6883      ymax=0
6884      xy=0
6885      ymin=0
6886      xsq=0
6887      errsqd=0
6888      sum=0
6889      maxslope=0
6890      FOR j=p TO q
6900        x=x+x(j)
6910        y=y+y(j)
6920        xsq=xsq+x(j)^2
```

```
6930      xy=xy+x(j)*y(j)
6935    NEXT j
6940    xxy=x*y/(q-p)
6945    xxx=x^2/(q-p)
6970    cone=(xy-xxy)/(xsq-xxx)
6980    ctwo=(y-(x*cone))/(q-p)
6990    FOR j=p TO q
6995      by=0
7000      naff=0
7010      by=cone*x(j)+ctwo
7020      naff=by-y(j)
7030      errsqd=naff^2
7040      sum=sum+errsqd
7050    NEXT j
7060    rmserr=SQR(sum)/(q-p)
7070    FOR j=p TO q
7080      IF x(j)<xmin THEN
7090          xmin=x(j)
7093          PRINT xmin
7095        ELSE
7097      ENDIF
7100    NEXT j
7110    PRINT xmin
7120    xmax=ABS(xmin)
7130    ymax=cone*xmax+ctwo
7140    ymin=cone*xmin+ctwo
7150    maxslope=((ymax+(3*rmserr))-
                                  -(ymin-(3*rmserr)))/(xmax-xmin)
7160    minslope=((ymax-(3*rmserr))-
                                  -(ymin+(3*rmserr)))/(xmax-xmin)
7170    PRINT "Maxslope= "maxslope
7180    PRINT "Minslope= "minslope
7190    PRINT "Meanslope= "cone
7200      PRINT "Added mass(Kg)= "ctwo
7210      PRINT "Error in A.M(%)= "rmserr*100/ctwo
7215      PRINT "Error in slope(%)= "((cone-minslope)/cone)*100
7290  ENDPROC
7300  REM:**********************************************
```

APPENDIX III

Appendix III

Equipment Inventory for Southampton Tests.

Two RM380Z Microprocessors.

Two (RM380Z) 8" Disc-Drive Units (2 drives per unit).

Amplifier and ribbon lead to microprocessor.

Sting (shroud), and leads to amplifier.

Extension stings; both sizes.

Oscillation mechanism plus support brackets.

Chart recorder and leads for amplifier.

Paper (chart recorder).

8" discs (approx 20) for 380Z.

Oscilloscope.

Tool Kit.

Pulley and clamp.

Two sets of weights (calibration).

Two 4-way electrical mains adaptors.

Test Run Remark Sheets.